nature COMMUNICATIONS

ARTICLE

https://doi.org/10.1038/s41467-019-09144-7 OPEN

Chronic *Chlamydia* infection in human organoids increases stemness and promotes age-dependent CpG methylation

Mirjana Kessler[1], Karen Hoffmann[1], Kristin Fritsche[1], Volker Brinkmann[1], Hans-Joachim Mollenkopf[1], Oliver Thieck[1], Ana Rita Teixeira da Costa[1], Elena I. Braicu[2], Jalid Sehouli[2], Mandy Mangler[3], Hilmar Berger[1] & Thomas F. Meyer[1]

Chronic infections of the fallopian tubes with *Chlamydia trachomatis* (*Ctr*) cause scarring and can lead to infertility. Here we use human fallopian tube organoids and genital *Ctr* serovars D, K and E for long-term in vitro analysis. The epithelial monolayer responds with active expulsion of the bacteria into the lumen and with compensatory cellular proliferation—demonstrating a role of epithelial homeostasis in the defense against this pathogen. In addition, *Ctr* infection activates LIF signaling, which we find to be an essential regulator of stemness in the organoids. Infected organoids exhibit a less differentiated phenotype with higher stemness potential, as confirmed by increased organoid forming efficiency. Moreover, *Ctr* increases hypermethylation of DNA, which is an indicator of accelerated molecular aging. Thus, the chronic organoid infection model suggests that *Ctr* has a long-term impact on the epithelium. These heritable changes might be a contributing factor in the development of tubal pathologies, including the initiation of high grade serous ovarian cancer.

[1] Department of Molecular Biology, Max Planck Institute for Infection Biology, Charitéplatz 1, 10117 Berlin, Germany. [2] Department of Gynecology, Charité University Medicine, Campus Virchow, Augustenburger Platz 1, 13353 Berlin, Germany. [3] Department of Gynecology and Obstetrics, Auguste-Viktoria-Klinikum, Rubensstr. 125, 12157 Berlin, Germany. These authors contributed equally: Mirjana Kessler, Karen Hoffmann. Correspondence and requests for materials should be addressed to T.F.M. (email: meyer@mpiib-berlin.mpg.de)

Understanding the mechanisms of fallopian tube (FT) homeostasis and pathology constitutes an important medical challenge, particularly in light of women's fertility and beyond. Notably, the FT is the likely tissue of origin of high-grade serous ovarian cancer (HGSOC), the deadliest gynecological malignancy[1]. Yet, progress in this area has been painstakingly slow, due to the absence of suitable experimental models as well as the lack of diagnostic tools. Among the most common causes of tubal pathology is the Gram negative pathogen *Ctr*, affecting 1.6 million people in 2016 in the USA alone[2]. It frequently leads to chronic infections due to a lack of symptoms and can result in tubal scarring and occlusion, the major cause of infertility and ectopic pregnancy[3,4].

As an obligate intracellular pathogen, *Ctr* has been shown in vitro to subvert host cell metabolism, block apoptosis, and impact genome integrity by causing DNA damage and triggering degradation of p53[5–7]. Nevertheless, key steps in the development of *Ctr*-induced tubal inflammation (salpingitis) remain obscure, including the natural progression of infections. In particular, there is a gap in our knowledge concerning the long-term consequences of *Ctr* infections on epithelial homeostasis. Several early studies reported structural damage to the FT[8,9]. Previously, we also showed that several paracrine pathways are activated in response to acute *Ctr* infection ex vivo[10], suggesting the existence of broader host defense mechanisms that include both infected and neighboring non-infected cells. Still, it has so far been impossible to analyze the molecular sequels of these initial events during the establishment of chronic *Ctr* infections in the human model. It is also unclear if protracted microbial colonization of the tube adds to the risk of cellular transformation and ovarian cancer development, since the epidemiological data remain inconsistent[11,12].

Establishment of long-term organoid cultures from human primary FT epithelial stem cells[13] has created an opportunity for a qualitatively new approach to study pathogen–host interactions during *Ctr* infection. Longevity of the organoids, genetic stability, preserved differentiation mechanisms, and high structural similarity of the organoid monolayer to the epithelium in vivo are all essential components of the model, making it an ideal system to investigate the molecular mechanisms of chronic *Ctr* infection. *Ctr* has 15 different serovars, which can be divided into three categories: A–C, which cause ocular disease, D–K, which cause urogenital infections, and L1–L3, which cause invasive lymphoma granuloma venerum (LGV).

Here, we report the establishment of a chronic *Ctr* infection model of FT organoids with genital serovars D, K, and E, which are the major drivers of tubal pathology in vivo. We identify sustained pathogen-driven changes in cellular differentiation of the epithelium that occur over the course of 9 months of infection, showing that *Ctr* not only alters the phenotype of host cells but also leaves a lasting mark in the epigenome.

Results

Human FT organoids as a model of chronic *Ctr* infection. We used organoid cultures from human FTs, as described previously[13], for infection with *Ctr* serovar D (*Ctr*D) and investigated its effect on epithelial homeostasis. In stark contrast to conventional infection models based on transformed cell lines, which allow *Ctr* propagation for only a single life cycle due to lysis of infected cells, the organoids accommodated the bacteria for extended periods of time and continued to expand at a normal rate, despite an ongoing productive infection. Immunofluorescence analyses suggested that ~30% of cells were initially infected. The life cycle duration of ~72 h did not detectably differ from that typically observed for *Ctr* in cell lines, as indicated by confocal microscopy at 3 d post-infection (p.i.; Fig. 1a). Confocal analysis at later time points revealed that large *Chlamydia* inclusions were still present in organoids at 1 and even 3 months p.i, although their numbers greatly decreased during that time (Fig. 1a). Actively replicating bacteria were detected in protein lysates at 3 days, 1 month, and 2 months, but at >4 months p.i. no signal was present, as judged by western blot analysis *of Ctr* HSP60 protein in relation to host cell actin levels in total cell lysates of infected organoids (Supplementary Figure 1a). The presence of chronic infection at 2 months p.i. was further validated in three independent donor cultures (Fig. 1a, WB panel). The infectious potential was determined by infectivity assay at 72 h and 1 month p.i. Successful infection of HeLa cells with retrieved elementary bodies (EBs) (Supplementary Figure 1b) at both time points proved that *Ctr* is able to complete multiple life cycles within the organoids and stay infectious over time. The titer of retrieved bacteria did gradually decrease, however, indicating the presence of defense mechanisms that contain and eventually eliminate the infection. We observed no large variation in retrieved bacteria between different donors, quantified by number of EBs/cell (Supplementary Figure 1b). Notably, organoid cultures infected with 10 µl of 4×10^8 (CFU ml^{-1}) *Ctr* EBs always survived, and we have successfully propagated chronically infected organoids for >3 months in 20 of 20 cases, indicating the robustness of this model. Overall, the long-term expandability of infected organoid cultures was maintained for >1 year, indicating that *Ctr* infection did not impair the stemness potential of the organoids. We wanted to analyze the dynamics of acute *Ctr* infection in organoids in more detail, including its progression beyond the first 72–96 h. Whole-mount labeling of the infected organoids, which enables a comprehensive 3D view of the epithelial structure, revealed large *Ctr* inclusions within the monolayer at 24 h p.i. In contrast, at 96 h p.i. the bacteria were predominantly located in the organoid lumen, suggesting the existence of a clearance mechanism (Fig. 1b).

To visualize these events in real time, live-cell imaging was performed from 24 to 72 h p.i. on an organoid line with pCT-Mem-GFP-labeled membranes infected with an mCherry-labeled *Ctr* strain. This revealed a fast and dynamic process of expulsion of intact *Ctr* inclusions and/or infected cells from the epithelial layer into the lumen, where they subsequently burst to release infective EBs (Fig. 1c, Supplemental Movie 1). Interestingly, this phenotype was the dominant route of resolution of *Ctr*-host interaction in the organoids, resulting in an almost complete preservation of epithelial integrity. This is evidence of an intact tissue defense mechanism that limits damage to the host epithelium and enables survival of the organoid. In stark contrast to this, the well-described phenotype of *Ctr* infection in monolayers results in widespread death of host cells, such that only induction of *Ctr* persistency by antibiotics can extend the life span of infected cultures beyond 3–4 days. The concurrent robust expulsion of the inclusions and/or infected cells we observed and the maintenance of an intact polarized monolayer with no detectable structural damage also suggest that pathways that respond to changes in cell density, tissue organization and mechano-transduction are involved in maintaining epithelial integrity during the infection. To test whether the observed infection pattern is similar for the other serovars clinically relevant for urogenital infections, we also infected organoids with *Ctr* K and E strains and confirmed the presence of replicative bacteria at 1 month p.i. by western blotting for hsp60 protein (Fig. 1d). This finding was further validated by immunofluorescence imaging (Supplementary Figure 1c), which revealed no differences in the dynamics of inclusion growth and inclusion shedding between the different strains. Therefore,

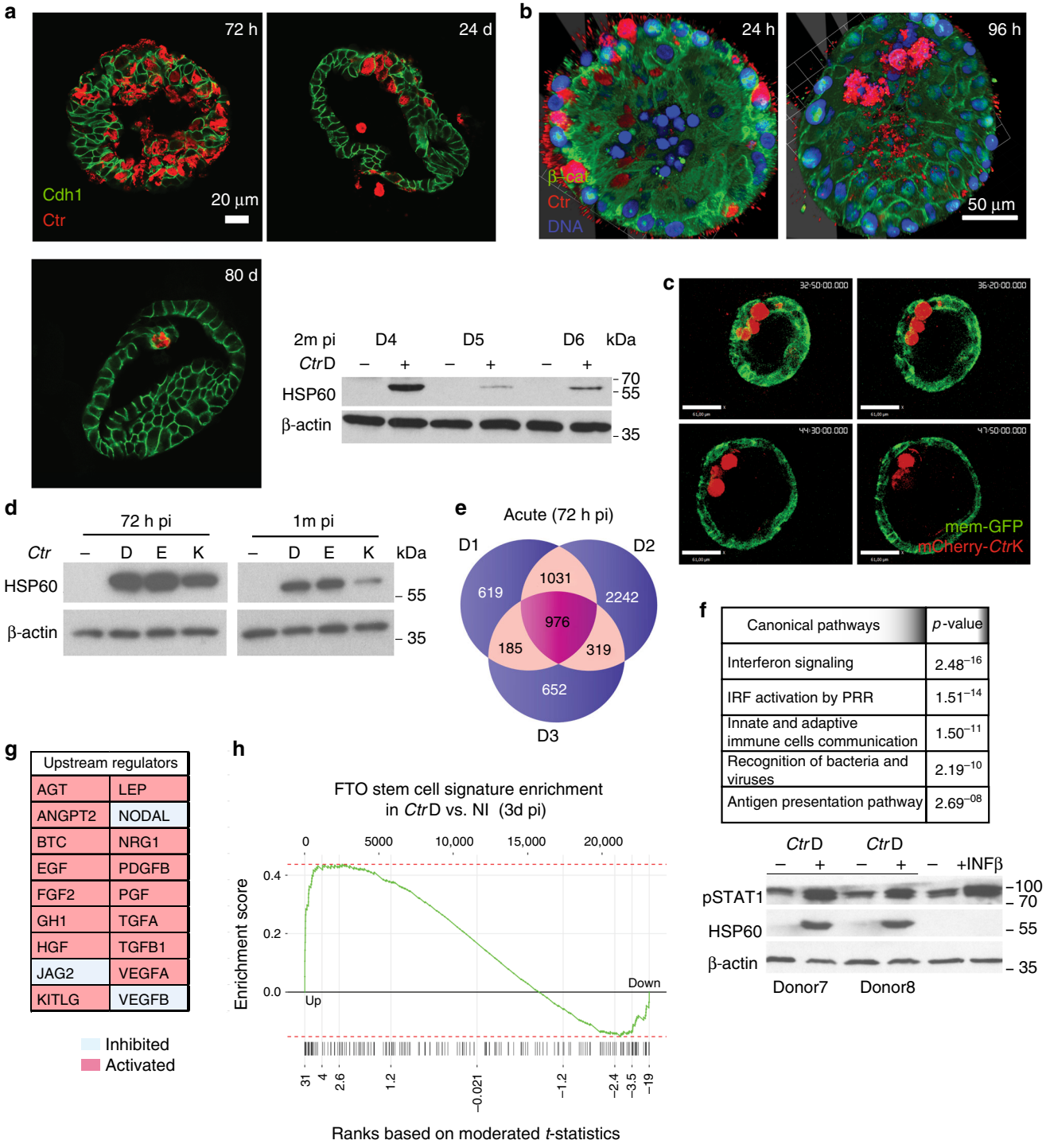

Fig. 1 Chronic *Ctr* infection of hFT organoids is characterized by early activation of inflammatory and paracrine signaling responses. **a** Representative confocal images of organoids infected with *CtrD* at 3, 24, and 80 d p.i., showing continuing presence of bacterial inclusions (red) within epithelial host cells (green). Scale bar: 20 µm. The WB of protein lysates from chronic infection at 2 months p.i. from three independent donors shows the presence of actively replicating bacteria (HSP60 protein). **b** Whole-mount 3D composite images of acute *Ctr* infection at 34 and 96 h p.i. showing a change in the localization of the bacteria (*Ctr*, red) from the inclusions within the primarily infected host cells (left panel) to the lumen of the organoid (right panel) (β-catenin, green). Scale bar: 50 µm. **c** Still images as a time course from Supplementary Movie 1 demonstrate stepwise extrusion of bacterial inclusions to the lumen. Scale bar: 60 µm. **d** Different genital *Ctr* serovars D, K, and E establish chronic infection in the organoids and maintain growth at 1 month p.i., as shown in the WB of the protein lysates harvested at acute and chronic phase. **e** Venn diagram showing extensive overlap between three different donors in the genes differentially expressed in response to *Ctr* infection, as detected by microarray analysis at 72 h p.i., with 976 genes regulated in all samples. **f** Ingenuity pathway analysis, suggesting strong activation of pro-inflammatory signaling, in particular interferon-β, which was independently confirmed by WB and detection of phospho STAT1 in infected samples with interferon-β treated organoids as positive control. **g** Table of activated paracrine pathways in the acute *Ctr* infection based on ingenuity upstream regulator analysis IPA. **h** GSEA analysis of fallopian tube (FT) organoid stem cell signature genes[13] compared to differential gene expression in infected vs. non-infected organoids at 3 d p.i. shows significant enrichment (ES = 0.44, $p < 0.001$, permutation test using 5000 permutations) among upregulated genes

we conclude that chronic organoid infection is likely to reflect the interaction of *Ctr* with the FT epithelium in vivo, regardless of the strain.

Gene expression profile of acute infection in the organoids. To investigate the global host–cell response during the acute phase of the infection, microarray analysis was performed on organoid cultures from three different donors infected with *Ctr*D for 72 h, while technical replicates were kept in long-term culture. Comparative analysis of differentially expressed genes revealed a largely similar response between different donors (Fig. 1e) to *Ctr* challenge, characterized by strong upregulation of large networks of genes involved in inflammation, pathogen recognition receptors, and communication between innate and adaptive immunity (Fig. 1f). Robust IFN-β signaling was the most prominent hallmark of acute infection, with the majority of known network components upregulated (Supplementary Figure 2a). Western blotting of whole-cell lysates from organoids confirmed that the main mediator of IFN-β signaling, the transcription factor STAT1, was strongly phosphorylated upon *Ctr* infection (Fig. 1f, lower panel) at levels comparable to that induced by stimulation with exogenous IFN-β. Interestingly, despite the absence of immune cells in our model, our microarray data revealed a strong upregulation of inducible nitric oxide synthase (NO2) (Supplementary Figure 2b) after *Ctr* infection, which was previously reported to depend on induction by activated T cells[14,15], suggesting that the epithelium responds to *Ctr* infection with a cell-autonomous, broad activation of inflammatory pathways. Importantly, in addition to the activation of regulatory networks involved in the innate immune response, we also observed differential regulation of important mediators of paracrine signaling, epithelial differentiation, and homeostasis. Analysis of upstream regulators using the Ingenuity Pathway Analysis IPA software platform identified activated (red) and inhibited (white) networks triggered by potent growth factors, such as EGF, PDGHFB, and TGF-β (Fig. 1g), with a wide range of functions that include control of cell growth, proliferation, and cell survival. As key regulators of epithelial homeostasis, these pathways have proved to be essential for control of epithelial integrity, response to injury, and wound healing in numerous other tissues, thus their activation in response to *Ctr* illustrates the extent of pathogen–host interaction in the organoids. In addition, we observed a strong upregulation of the leukemia inhibitory factor (LIF) signaling pathway, including LIF itself, as well as its downstream targets, e.g., OCT4, SOCS1, TNF-α, and IGF3BP[16] (Supplementary Figure 3), which suggests changes in both differentiation and inflammation. In confirmation, gene set enrichment analysis (GSEA) (Fig. 1h) comparing the acute infection response to a published set of NOTCH-regulated stemness genes detected in FT organoids[10] revealed a significant enrichment in the group of upregulated genes, suggesting that at 3 days p.i. organoids exhibit an increase in stemness. Taken together, acute *Ctr* infection of FT organoids triggers a sustained innate inflammatory response coupled with activation of homeostatic mechanisms to repair the injury. These findings are in agreement with the observed phenotypic changes in organoids at early stages of the infection process. Newly infected cultures are characterized by the presence of cellular debris derived from apoptotic cells, as confirmed by the presence of activated caspase-3 during the first 48 h (Supplementary Figure 4a), likely initiated by an early stress response. The absence of caspase-3 activation at 72 h, a time point when intense shedding of inclusions and/or cells occurs, confirms that infected cells do not die by apoptosis. Indeed, confocal images of infected organoids revealed that active caspase-3 signal does not co-localize with inclusion-bearing cells (Supplementary Figure 4b), thus cell death is likely triggered by a paracrine mechanism in the neighbouring uninfected cells.

Infected organoids regain homeostasis by increased proliferation. In contrast to the acute infection, chronically infected organoids phenotypically resemble controls (Supplementary Figure 4c). Long-term infected cultures also maintain a constant expansion rate over many passages and are passaged at the same time points and ratios as their non-infected sister organoids over the course of many months. We therefore hypothesized that newly infected organoids undergo increased proliferation in order to compensate for the initial cell loss. Analysis of confocal images at 7 d p.i. revealed increased numbers of Ki67+ cells in infected cultures. Positive nuclei were predominantly present in non-infected cells in close proximity to infected cells (Fig. 2a). FACS-based analysis over the course of one month to determine the proportion of EdU-labeled cells in infected vs uninfected organoids from six different donors revealed a significant increase in the proliferation rate, with a peak at 7 d p.i. (Fig. 2b, Supplementary Figure 5a). By 30 d, the proliferation rate in infected organoids had returned to control levels, in congruence with the observed lack of differences in the long-term expansion rate. This suggests that in order to maintain epithelial integrity, non-infected cells transiently increase their expansion rate to replace infected cells that have been extruded from the epithelium. Nevertheless, the observed robust activation of paracrine networks controlling not only cell growth and proliferation but also differentiation and cell fate in general, suggests that *Ctr* infection has pervasive long-term consequences on the organoid epithelium. We therefore went on to analyze pathways with dual functions that could potentially connect inflammatory responses with those involved in epithelial homeostasis.

LIF signaling regulates organoid formation and differentiation. LIF belongs to the IL-6 family of cytokines and is one of the major regulators of pluripotency during early embryogenesis as well as a crucial determinant of uterine receptivity during implantation in humans. In addition, it has potent anti-inflammatory effects, regulating IL-1β, IL-6, IL-7, IL-2Rα, and IFN-γ in a cutaneous inflammation model[17] and limiting the degree of lung injury from *E. coli* infection[18]. Our microarray data revealed that acute *Ctr* infection consistently triggers LIF upregulation in all three donors. In agreement with this, increased expression of the LIF target gene OCT4 in infected vs non-infected cells was confirmed by qPCR (Fig. 2c, upper panel). Western blot analysis further validated these findings, by revealing increased amounts of LIF protein from as early as 8 h until at least 72 h p.i. (Fig. 2c, lower panel). Considering the functional importance of LIF in preserving stemness in other models, we were interested in whether its induction during acute *Ctr* infection could contribute to infection-driven changes in homeostasis.

Interestingly, western blot analysis showed that phospho-STAT3, the main downstream effector of LIF, was constitutively active in FT organoids (after 1 d post-seeding), while the passaging procedure induced a transient dephosphorylation that lasted for 8 h, indicating changes in the STAT3 LIF/STAT3 signaling axis during organoid development, which is reinitiated after every passage (Supplementary Figure 5b). This suggests that the LIF/STAT3 axis may also be involved in the regulation of epithelial homeostasis and differentiation in the FT. Indeed, depletion of LIF transcript via shRNA greatly decreased organoid-forming capacity in epithelial isolates with only few organoids forming (Fig. 2d). Depending on the virus titer, the number of organoids generated dropped to <2% of that observed

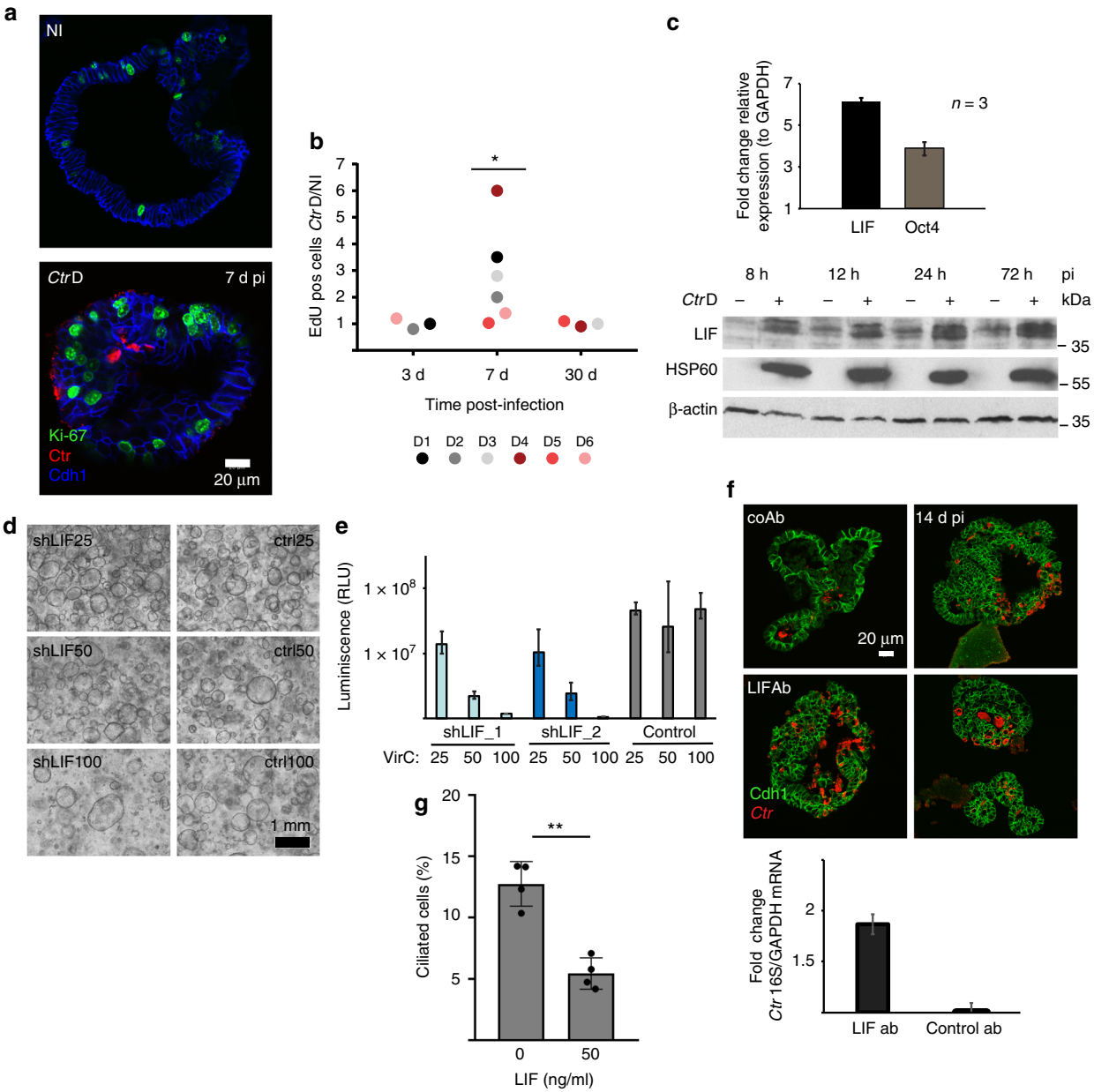

Fig. 2 LIF controls organoid homeostasis and limits replication of *Ctr* in the epithelium. **a** Confocal images showing that in infected organoids actively proliferating Ki67+ cells (green) are more frequent in cells neighboring infected cells (Ctr: red, Cdh1: blue) at 7d p.i. Scale bar: 20 µm. **b** Quantification of the time course experiments from 6 *Ctr* infections (Donors D1-D6), by number of EdU-positive cells in the infected sample, as detected by FACS normalized to the control. Infected organoids exhibit a transient peak in proliferation at one week p.i., while long-term growth rate, measured at 30 days p.i. remains constant. Significance was determined by paired Student's *t*-test of EdU measurement data sets in non-infected (NI) and infected (*Ctr*D) conditions. **c** Upregulation of LIF and its target gene Oct4 in acute *Ctr* infection was validated by qPCR in three independent donors at 72 h p.i. Data are presented as mean ± sd. Induction of LIF starts from the early phase of *Ctr* infection, as increased protein levels are already detected at 8 h p.i. by western blot analysis of the first 3 days. **d** Phase contrast images showing that lentiviral transduction of shRNA against LIF (at 25, 50, or 100 of viral units) greatly reduces the number of generated organoids in a dose-dependent manner. Ctrl: control vector pLKO.5. **e** The effect on organoid formation upon LIF knockdown by using different concentrations of virus particles (VirC) was quantified by ATP-based viability assay, which detects luminescence signal. Error bars represent technical variation between triplicate wells ± SD. **f** Inhibition of LIF activation by neutralizing antibody leads to increased bacterial load (*Ctr* red, Cdh1 green) detected in confocal images at 14 d p.i.; scale bar: 20 µm. The difference was quantified by qPCR at the same time point as the change in abundance of bacterial 16S relative to GAPDH level of the host cells. Data are representative of two independent experiments and presented as mean ± sd of technical replicates. CoAb: control antibody against *H. pylori* Cag A protein. **g** Active LIF, at 50 ng/ml promotes a secretory phenotype in the organoids as evidenced by reduction in the number of ciliated cells. Data are representative of two independent experiments. Quantification is performed as number of ciliated cells/nuclei in five independent fields of view (dot plot) (>1000 nuclei/sample) ± sd represents variation between individual images. $^{**}p < 0.01$ ($p = 0.0057$) was calculated by paired Student's *t*-test

after transduction with control vector, as quantified by the Cell Titer-Glo® assay, which measures the number of live cells via the ATP content (Fig. 2e). The organoids that did grow still expressed basal levels of LIF protein that were the same between cultures transduced with different amounts of virus particles, suggesting that LIF is essential for organoid growth in vitro (Supplementary Figure 5c). Therefore, we conclude that LIF has a central role during organoid formation, and thus ultimately controls epithelial renewal in the FT. Interestingly, blocking LIF pathway activation with soluble neutralizing antibody at the time of infection increased the chlamydial load in the organoids (Fig. 2f), as visualized by immunofluorescence analysis at 14 d p.i. and confirmed in a separate experiment by qPCR of *Ctr* 16s (Fig. 2f). While activation of LIF signaling thus limits replication of the pathogen, we were interested in whether it also affects the organoid phenotype. Adding recombinant LIF to non-infected cultures resulted in a reduced percentage of ciliated cells, quantified as the number of cilia per nuclei (Fig. 2g), suggesting that amplification of the LIF signal alone is sufficient to shift the balance of cell types within the epithelium towards a less differentiated, secretory phenotype.

Chronic infection leads to increased stemness in organoids. The robust changes in signaling and in the regulation of cell fate and differentiation factors during the acute phase of the infection suggested that *Ctr* infection potentially has long-lasting consequences on the epithelium. Quantification of the cell types found in chronically infected cultures by analysis of confocal images of serial sections, revealed that the percentage of ciliated cells significantly decreased by 3 months p.i., as determined by the number of cilia/nuclei compared to non-infected control cultures in chronic infections of organoids from five different donors (Fig. 3a). To test whether this reduction is linked to an increase in the proportion of less differentiated cells, we used FACS to analyze the number of cells expressing stem cell surface markers. Indeed, chronic infection led to an increase in the number of $CD24^+/EpCam^+$ cells (Fig. 3b, Supplementary Figure 6a), in four different donors, in agreement with the general shift towards a less differentiated state. Stem cells of both healthy and diseased upper genital tract tissue have previously been defined as $CD24^+/EpCam^+$[19]. In addition, in 2 out of 3 donors, infected organoids contained an increased proportion of cells positive for CD133, a surface marker that is associated with an increase in stemness potential[20] (Supplementary Figure 6b). Thus, both cell-type composition of the organoids, as well as surface-marker distribution, strongly suggest changes in the homeostasis of chronically infected cultures compared to controls. To test whether there is also a difference in stemness potential, we dissociated organoids to single cells and quantified their organoid forming efficiency. Indeed, cells from chronically infected organoids had a significantly higher organoid forming capacity, as quantified by Cell Titer-Glo 3D viability assay (Fig. 3c). Thus, we conclude that chronic *Ctr* infection leads to increased stemness of the organoid epithelium. Expansion of the secretory cell phenotype in the FT has been postulated as a cornerstone of transformation during the development of HGSOC[1]. In line with our previous observations in FT organoids[13], lineage tracing in mice has recently confirmed that secretory cells are in fact the precursors of ciliated cells[21]. Therefore, the *Ctr*-induced expansion of the secretory phenotype due to decreased terminal differentiation may be a potential risk factor for the initiation of sequels that could lead to transformation.

To obtain comprehensive insight into the signaling events that characterize long-term *Ctr* infection in the organoid model, we generated exploratory data sets at multiple time points during chronic infection of organoids from independent donors. As the strongest risk factor for *Ctr*-driven pathology is known to be the number of episodes of recurrent disease or reinfections, we added groups to examine whether such infections could facilitate long-lasting or even heritable changes—which would likely be mediated via epigenetic CpG methylation. To this end, we carried out global gene expression analysis at 72 h and 1 month p.i., and also at 4 months p.i. At this point, cultures were cured and re-infected (chronic infected + reinfected) and compared to the acute infection of organoids from the non-infected arm kept in culture from the start of the experiment (long-term, acute infected) (Fig. 3d). To ensure any residual bacteria were cleared prior to reinfection, all cultures were treated with antibiotics, and the absence of viable bacteria confirmed by infectivity assay (Supplementary Figure 7a). Finally, re-infected organoids were maintained in culture for an additional 4 months and analyzed for changes in DNA methylation in comparison to the methylation profile of non-infected parallel control cultures as well as "baseline" organoid cultures from the same donors, from which genomic DNA had been isolated at passage 0.

The gene expression pattern of organoids infected for 4 months followed by 7 days of antibiotic treatment (chronic infected + cured) compared to control organoids of the same age (long-term non-infected) showed that a number of genes remained dysregulated beyond resolution of infection. We identified 91 significantly regulated genes between cured and never infected samples (log2 fold change <-0.7 or >0.7, $p < 0.01$ with an FDR < 61%; Supplementary Data 1. Statistics based on moderated *t*-test and adjusting *p*-values for multiple testing using Benjamini–Hochberg procedure). Interestingly, one of the genes that was consistently upregulated in cultures from all three donors was osteopontin (SPP1) (Fig. 3f). This secreted matricellular protein can mediate migration and cell survival and is involved in the pathogenesis of multiple chronic diseases involving cancer and chronic inflammation[22]. Also, chronically infected, cured organoids show sustained overexpression of TNFSF14 (LIGHT), a member of the TNF family of ligands. Among the downregulated genes was the homeobox gene HOXA4, a prognostic factor in ovarian cancer that suppresses growth and cell motility[23], as well as HOXA5[24], which has been shown to prevent cellular transformation and positively regulates p53 expression. Downregulated genes with major roles in the modulation of the adaptive immunity included ILR17RB receptor, CCR7 or KLRF1.

Interestingly, despite these differences, we did not observe relevant changes in the cellular responses to acute *Ctr* infection between organoids that were previously chronically infected and cured, and control cultures (short or long term) that had not been infected previously. In particular, major immune response effectors like IFN-β1, TNF, IL-1β, LIF, STAT1, and NOS1 were strongly upregulated in all acute infection conditions, while chronically infected (1 month) and cured samples did not show such changes (Fig. 3e), suggesting that inflammatory responses subsided. This likely reflects the progressive reduction of bacterial numbers in the organoids over time, as confirmed by qPCR of bacterial 16S rRNA (Supplementary Figure 7b).

Thus, we concluded that while previous chronic *Ctr* infection does not change the immediate response of the fallopian epithelium to a fresh acute challenge, it does cause prolonged changes in the cellular composition of the organoid monolayer and the distribution of stemness markers. Moreover, there is evidence that chronic *Ctr* infection alters the interaction between the epithelium and the microenvironment, due to changes in expression levels of active extracellular proteins (SPP1, SULF1, IGF1) and immunomodulators (CCR7, IL17 RB). This finding could be of great importance for understanding the development

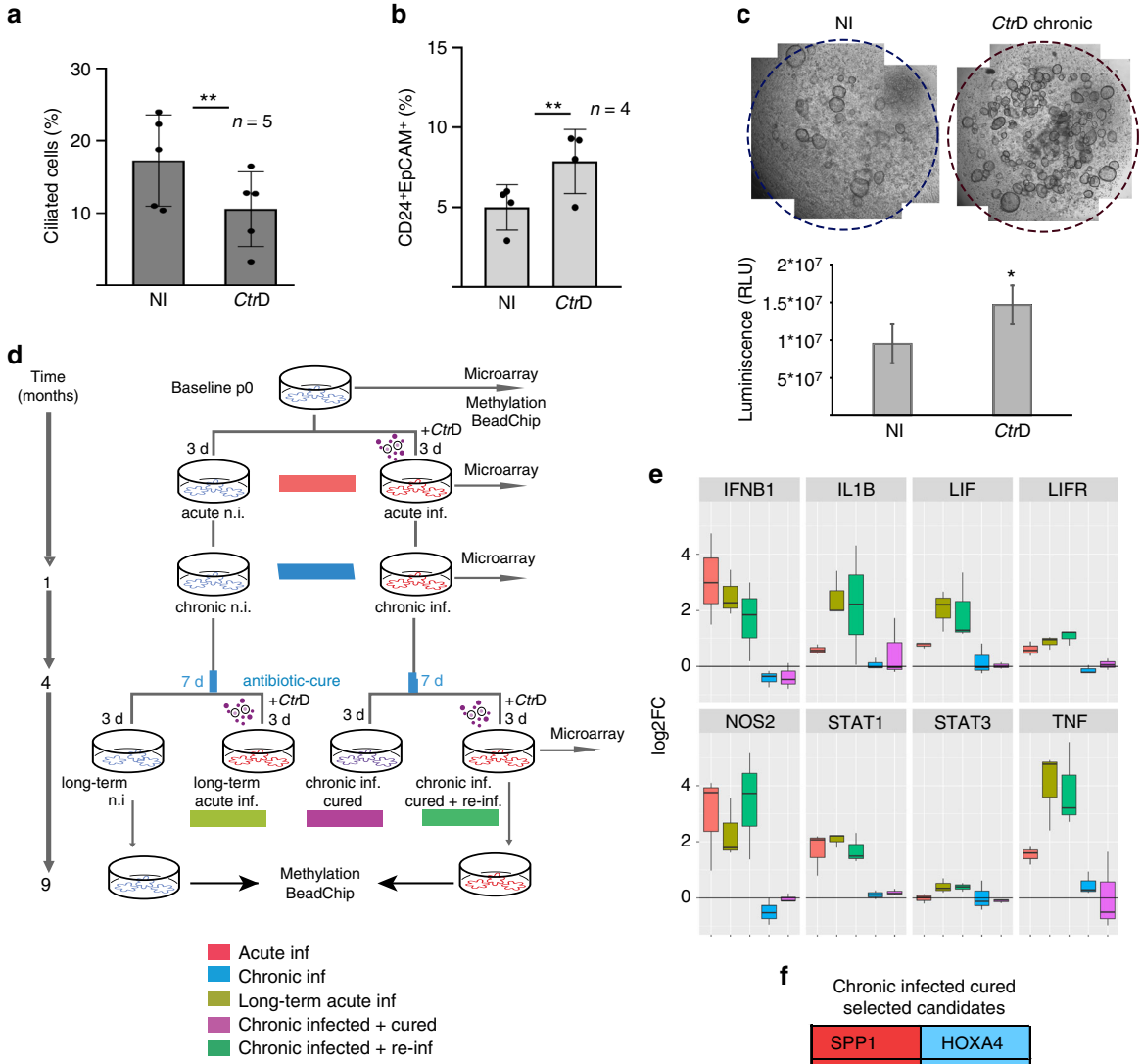

Fig. 3 Chronic *Ctr* infection leads to fewer ciliated cells, increased stemness markers and downregulation of immunomodulators. **a** Chronic infection (>3 months) significantly reduces the number of ciliated cells in the organoids. Percentage of ciliated cells was calculated as the number of ciliated cells per nuclei per field of view. Data represent mean ± SD from five independent experiments; dot plot reflects data points from independent infections $^{**}p = 0.0059$, paired Student's *t*-test. **b** Chronically infected organoids show increased numbers of CD24+/EpCam+ cells, as determined by FACS profiling. Data represent mean ± SD of four independent chronic infections. Data points from independent experiments are represented on dot plot. $^{**}p = 0.0071$ paired Student's *t*-test. **c** Chronic *Ctr* infection causes increase in organoid forming efficiency as visible on phase contrast images of comparative *Ctr*+/− wells of organoids grown from respective single cells suspensions. The effect was quantified by Cell Titer-Glo® assay. $^{*}p < 0.05$, paired Student's *t*-test, calculated from measurements of technical replicates. Data are representative of three independent experiments. **d** Experimental outline of acute/chronic infections, indicating time points at which samples for microarray and methylation analysis were collected. For each infected sample, the non-infected control sample at the same time point served as control. **e** Differential expression of selected genes across acute (3 d p.i.), chronic (1 m p.i.), and cured (4 m p.i.) infection experiments compared to non-infected control (as determined by microarray analysis) shows a conserved inflammatory response to *Ctr*, which subsides at later stages of infection and after clearance of the pathogen. Samples are colour-coded as in **d**, each was compared to the non-infected control culture at the same time point, as shown in **d**. Box plots show median, quartiles, maximum, and minimum of the log2 fold-changes of three donors. **f** Selected genes from the table of jointly regulated candidates (Supplementary Data 1) that remained differentially regulated after curing of chronic infection (red: upregulated, blue: downregulated). Genes include regulators of extracellular signaling (SPP1, SULF1), developmental genes (HOX4A and HOX5A), and immunomodulators (CCR7 and IL17 RB)

and clinical sequels of *Ctr*-driven pathology, especially in the context of recurrent episodes of asymptomatic salpingitis.

CpG hypermethylation is increased upon chronic infection. To understand how chronic *Ctr* infection leads to long-lasting changes in gene expression even after the infection is cured, we examined whether it affects the epigenome of host cells. To identify DNA methylation pattern changes, genomic DNA from organoids cultured for a total of 9 months, which were cured and re-infected at 4 months (Fig. 3d), was analyzed using the Illumina

Infinium® Methylation EPIC BeadChip, covering >850,000 CpGs of the human genome. We first tried to identify changes across three independent donors between long-term infected and non-infected conditions. Applying a threshold of at least 20% differential methylation and a *p*-value of 0.05, we identified 603 CpGs at a minimal false discovery rate of 76%, of which 179 were located in promoter regions (Supplementary Data 2). For most genes, only a single CpG out of many represented on the array was affected, indicating that there was no strong deterministic effect of long-term infection on DNA methylation compared to control.

As stochastic processes have been implicated in the formation of differentially methylated regions[25], we hypothesized that infection might lead to stochastic changes in DNA methylation that may not be detectable in organoid cultures due to the limited number of stem cells that contribute to long-term maintenance. We thus analyzed samples from two different donors to determine differentially methylated CpGs in both infected and non-infected samples, as compared to the baseline DNA methylation profile of the parental organoid cultures. We used data from a control experiment on gastric primary cells to define the magnitude of relevant changes in the absence of replicates (Supplementary Figure 8a, b) and concluded that methylation changes of >20% in any direction most likely represent real biological changes. Using this threshold, ~10–12% of all CpGs on the array were found to be differentially methylated during the course of the experiment. Notably, while changes in DNA methylation were detected in both arms of the experiment, infected samples showed an increased number of hypermethylated CpGs in both donors (Fig. 4a) compared to non-infected samples (χ^2 test, $p < 0.001$ for both replicates, Supplementary Figure 8c), leading to an increase in the number of hypermethylated genes (Fig. 4b). In order to determine whether there are any common functional denominators or distribution patterns among affected CpGs, data were subjected to Locus overlap analysis (LOLA)[26]. Identification of the genomic regions where changes in the DNA methylation occurred revealed that differentially methylated CpGs are not randomly distributed. Globally, they are enriched for laminin B1-associated domains (LAD) and depleted for transcriptionally active genomic regions, including transcription start sites (TSS), transcribed segments, and for CpG islands (Fig. 4c). Instead, hypermethylated CpGs in both conditions were enriched for enhancer and promoter flanking sites, as well as regions that, in human embryonic stem cells, are known to bind the polycomb repressive complex 2 (PRC2) members EZH2 and SUZ12—and to show histone modification H3K27me3[27]. Regulation of DNA methylation by PRC2 and hypomethylation of repetitive genomic regions have both been implicated in the process of molecular ageing across a number of sectional studies[28–30]. To analyze if the detected methylation changes correlate with the gene expression profiles of aged organoid cultures, we have performed microarray analysis of infected and non-infected long-term cultures at 9 months from both donors. At this time point, we could not conclusively confirm a significant correlation, which could be due to the small sample size or the inherent complexity of the regulatory mechanisms that mediate the effect of individual CpGs on gene transcription. Still, we detected distinct changes in the gene expression profile of long-term cultures over time, and upregulation of numerous genes involved in packaging of DNA, chromosome assembly and segregation (K4H20 demethylase network), regulation of replication (MCM4 and MCM10), control of cell cycle (BUB1B, CDKN3) and process of cellular ageing (EZH2, PIF1). All these markers provide a broader context regarding the set of molecular changes at the genomic level that characterize prolonged cultivation of adult stem cells. Interestingly, the heatmap of candidate genes (Fig. 4d) shows a tendency for higher expression levels in the infected cultures compared to non-infected aged controls, which also supports the conclusion that infection promotes the process of aging.

Taken together, our findings demonstrate sustained age-related changes in DNA methylation during a longitudinal study in a controlled experimental model. Thus, organoids appear to undergo an in vitro ageing process that is highly similar to that observed in vivo, further validating the authenticity of this model. Importantly, although there are no apparent qualitative differences in the pattern of CpG changes between experimental arms —indicating that the same underlying process is at work— chronic *Ctr* infection appears to accelerate this process in vitro. Interestingly, while the gene expression data of acute *Ctr* infection suggests an initial downregulation of the EZH2 transcription factor and corresponding target genes, long-term culture leads to sustained upregulation of EZH2. Overexpression of EZH2 is frequently detected in HGSOC tissue and is a potential therapeutic target[31]. Further studies are needed to determine whether there is a causative relationship between the transcriptional changes in EZH2 and the observed differences in CpG methylation. Altogether, our data provide experimental evidence that chronic *Ctr* infection causes long-term changes in homeostasis of the host epithelium, gene expression, and the epigenetic landscape, which are maintained beyond the end of the infection.

Discussion

Previous investigations of the effects of *Ctr* infection on human host cells were performed in 2D models mostly using transformed cell lines. Such models correlate poorly with the structural complexity and cell–cell communication that are key features of the healthy epithelial lining in the genital tract. Importantly, due to the aggressive nature of the *Ctr* lytic cycle in monolayer culture, it is also impossible to follow the process of infection long-term without induction of persistence. However, it is chronic and asymptomatic *Ctr* infections that are the main drivers of pathology in the upper genital tract. Thus, there is a great medical need for developing new *Ctr* infection models in order to understand the molecular basis of disease development.

Analysis of the long-term consequences of both acute and chronic ascending infections in vivo is greatly impeded by the inaccessibility of the FTs to clinical diagnostic tools. Instead, past infections are not usually documented until years later, and based solely on the evidence of positive *Ctr* serology and structural damage to the tube. Our chronic *Ctr* infection model now provides unique insights into the nature and cellular mechanisms of *Ctr*-driven pathogenesis in a human primary FT epithelium that closely resembles the characteristics of the native tissue. We show that chronic infection can be established in organoids with all tested *Ctr* genital serovars (D, K, E), which underlines the validity of the model for studying the general mechanisms of *Ctr* infection and for investigating the mechanisms that lead to the associated pathology. Our data were generated by thorough long-term analysis of expression data from organoid cultures from 4 different donors, and analysis of methylation changes in organoids from 3 donors, infected with *Ctr* for 9 months. It thus offers a first insight into the events that characterize the long-term effects of chronic *Ctr* infection. In addition to data presented here, which originate from 10 donors, we have performed additional chronic infection experiments (>3 months), all of which followed a consistent pattern in terms of course of infection—confirming the robustness of the infection model and the conserved response to *Ctr* infections, regardless of genetic background.

Our results indicate a profound, yet homeostatic, effect of *Ctr* infection on the regulation of cell fate and differentiation. By

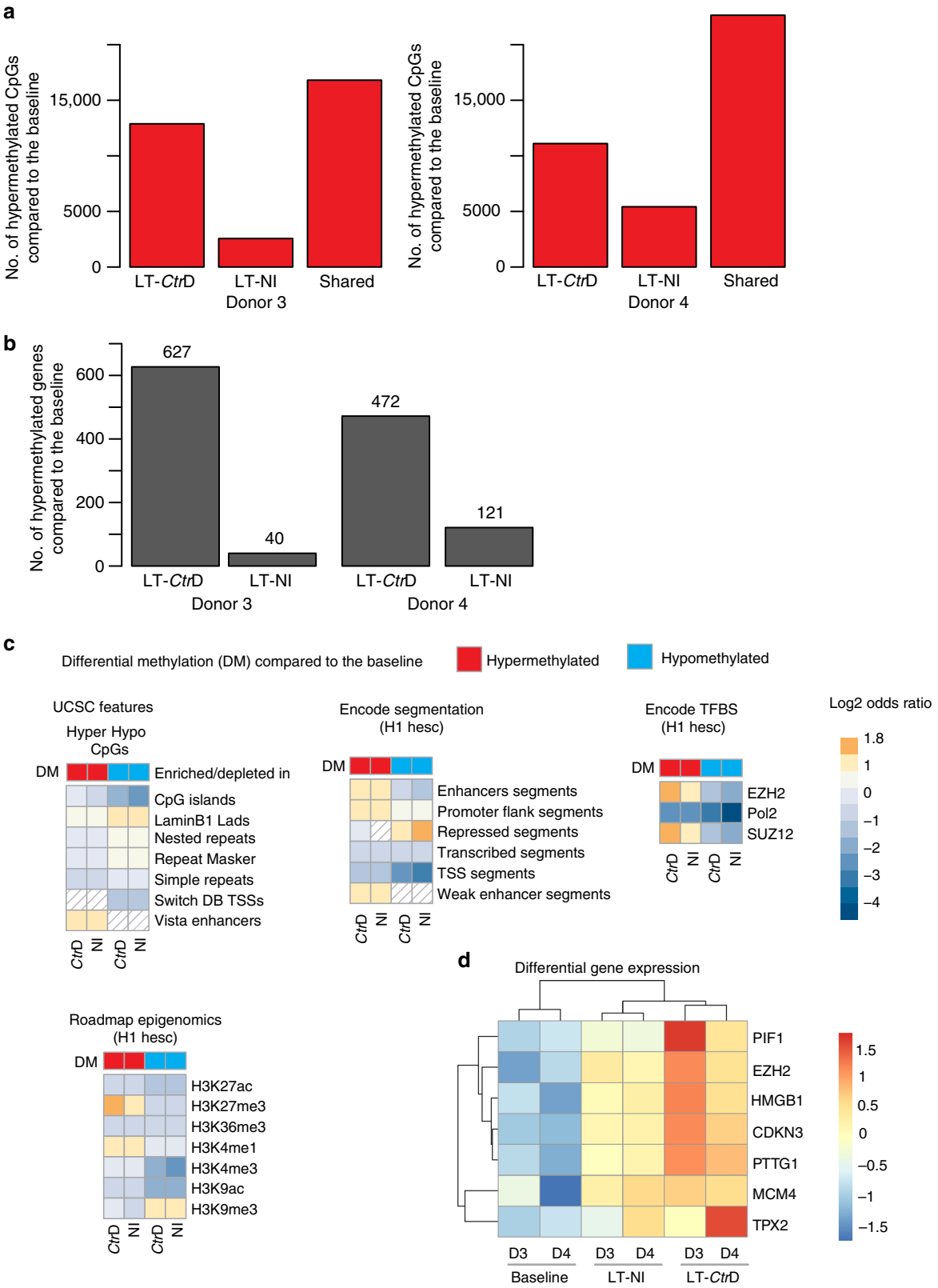

using organoids, it was possible to demonstrate that the epithelium limits the physical damage resulting from infection by efficiently extruding inclusions and infected cells into the lumen. While rupture of the inclusion membrane appears to occur mostly after extrusion from the monolayer, we could not conclusively determine the fate of the infected cells. However, it is clear that *Ctr* bacteria are able to maintain a prolonged infection in the organoid epithelium, during which shedding into the lumen is followed by fresh cycles of infection and active bacterial replication. The diminishing *Ctr* titer over time is evidence of a successful defense mechanism of the host epithelium. However, we cannot rule out that it could also reflect limitations of the

Fig. 4 Impact of chronic *CtrD* infection on the methylome. **a** Barplots showing the numbers of CpGs that increase in DNA methylation (hypermethylation; delta beta > 0.2) specifically in long-term (LT; 9 months; compare experimental design in Fig. 3c) infected (*Ctr*D) or non-infected (NI) samples compared to baseline, as well as those which are hypermethylated in both arms of the experiment (shared) in donor 3 (left) and donor 4 (right). **b** Barplot displaying the number of genes where hypermethylation, specifically for infected or non-infected samples compared to the baseline, affects at least three CpGs/gene. **c** Heatmaps of enriched and depleted genomic features among differentially methylated CpGs. The color code indicates a significant enrichment (orange) or depletion (blue) based on the log2 odds ratio and a FDR < 5%. No significant enrichment or depletion (FDR > 5%) is displayed by dashed squares. DM differential methylation, H1 hesc H1 human embryonic stem cell line, TFBS transcription factor binding sites. **d** Heatmap representing the differential expression of selected genes comparing baseline, long-term (9 months) non-infected, and infected organoids. The standardized gene expression data (*z*-score) of two patients (D3 and D4) were obtained from single-color microarray analysis

model, e.g., the inevitable loss of infectious EBs into the medium when organoids are broken up for passaging.

Although the acute infection leads to activation of multiple paracrine growth factors (TGF-β1, EGF, FGF etc.), we identify LIF as a key player in the maintenance of stemness in tubal organoids. This underscores the fundamental role of LIF signaling in the female genital tract, as evidenced by the fact that LIF mutant mice are sterile and have an underdeveloped uterus[32]. The *Ctr*-driven amplification of LIF signaling we observed suggests a mechanistic molecular basis for the link between salpingitis and the risk of ectopic pregnancy, which has previously been connected to overexpression of LIF in the FT[33]. Due to the dual function of the LIF signaling network in regulating stemness[34,35] and mediating anti-inflammatory effects, it is possible that the peak in LIF activity is primarily triggered by innate immune mechanisms in order to limit bacterial replication, as evidenced by our pharmacological inhibition of LIFR. Stemness-related changes may be a by-product in the course of chronic infection.

The observed gradual decrease in the number of ciliated cells and increase in CD24+Epcam+ and CD133+ cells suggest a sustained shift in the regulation of epithelial renewal during infection. This effect establishes a link towards cell transformation, since expansion of non-ciliated, secretory cells generally precedes HGSOC development[1]. It is important to note that the increase in stemness, as measured by the increased organoid forming efficiency, does not imply complete functional competence of the ageing stem cells, as previously demonstrated in other models[36]. Equally important may be our observation that chronically infected organoids show changes in the expression of the potent immunomodulators IL17 RB, CCR7, and KLRF1, and that this effect persists after the clearance of the bacteria. In context with the detected upregulation of SPP1 and reduction of HOXA4 and HOXA5, this may modify the way the epithelium interacts with the surrounding tissue, including adaptive immune cells. However, determining the precise implications of these findings will require more extended experimental settings, involving immune cells as well as larger numbers of donors to control for individual differences.

Strikingly, our methylation data support a potential role of chronic *Ctr* infection as an epigenetic modulator. The molecular mechanisms that lead to the observed increase in differential CpG hypermethylation of genes known to be regulated by polycomb in mouse and human embryonic stem cells[27,37] are yet to be determined. Yet, it is conceivable that this process is influenced by the transient spike in proliferation during the early phase of *Ctr* infection and the activation of signaling pathways known to maintain crosstalk with EZH2 polycomb networks[38]. Studies of hematopoietic stem cells first reported epigenomic changes that enhance self-renewal in the context of ageing[29]. In this context, it is interesting that we also observed an increase in stemness in chronically infected organoids. It remains to be seen if the shift towards a more de-differentiated phenotype is connected to these epigenetic changes. Notably, though, the number of cilia in non-infected organoids remained constant over time, in congruence with our previous observations[13]—despite the changes in CpG methylation and molecular ageing that were also observed in the non-infected samples. Therefore, these types of epigenetic changes do not appear to be sufficient to alter organoid composition and imply involvement of additional cellular mechanisms triggered by infection.

Taken together, this study highlights progress in the establishment of a next-generation human epithelial in vitro model, enabling investigation of important aspects of the *Ctr*-host interaction. Human FT organoids maintain stemness and differentiation programs—both of which are necessary to allow for detection of the long-term effects of infection on the host epithelium. Such programs are not present in standard monolayer cultures, in particular transformed cell lines. Our findings shed tantalizing new light on the effects of *Ctr* on the tubal epithelium that may have a role in the development of tubal pathology. Although *Ctr* has a relatively high rate of upper genital tract colonization, estimated at ~10% of all infected women, it remains underreported due to the frequent asymptomatic clinical presentation. Given the interference with core developmental mechanisms of epithelial homeostasis, the epigenetic changes and the expression of immune system modifiers we observed, it is clear that future investigation of the long-term consequences of *Ctr* infection is imperative and will need to take into account the interplay between infected epithelium and its tissue microenvironment. This new approach will thus contribute to a better understanding of the long-term effects of *Ctr* infections, including its potential to contribute to cell transformation and the etiology of HGSOC.

Methods

Patient material. FT samples were provided by the Department of Gynecology, Charité University Hospital, Campus Virchow Clinic and August-Viktoria Klinikum Berlin, Department of Gynecology and Obstetrics. Scientific usage of the samples for experimental purposes was approved by the Ethics Commission of the Charité, Berlin (EA1/002/07) and informed consent was obtained from all donors. Fragments were sourced from standard surgical procedures for benign gynecological disease. Only anatomically normal FTs were used. Tubes were transported and dissected within 2 to 3 h of removal.

Organoid cultivation. Generation and culture of FT organoids was performed as described in Kessler et al[13]. In brief, epithelial progenitors from human FT tissue samples were isolated by enzymatic digestion with collagenase I (Sigma). The retrieved primary cells were seeded in 2D culture for 5–7 days (ADF medium with 12 mM HEPES, 1% GlutaMAX™, 10 ng ml^{-1} human EGF and 9 µM Y-27632) before seeding in Matrigel™ (~30,000 cells/50 µl) for 3D organoid formation. Once the Matrigel™ had set, cultures were overlaid with medium containing a specific growth factor cocktail to preserve stemness and support differentiation (ADF, 25% conditioned mouse Wnt3A-medium as described in Willert et al.[39] and 25% conditioned mouse RSPO1 medium[40], supplemented with 12 mM HEPES, 1% GlutaMAX™, 2% B27, 1% N2, 10 ng ml^{-1} human EGF (all from Invitrogen), 100 ng ml^{-1} human noggin, 100 ng ml^{-1} human FGF-10 (both from Peprotech), 1 mM nicotinamide, 9 µM ROCK inhibitor (Y-27632, both from Sigma) and 0.5 µM TGF-β RI Kinase Inhibitor IV (SB431542, Calbiochem)). For propagation, organoids were split every 2 to 3 weeks at a ratio of 1:2 to 1:3 using mechanical splitting with a

syringe and needle (26 G gauge). Organoids were kept in a humidified incubator at 5% CO_2 and 37 °C, or 35 °C once infected.

Organoid formation assay. Single cells were prepared from long-term infected organoids (>2 months p.i.) by digestion with collagenase and reseeded at 40,000 cells/25 µl Matrigel™ in triplicate. At 3 weeks post-seeding, cell viability assay was performed on all wells. The Cell Titer-Glo® 3D Cell Viability kit (Promega # G9681) was applied to each well according to the manufacturer's protocol and the luminescence measured using a plate reader.

Antibodies. The following antibodies were used in this study: primary—mouse anti-E-Cadherin (1:200 610181, BD Transduction Lab), mouse anti-β-actin (1:200, A5441, Sigma), goat anti-*Ctr* (OBT0978, AbD Serotec), mouse anti-HSP60 (1:5000, ALX-804-701, Alexis), rabbit anti-Ki67 (9027, Cell Signaling), rabbit anti-pSTAT1 (1:1000, 9167, Cell Signaling), rabbit anti-pSTAT3 (Tyr705) (1:1000 9145, Cell Signaling), cleaved caspase-3 (1:1000, 9664, Cell Signaling), goat anti-LIF (1:500, AF-250-NA, R&D Systems); secondary - sheep anti-mouse-HRP (1:3000, NA931, Amersham), donkey anti-rabbit-HRP (1:3000, NA934, Amersham), donkey anti-goat-HRP (1:3000, 800073, Biomol), donkey anti-mouse-Alexa488 (1:300, 715-546-140, Dianova), donkey anti-goat-Cy3 (1:300, 705-165-003, Dianova), donkey anti-rabbit-Alexa488 (1:300, 711-546-152, Dianova), donkey anti-mouse-Dylight 647 (1:300, 715-605-150, Dianova), CD326 (EpCAM)-FITC antibody (1:50, 130-080-301, Miltenyi), mouse anti-human CD24-BV711 antibody (1:200, 563371, BD Biosciences), mouse anti IgG1-APC (1:100, 130-098-846, Miltenyi), and mouse anti-human CD133/1 (AC133)APC (1:100, 130098829, Miltenyi). As a DNA-labeling agent, Draq5 (5 µM, 62252, Thermo Scientific) was used.

Single cell preparation and fixation. To prepare single cells, organoids were released from Matrigel using cold PBS, pelleted by centrifugation (5 min, 300 × *g*), resuspended in 0.5–1 ml TrypLE and incubated for 15 min at 37 °C. Organoid fragments were then mechanically disrupted by passing 3–4× through a 26 G gauge needle. Next, the cells were taken up in 3 ml Advanced DMEM/F12 and passed through a 40 µm filter. The single cell suspension was pelleted by centrifugation and resuspended in 500 µl 3.7% PFA for 30 min. Cells were then washed by addition of 3 ml PBS/1% BSA, centrifuged (5 min, 300 × *g*), resuspended in 1 ml PBS/1% BSA and kept at 4 °C for further processing.

Proliferation assay. To determine the number of proliferating cells, the Click-iT-EdU assay (Thermo Fischer, #C10425) was applied. Organoids were treated with 10 µM EdU for 2 h in culture medium, triturated into single cells and fixed with 3.7% PFA. Labeling of the EdU-positive cells with Alexa488 was done as per manufacturer's instructions. Flow cytometric analysis was performed using a BD FACS CANTOII flow cytometer and the FlowJo vX.0.6 software.

Flow cytometry. Single cells derived from organoids were labelled in 1×PBS/1% BSA using mouse anti-human CD326 (EpCAM)-FITC antibody, mouse anti-human CD24-BV711 antibody and mouse anti-human CD133/1 (AC133)APC. Labeling was performed for 30 min on ice in the dark. Afterwards, cells were washed using 1 ml PBS. Finally, cells were pelleted and resuspended in PBS. The flow cytometric analysis was done using a BD FACS CANTOII flow cytometer and the FlowJo vX.0.6 software.

Quantitative real-time polymerase chain reaction (qRT-PCR). Determination of RNA levels was performed by qRT-PCR using the AB Power SYBR® Green RNA-to-CT™ 1-Step Kit (Applied Biosystems™), StepOnePlus™ Real-Time PCR System (Applied Biosystems™), and StepOne™ Software (v2.3, Applied Biosystems).

A mixture of 10 µl RNA (2–5 ng µl^{-1}), 10 µl SYBR® green mix, 4.3 µl H_2O, 0.2 µl Reverse Transcriptase enzyme mix and 0.5 µl Primer mix (10 µM) was subjected to the following PCR cycler program: 30 min 48 °C; 10 min 95 °C; followed by 40× cycles of 15 s 95 °C/60 s 60 °C.

Each sample was measured in triplicate. The expression levels of all target genes were normalized to expression of the housekeeping gene *glyceraldehyde-3-phosphate dehydrogenase* (*GAPDH*). Relative expression levels were determined by calculating $\Delta\Delta C_t$. Fold change was calculated as an average of $\Delta\Delta C_t$ of independent biological replicates ($2-\Delta\Delta C_t$), while s.d. was calculated as $\Delta\Delta C_t + s$ and $\Delta\Delta C_t - s$, where s is the pooled s.d. of the ΔC_t and ΔC_t control values ($s = \sqrt{\mathrm{sd(ctt)}^2 + \mathrm{sd(ctc)}^2}$).

The following primers were used: *GAPDH*—forward 5′-GGTATCGTGGAAGG ACTCATGAC-3′, reverse 5′-ATGCCAGTGAGCTTCCCGTTCAG-3′; *LIF*—forward 5′-CAGGAGTTGGGTCCAGATGT-3′, reverse 5′-GTCCACAATCTCC CAGAGGA-3′; *Oct4*—forward 5′-GATGTGGTCCGAGTGTGGTTCT-3′, reverse 5′-TTGTGCATAGTCGCTGCTTGA-3′; *CtrD 16S rRNA*—forward 5′-GGTATCG TGGAAGGACTCATGAC-3′, reverse 5′-TCAAATCCAGCGGGTATTAACCG CCT-3′.

Lentiviral manipulation. Replication-deficient lentiviral particles were produced by transfection of 293T cells with a mixture of the respective lentiviral plasmids and Fugene6 (Promega, #E2691) diluted in Opti-MEM™ (Gibco, # 31985088). For a 10 cm dish, 15.6 µl Fugene6 was mixed with 192.4 µl OPTI-MEM and added to 3 µg lentiviral target plasmid, 2.25 µg psPAX2 packaging vector and 0.75 µg pMD.2 G (VSVG) envelope vector diluted in 52 µl OPTI-MEM. After 30 min incubation at RT, the mixture was pipetted dropwise onto the 293T cells. 16 h post transfection the medium was replaced with 10 ml fresh DMEM. 24 h later the medium was aspirated, filtered at 45 µm and mixed with Lenti-X™ Concentrator (Clontech Laboratories, #631231). After concentration, the virus pellet was resuspended in 1 ml ADF (10x concentration) and stocked at −80 °C.

LIF shRNA lentiviral plasmids and the corresponding vector control were obtained from Sigma (pLKO.5, SHC201; pLKO.5-LIFshRNA: TRCN0000308277, 5′-ACCGCATAGTCGTGTACCTTG-3′; pLKO.1-LIFshRNA: TRCN0000058586, TAAGCAGATCATCGCCGTGTT). The pCT-Mem-GFP plasmid was obtained from System Biosciences (#CYTO100-VA-1).

For transduction, early passage 2D primary FTECs at ~70% confluence in a 6-well plate were treated with 1×, 0.5×, or 0.25× concentrated virus diluted in ADF medium supplemented with 12 mM HEPES, 1% GlutaMAX, 10 ng ml^{-1} human EGF, 9 mM ROCK inhibitor and 5 µg ml^{-1} polybrene (Sigma, #H9268). The cells were incubated overnight with the virus at 37 °C. When the cells reached ~90% confluence, organoids were prepared and selection with puromycin (0.5 µg ml^{-1}) was started.

RNA and DNA isolation. RNA and DNA were isolated using the Allprep Qiagen Kit.

Microarray RNA isolation, quantification, and quality control. Total RNA was isolated with TRIzol (Life Technologies) according to the supplier's protocol using glycogen as carrier. Quality control and quantification of total RNA was assessed using an Agilent 2100 Bioanalyzer with an RNA Nano 6000 microfluidics kit (Agilent Technologies) and a NanoDrop 1000 UV-Vis spectrophotometer (Kisker).

Microarray expression profiling and data analysis. Microarray experiments were performed as dual-color or single-color hybridizations on either 4 × 44 K human catalogue (Agilent-026652) or 8 × 60 K human custom (Agilent-048908) microarrays comprising identical features for coding genes. In order to compensate dye-specific effects and to ensure statistically relevant data, color-swap dye-reversal hybridizations were performed[41]. RNA labeling was done either with a two-color Quick Amp Labeling Kit (4 × 44 K arrays) or with a Low Input Quick Amp Kit (6 × 60 K arrays) according to the supplier's recommendations (Agilent Technologies). In brief, mRNA was reverse transcribed and amplified using an oligo-dT-T7 promoter primer, and labeled with Cyanine 3-CTP or Cyanine 5-CTP. After precipitation, purification, and quantification, 1 µg (4 × 44 K arrays) or 300 ng (8 × 60 K arrays) of each labeled cRNA was fragmented and hybridized to whole genome multipack microarrays according to the manufacturer's protocol (Agilent Technologies). Scanning of microarrays was performed with 5 µm resolution and XDR extended range (4 × 44 K arrays) or 3 µm resolution (8 × 60 K arrays) using a G2565CA high-resolution laser microarray scanner (Agilent Technologies). Microarray image data were analyzed and extracted with the Image Analysis/Feature Extraction software G2567AA v. A.11.5.1.1 (Agilent Technologies) using default settings and the protocol GE2_1100_Jul11. The extracted MAGE-ML files were subsequently analyzed with the Rosetta Resolver, Build 7.2.2 SP1.31 (Rosetta Biosoftware). Ratio profiles comprising single hybridizations were combined in an error-weighted fashion to create ratio experiments. A 1.5-fold change expression cut-off for ratio experiments was applied together with anti-correlation of ratio profiles, rendering the microarray analysis highly significant, robust, and reproducible. Additionally, raw data txt files were analyzed with R packages from the Bioconductor repository. The networks and functional analyses of microarray data were generated via Ingenuity Pathway Analysis (QIAGEN Inc., [https://www.qiagenbioinformatics.com/products/ingenuity-pathway-analysis])[42]. The data discussed in this publication have been deposited in NCBI's Gene Expression Omnibus and are accessible through GEO Series accession number GSE107712.

GSEA analysis. We derived a stem cell signature using published gene expression data (GSE60919)[13] from FT organoids upon DBZ treatment. Raw data were normalized using method LOESS and differentially expressed genes determined using R and the BioConductor package LIMMA package[43]. We selected downregulated genes with FDR < 10% and log2 fold change <−1.5 as putative FT stem cell signature genes. We performed GSEA on those genes pre-ranked by gene expression-based *t*-score between infected and non-infected samples at 3 d p.i., using the fgsea R package[44] with 5000 permutations.

Live-cell imaging. FT epithelial cells were transduced with a plasmid carrying a GFP-membrane tag (pCT-Mem-GFP plasmid, System Biosciences #CYTO100-VA-1). After selection, GFP mem transduced organoids were infected with mCherry-labeled *Chlamydia* stock according to the standard protocol, seeded into Matrigel in ibidi µ dishes, incubated for 24 h and transferred to an inverted Leica TCS-SP5 confocal microscope equipped with a cell culture incubator. For about

50 h, confocal stacks of about 30 frames were generated every 10 min. These stacks were used for 3D reconstruction and videos using Volocity 6.3.

Transformation of *Chlamydia* with RFP. The protocol was adapted from procedures developed by Wang and colleagues[45,46]; Agaisse and Derré[47]; Song and colleagues[48] and Bauler and Hackstadt[49]. In brief, *Chlamydia trachomatis* K (*Ctr* K, a kind gift from Lars Köhler) EBs were transformed with p2TK2-SW2_IncDProm-mCherry-IncDTerm plasmid DNA. The transformed strain was then selected with increasing concentrations of penicillin G for 7 passages until 100 units ml^{-1} for further propagation of transformed *Ctr* K mcherry stock. For the preparation of mCherry *Ctr* K stocks, chlamydial EBs were propagated in HeLa cells (ATCC® CCL-2) in T150 cm^3 cell culture flasks with 25 ml of culture medium. Cells were infected with lysates from earlier passages and incubated at 35 °C in a cell culture incubator under humidified atmosphere with 5% CO_2 until time of harvest at 48 h p.i., as described above. The resulting supernatant was collected and centrifuged at 20,000 rcf for 40 min at 4 °C in an SS-34 rotor (Sorval RC 5 C Plus) to pellet chlamydial EBs. The harvested bacteria were resuspended in 5 ml SPG buffer (4 °C). A second centrifugation was performed and the pellet resuspended in 4 ml of SPG buffer (4 °C) and frozen at −80 °C.

Chlamydia infection, cure, and re-infection of FT organoids. For infection with *CtrD* (ATCC® VR-885TM), *CtrE* (ATCC® VR-348B™) and *CtrK*, 2 wells of organoids were released from Matrigel™ with cold DPBS, pooled and mechanically disrupted by passing them through a 26 gauge needle. The fragmented organoids were divided evenly into 2 tubes for infection and mock control. After centrifugation (300 × *g*, 5 min) and removal of the supernatant, 10 µl *Ctr*D (from a frozen stock with 10^8 IFU ml^{-1} as determined by titration on HeLa cells) were added to one tube with the pelleted organoids. The suspension was mixed by pipetting and incubated for 15 min at 35 °C followed by 5 min on ice. The mock control was treated in the same way, but without addition of *Ctr*D. Finally, 50 µl Matrigel™ was added to each tube, the organoids seeded and placed in a humidified incubator at 5% CO_2 and 35 °C. Splitting of organoids was done every 3–4 weeks. RNA samples were taken at 72 h p.i. and 1 month p.i.

At around 4 months p.i. the infection was cured by applying a mixture of penicillin (100 U ml^{-1}) and streptomycin (100 µg ml^{-1}) to the organoid culture for one week. After curing, re-infection was carried out in the same way as the first infection with mechanical splitting, adding of *Ctr*D to one half of the organoids and mock treatment of the other half. Control organoids initially infected with *Ctr*D were infected or mock-treated again. 72 h post seeding, RNA samples were taken of the now 2× infected (chronic infected + re-infected), chronic infected (chronic cured), acute infected (long-term acute inf), and the never infected organoids (Fig. 3d).

RNA samples for microarray. At the respective time points (3 d p.i., 1 month p.i. and 4 months p.i.) organoids were released from Matrigel™ with ice-cold DPBS and centrifuged (300 × *g*, 5 min). The cell pellet from one Matrigel™ drop was resuspended in 750 µl TRIzol® reagent (Invitrogen # 15596026) and stored overnight at −80 °C until further isolation.

Infectivity assay. One day before the infectivity assay, HeLa cells were seeded at a density to achieve ~ 70% confluence at the time of infection. Both *Ctr*-infected and non-infected FT organoids were treated as follows: Medium was removed and Matrigel™ dissolved in 1 ml ice-cold RPMI w/o FCS. Organoids were centrifuged for 4 min at 300 × *g*. After removal of the supernatant, cells were resuspended in 1 ml RPMI and homogenized by passing three times through a 26 G gauge needle. After another round of centrifugation and addition of 1 ml ice-cold RPMI, the pellet was transferred to a 50 ml falcon tube with 1 ml sterile glass beads. EBs were released by vigorous vortexing for 5 min. After centrifugation for 4 min at 300 × *g*, the supernatants were transferred to the prepared HeLa cells containing fresh medium. After 24 h (at 35 °C, 5% CO_2) cells were fixed in PFA and subjected to IF staining for detection of inclusions.

Immunofluorescence staining. Organoids were fixed with 3.7% PFA, embedded in paraffin, sectioned and stained for confocal imaging as described previously[13].

Whole-mount staining. Organoids were released from Matrigel with 1xPBS and pelleted by gravitational flow to maintain 3D structure. After fixing with 3.7% PFA for 1 h at RT, organoids were permeabilized and blocked overnight at 4 °C in 5% donkey serum, 1% FCS, 0.05% Tween-20, 0.5% Triton X-100 and 0.02% sodium azide in 1×PBS. Staining with primary antibodies was performed in blocking buffer (0.0025% Triton X-100) at a dilution of 1:200 for 3 days at 4 °C. Washing (5 × 45 min in 1×PBS with 5% glycerol) was followed by staining with Draq5 and secondary antibody in blocking solution (0.0025% Triton X-100) at a dilution of 1:200 for 2 days at 4 °C. After washing, organoids were transferred onto an ibiTreat µ-slide (ibidi #003031) and *z* stacks performed using confocal microscopy. The 3D structure was reconstructed and visualized using Fiji (ImageJ).

Western blot. Organoid samples were treated with ice-cold PBS to remove Matrigel, centrifuged (300 × *g*; 5 min; 4 °C), supernatant was removed and the cell pellet resuspended in 100 µl SDS sample buffer (4% SDS, 32% glycerol, 125 mM Tris pH 6.8, 200 mM β-mercaptoethanol, and bromphenol blue). Samples were boiled for 7 min at 96 °C, then separated via SDS-Page electrophoresis (~90 min at 150 V const) and transferred to a PVDF membrane (2.5 h at 250 mA const. at 4 °C). Membranes were blocked in 5% skim milk/TBS-Tween-20 (0.1%) for 60 min. Primary antibodies were diluted 1:500 or 1:1000 in 5% skim milk/TBS-Tween-20 (0.1%) and incubated with the blocked membranes at 4 °C overnight. After extensive washing in TBS-T for 45 min in total, secondary antibodies anti-mouse- or anti-rabbit-HRP were diluted 1:3000 in 5% skim milk/TBS-Tween-20 (0.1%) and incubated for 1 h at room temperature. ECL detection was performed according to the manufacturer's protocol after washing the membranes with TBS-T for 1 h. Uncropped scan images of all blots are provided in Supplementary Figure 9.

LIF neutralization. For LIF neutralization the general protocol for *CtrD* infection of organoids (as described above) was carried out. Differing from this protocol, the fragmented organoids were resuspended in 90 µl ADF++, which was added with or without *CtrD*, and subsequently mixed with 10 µl of 1:40 pre-diluted antibodies. Neutralization was done using 0.5 µg ml^{-1} anti-LIF antibody (R&D, #AF-250-NA, from goat, 200 µg ml^{-1}) and mock control using 0.5 µg ml^{-1} goat anti-CagA (Santa Cruz, #sc-6085, 200 µg ml^{-1}). After the specified incubation time for infection, the organoids were seeded in Matrigel and culture medium was added. 14 days p.i. organoids were fixed, embedded and IF labeled for detection of *Chlamydia*.

Methylation array and bioinformatic analysis. For genome-wide DNA methylation analysis, bisulfite conversion of the genomic DNA and hybridization to the Illumina Infinium® MethylationEPIC BeadChip were performed at Life&Brain (Bonn, Germany), according to the manufacturer's protocol. Data analysis was carried out in the R environment[50]. Preprocessing and quality control (QC) were performed following the ChAMP package[51] default filtering steps (probes with a detection *p*-value > 0.01 and with a bead count < 3 were excluded), as well as probes where the sequence overlaps single-nucleotide polymorphisms (SNPs) or that were shown to cross-hybridize according to Zhou et al.[52] Subset-quantile within array normalization (SWAN) was applied in order to adjust for the type I and type II bias of the methylation array[53]. Differentially methylated CpGs between infected (*Ctr*D) and non-infected (NI) organoids were determined using limma[43] and a moderated paired *t*-test. A false discovery rate (FDR) was computed by adjusting *p*-values for multiple testing using the Benjamini–Hochberg procedure. For patient-specific DM CpGs upon infection and long-term culture, a cut-off of delta beta > 20% was applied and justified with data from a control experiment (Supplementary Figure 8a,b). Unique DM CpGs compared to the baseline were subjected to a locus overlap analysis (LOLA)[26] using the databases ENCODE transcription factor binding sites (TFBSs), ENCODE segmentation[37], UCSC features[54] as well as Roadmap Epigenomics[55]. For the χ^2 test, for each donor the frequency of hypomethylated or unchanged CpGs in each arm was compared with the corresponding number of hypermethylated CpGs. The Methylation BeadChip data generated in this study have been deposited in the National Centre for Biotechnology Information Omnibus (GEO) under the accession code GSE108202.

Reporting summary. Further information on experimental design is available in the Nature Research Reporting Summary linked to this article.

Data availability

The microarray and methylation BeadChip data from this manuscript have been deposited in the National Centre for Biotechnology Information Omnibus (GEO) under accession codes GSE107712 and GSE108202. Raw data associated with Figs. 3f and 4 can be found in Supplementary Data 1 and 2, respectively. Other data supporting the findings of this study are available within the paper and its Supplementary Information files, or from the corresponding author upon request. As far as ethical and legal constrains permit, all biological materials are available upon request from the corresponding author.

Received: 4 January 2018 Accepted: 22 February 2019
Published online: 18 March 2019

References

1. Bowtell, D. D. et al. Rethinking ovarian cancer II: reducing mortality from high-grade serous ovarian cancer. *Nat. Rev. Cancer* **15**, 668–679 (2015).
2. CDC. *Sexually Transmitted Disease Surveillance 2016* (Department of Health and Human Services, Atlanta, GA, 2017).
3. Price, M. J. et al. How much tubal factor infertility is caused by *Chlamydia*? Estimates based on serological evidence corrected for sensitivity and specificity. *Sex. Transm. Dis.* **39**, 608–613 (2012).

4. Shaw, J. L. et al. *Chlamydia trachomatis* infection increases fallopian tube PROKR2 via TLR2 and NFkappaB activation resulting in a microenvironment predisposed to ectopic pregnancy. *Am. J. Pathol.* **178**, 253–260 (2011).
5. Chumduri, C., Gurumurthy, R. K., Zadora, P. K., Mi, Y. & Meyer, T. F. *Chlamydia* infection promotes host DNA damage and proliferation but impairs the DNA damage response. *Cell Host Microbe* **13**, 746–758 (2013).
6. Gonzalez, E. et al. Chlamydia infection depends on a functional MDM2-p53 axis. *Nat. Commun.* **5**, 5201 (2014).
7. Sharma, M. & Rudel, T. Apoptosis resistance in *Chlamydia*-infected cells: a fate worse than death? *FEMS Immunol. Med. Microbiol.* **55**, 154–161 (2009).
8. Cooper, M. D., Rapp, J., Jeffery-Wiseman, C., Barnes, R. C. & Stephens, D. S. *Chlamydia trachomatis* infection of human fallopian tube organ cultures. *J. Gen. Microbiol.* **136**, 1109–1115 (1990).
9. Hvid, M. et al. Interleukin-1 is the initiator of fallopian tube destruction during *Chlamydia trachomatis* infection. *Cell. Microbiol.* **9**, 2795–2803 (2007).
10. Kessler, M. et al. *Chlamydia trachomatis* disturbs epithelial tissue homeostasis in fallopian tubes via paracrine Wnt signaling. *Am. J. Pathol.* **180**, 186–198 (2012).
11. Lin, H. W. et al. Risk of ovarian cancer in women with pelvic inflammatory disease: a population-based study. *Lancet Oncol.* **12**, 900–904 (2011).
12. Ness, R. B. et al. *Chlamydia trachomatis* serology in women with and without ovarian cancer. *Infect. Dis. Obstet. Gynecol.* **2008**, 219672 (2008).
13. Kessler, M. et al. The Notch and Wnt pathways regulate stemness and differentiation in human fallopian tube organoids. *Nat. Commun.* **6**, 8989 (2015).
14. Igietseme, J. U. Molecular mechanism of T-cell control of *Chlamydia* in mice: role of nitric oxide in vivo. *Immunology* **88**, 1–5 (1996).
15. Jayarapu, K., Kerr, M., Ofner, S. & Johnson, R. M. Chlamydia-specific CD4 T cell clones control *Chlamydia muridarum* replication in epithelial cells by nitric oxide-dependent and -independent mechanisms. *J. Immunol.* **185**, 6911–6920 (2010).
16. Sherwin, J. R. et al. Identification of genes regulated by leukemia-inhibitory factor in the mouse uterus at the time of implantation. *Mol. Endocrinol.* **18**, 2185–2195 (2004).
17. Zhu, M., Oishi, K., Lee, S. C. & Patterson, P. H. Studies using leukemia inhibitory factor (LIF) knockout mice and a LIF adenoviral vector demonstrate a key anti-inflammatory role for this cytokine in cutaneous inflammation. *J. Immunol.* **166**, 2049–2054 (2001).
18. Quinton, L. J. et al. Leukemia inhibitory factor signaling is required for lung protection during pneumonia. *J. Immunol.* **188**, 6300–6308 (2012).
19. Gao, M. Q., Choi, Y. P., Kang, S., Youn, J. H. & Cho, N. H. CD24+ cells from hierarchically organized ovarian cancer are enriched in cancer stem cells. *Oncogene* **29**, 2672–2680 (2010).
20. Kryczek, I. et al. Expression of aldehyde dehydrogenase and CD133 defines ovarian cancer stem cells. *Int. J. Cancer* **130**, 29–39 (2012).
21. Ghosh, A., Syed, S. M. & Tanwar, P. S. In vivo genetic cell lineage tracing reveals that oviductal secretory cells self-renew and give rise to ciliated cells. *Development* **144**, 3031–3041 (2017).
22. Shevde, L. A. & Samant, R. S. Role of osteopontin in the pathophysiology of cancer. *Matrix Biol.* **37**, 131–141 (2014).
23. Klausen, C., Leung, P. C. & Auersperg, N. Cell motility and spreading are suppressed by HOXA4 in ovarian cancer cells: possible involvement of beta1 integrin. *Mol. Cancer Res.* **7**, 1425–1437 (2009).
24. Teo, W. W. et al. HOXA5 determines cell fate transition and impedes tumor initiation and progression in breast cancer through regulation of E-cadherin and CD24. *Oncogene* **35**, 5539–5551 (2016).
25. Landan, G. et al. Epigenetic polymorphism and the stochastic formation of differentially methylated regions in normal and cancerous tissues. *Nat. Genet.* **44**, 1207–1214 (2012).
26. Sheffield, N. C. & Bock, C. LOLA: enrichment analysis for genomic region sets and regulatory elements in R and Bioconductor. *Bioinformatics* **32**, 587–589 (2016).
27. Lee, T. I. et al. Control of developmental regulators by Polycomb in human embryonic stem cells. *Cell* **125**, 301–313 (2006).
28. Fernandez, A. F. et al. H3K4me1 marks DNA regions hypomethylated during aging in human stem and differentiated cells. *Genome Res.* **25**, 27–40 (2015).
29. Sun, D. et al. Epigenomic profiling of young and aged HSCs reveals concerted changes during aging that reinforce self-renewal. *Cell Stem Cell* **14**, 673–688 (2014).
30. Zampieri, M. et al. Reconfiguration of DNA methylation in aging. *Mech. Ageing Dev.* **151**, 60–70 (2015).
31. Jones, B. A., Varambally, S. & Arend, R. C. Histone methyltransferase EZH2: a therapeutic target for ovarian cancer. *Mol. Cancer Ther.* **17**, 591–602 (2018).
32. Kimber, S. J. Leukaemia inhibitory factor in implantation and uterine biology. *Reproduction* **130**, 131–145 (2005).
33. Krishnan, T. et al. The role of leukemia inhibitory factor in tubal ectopic pregnancy. *Placenta* **34**, 1014–1019 (2013).
34. Liu, J. W., Hsu, Y. C., Kao, C. Y., Su, H. L. & Chiu, I. M. Leukemia inhibitory factor-induced Stat3 signaling suppresses fibroblast growth factor 1-induced Erk1/2 activation to inhibit the downstream differentiation in mouse embryonic stem cells. *Stem Cells Dev.* **22**, 1190–1197 (2013).
35. Niwa, H., Ogawa, K., Shimosato, D. & Adachi, K. A parallel circuit of LIF signalling pathways maintains pluripotency of mouse ES cells. *Nature* **460**, 118–122 (2009).
36. Pollina, E. A. & Brunet, A. Epigenetic regulation of aging stem cells. *Oncogene* **30**, 3105–3126 (2011).
37. ENCODE Project Consortium. An integrated encyclopedia of DNA elements in the human genome. *Nature* **489**, 57–74 (2012).
38. Ringrose, L. & Paro, R. Epigenetic regulation of cellular memory by the Polycomb and Trithorax group proteins. *Annu. Rev. Genet.* **38**, 413–443 (2004).
39. Willert, K. et al. Wnt proteins are lipid-modified and can act as stem cell growth factors. *Nature* **423**, 448–452 (2003).
40. Farin, H. F., Van, Es,J. H. & Clevers, H. Redundant sources of Wnt regulate intestinal stem cells and promote formation of Paneth cells. *Gastroenterology* **143**, 1518–1529.e1517 (2012).
41. Churchill, G. A. Fundamentals of experimental design for cDNA microarrays. *Nat. Genet.* **32**(Suppl), 490–495 (2002).
42. Krämer, A., Green, J., Pollard, J. Jr & Tugendreich, S. Causal analysis approaches in ingenuity pathway analysis. *Bioinformatics* **30**, 523–530 (2013).
43. Ritchie, M. E. et al. limma powers differential expression analyses for RNA-sequencing and microarray studies. *Nucleic Acids Res.* **43**, e47 (2015).
44. Sergushichev, A. An algorithm for fast preranked gene set enrichment analysis using cumulative statistic calculation. Preprint at https://doi.org/10.1101/060012 (2016).
45. Wang, Y. et al. Development of a transformation system for Chlamydia trachomatis: restoration of glycogen biosynthesis by acquisition of a plasmid shuttle vector. *PLoS Pathog.* **7**, e1002258 (2011).
46. Wang, Y. et al. Genetic transformation of a clinical (genital tract), plasmid-free isolate of *Chlamydia trachomatis*: engineering the plasmid as a cloning vector. *PLoS ONE* **8**, e59195 (2013).
47. Agaisse, H. & Derre, I. A *C. trachomatis* cloning vector and the generation of *C. trachomatis* strains expressing fluorescent proteins under the control of a *C. trachomatis* promoter. *PLoS ONE* **8**, e57090 (2013).
48. Song, L. et al. Plasmid-mediated transformation tropism of chlamydial biovars. *Pathog. Dis.* **70**, 189–193 (2014).
49. Bauler, L. D. & Hackstadt, T. Expression and targeting of secreted proteins from *Chlamydia trachomatis*. *J. Bacteriol.* **196**, 1325–1334 (2014).
50. RC Team. *R: A Language and Environment for Statistical Computing* (R Foundation for Statistical Computing, Vienna, Austria, 2011). http://www.r-project.org.
51. Morris, T. J. et al. ChAMP: 450k chip analysis methylation pipeline. *Bioinformatics* **30**, 428–430 (2014).
52. Zhou, K. R. et al. ChIPBase v2.0: decoding transcriptional regulatory networks of non-coding RNAs and protein-coding genes from ChIP-seq data. *Nucleic Acids Res.* **45**, D43–d50 (2017).
53. Maksimovic, J., Gordon, L. & Oshlack, A. SWAN: Subset-quantile within array normalization for illumina infinium HumanMethylation450 BeadChips. *Genome Biol.* **13**, R44 (2012).
54. Casper, J. et al. The UCSC genome browser database: 2018 update. *Nucleic Acids Res.* **46**, D762–D769 (2017).
55. Kundaje, A. et al. Integrative analysis of 111 reference human epigenomes. *Nature* **518**, 317–330 (2015).

Acknowledgements

We would like to thank Ina Wagner, Susan Jackisch, and Jörg Angermann, for technical support, Rike Zietlow for editing the manuscript and Diane Schad for help with graphics. We are also grateful to Per Hoffmann und Stefan Herms from Life & Brain Center/University Bonn for performing bisulfite conversion of genomic DNA and hybridization to the BeadChip. This study was supported by the BMBF through the Infect-ERA project CINOCA (FK 031A409A).

Author contributions

M.K. and T.F.M. conceived the project and designed experiments, which were conducted by M.K., K.H., O.T., and A.R.C.; V.B. conducted the live-cell imaging experiment. K.F. and H.B. analyzed methylation Chip data. H.B. and H.-J.M. analyzed microarray data, M.M., J.S. and E.B. selected the patients and provided human FT samples. M.K. and T.F.M. wrote the manuscript, and T.F.M. supervised the project.

Additional information

Supplementary Information accompanies this paper at https://doi.org/10.1038/s41467-019-09144-7.

Competing interests: The authors declare no competing interests.

Reprints and permission information is available online at http://npg.nature.com/reprintsandpermissions/

Journal peer review information: *Nature Communications* thanks Toni Darville, Adam Karpf and the other anonymous reviewer(s) for their contribution to the peer review of this work.

Publisher's note: Springer Nature remains neutral with regard to jurisdictional claims in published maps and institutional affiliations.

Supplementary Information

Chronic *Chlamydia* infection in human organoids increases stemness and promotes age-dependent CpG methylation

Kessler M et al

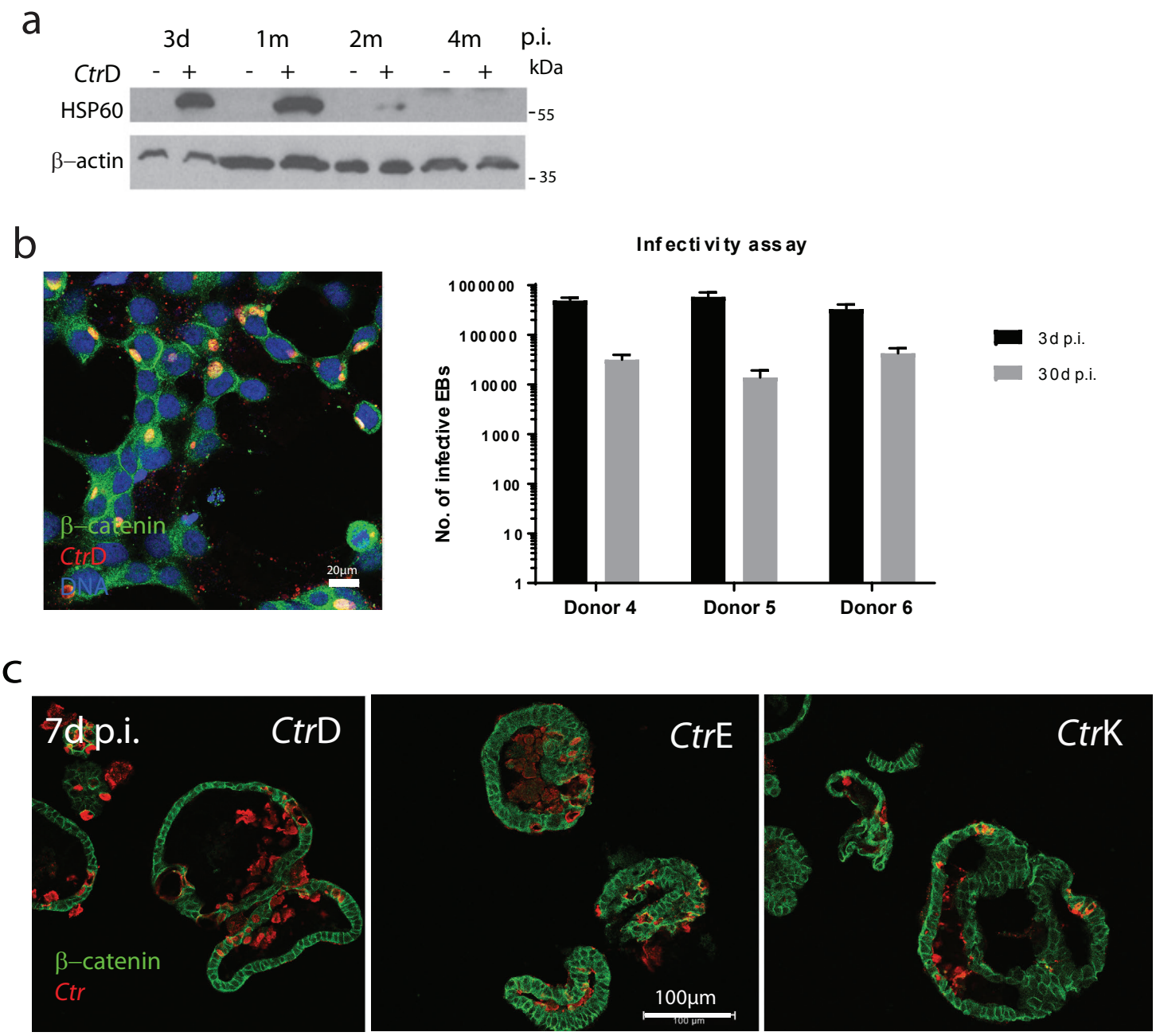

Supplementary Figure 1. Chronic, productive *Ctr* infections in organoids gradually decreases in titer a) Representative blot of HSP60 protein levels from one chronically infected culture at 3 d, 1 month and 4 month p.i. While bacterial load is high at 3 dp.i and remains substantial at 1 month p.i. it decreases to undetectable levels by 4 months p.i. b) Confocal image of HeLa cells containing inclusions filled with *Ctr*, confirming infectious potential of EBs retrieved from infected organoids. The graph represents quantification from 3 independent chronic infections in 3 donors at 3 d and 1 m p.i. ± sd calculated based on inclusion counts from different fields of view. c) Confocal images of representative organoids infected with serovars D, E and K at 7 d p.i. reveals similar infection rates and accumulation of bacteria shed in the organoid lumen.

a

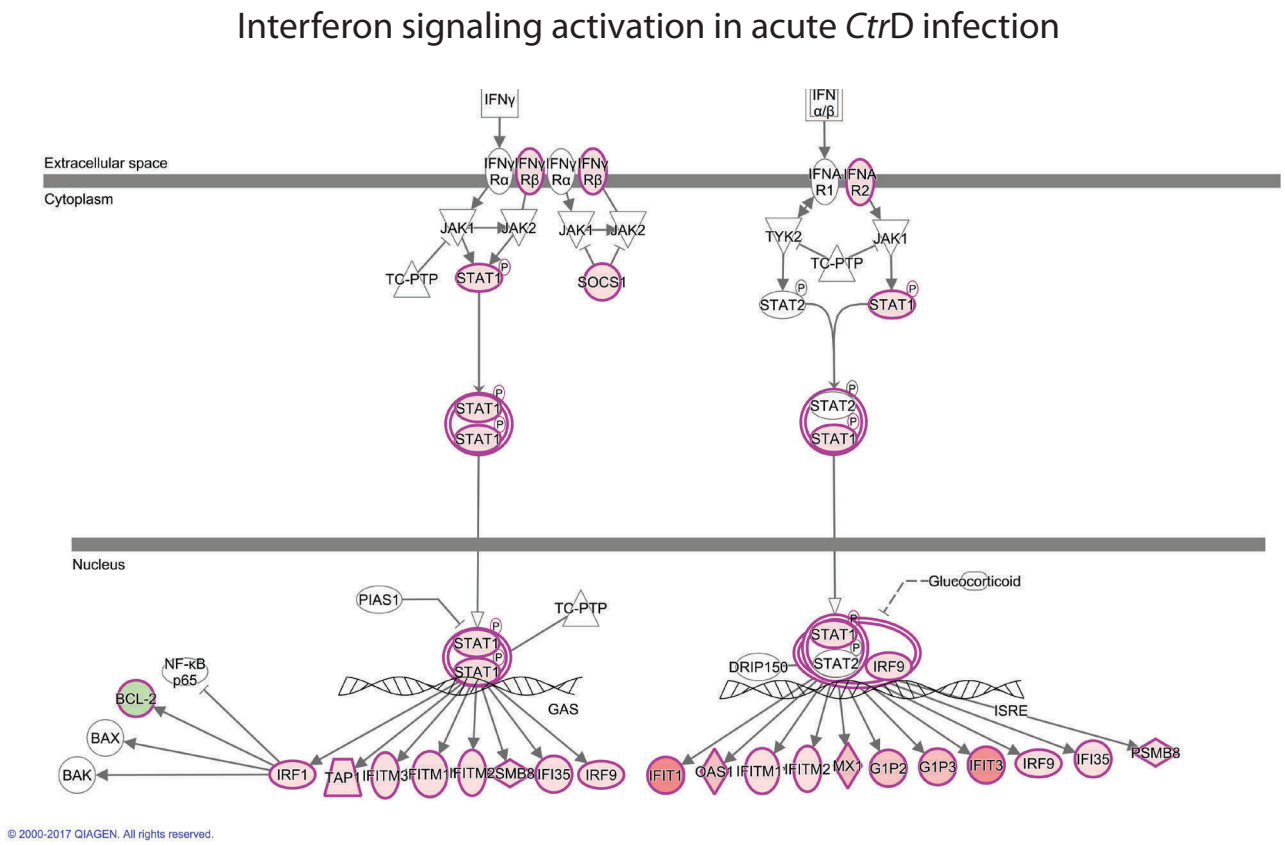

b

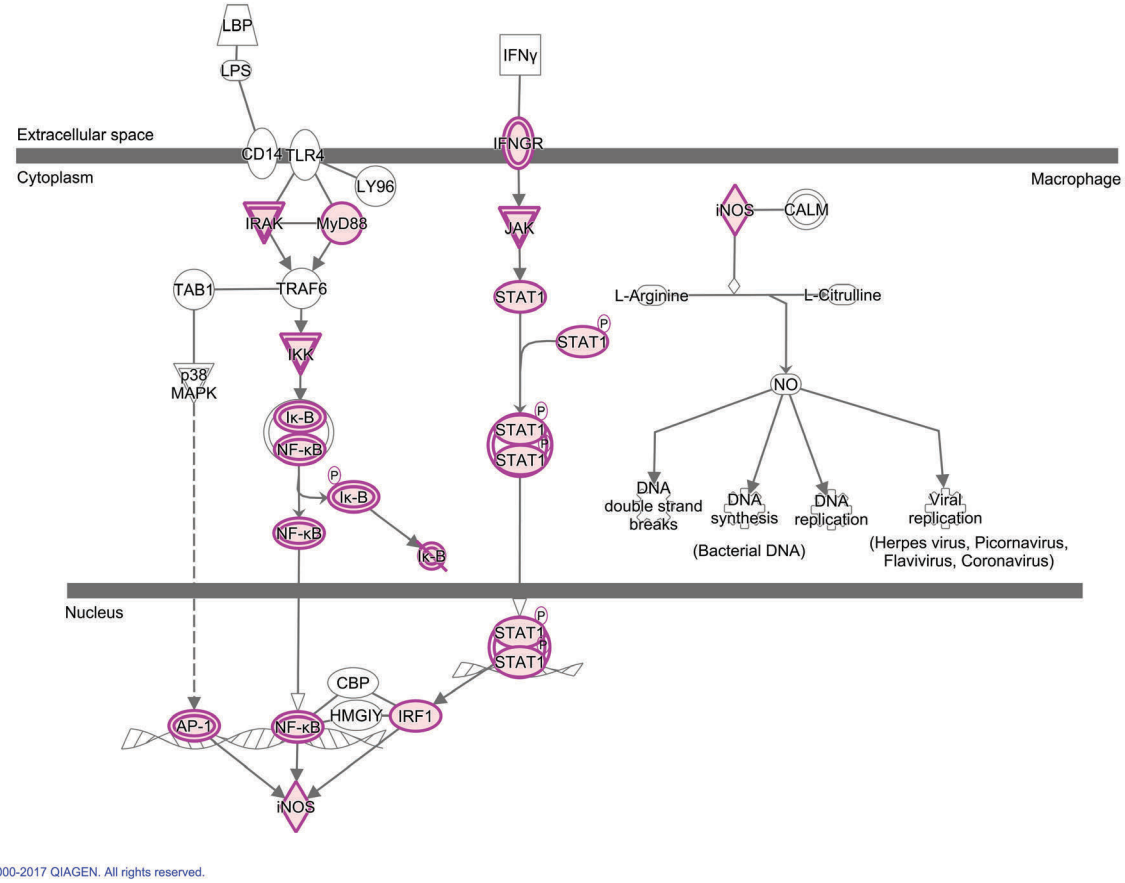

Supplementary Figure 2. Acute *Ctr* infection triggers strong upregulation of interferon response a) Genes in the interferon signaling network that were upregulated (red) during acute *Ctr* infection. b) Genes in the iNOS pathway upregulated during acute *Ctr* infection. Pathways were generated on the IPA^{tm} platform by overlay of canonical networks with microarray data of genes that are regulated in an identical fashion in all 3 donors.

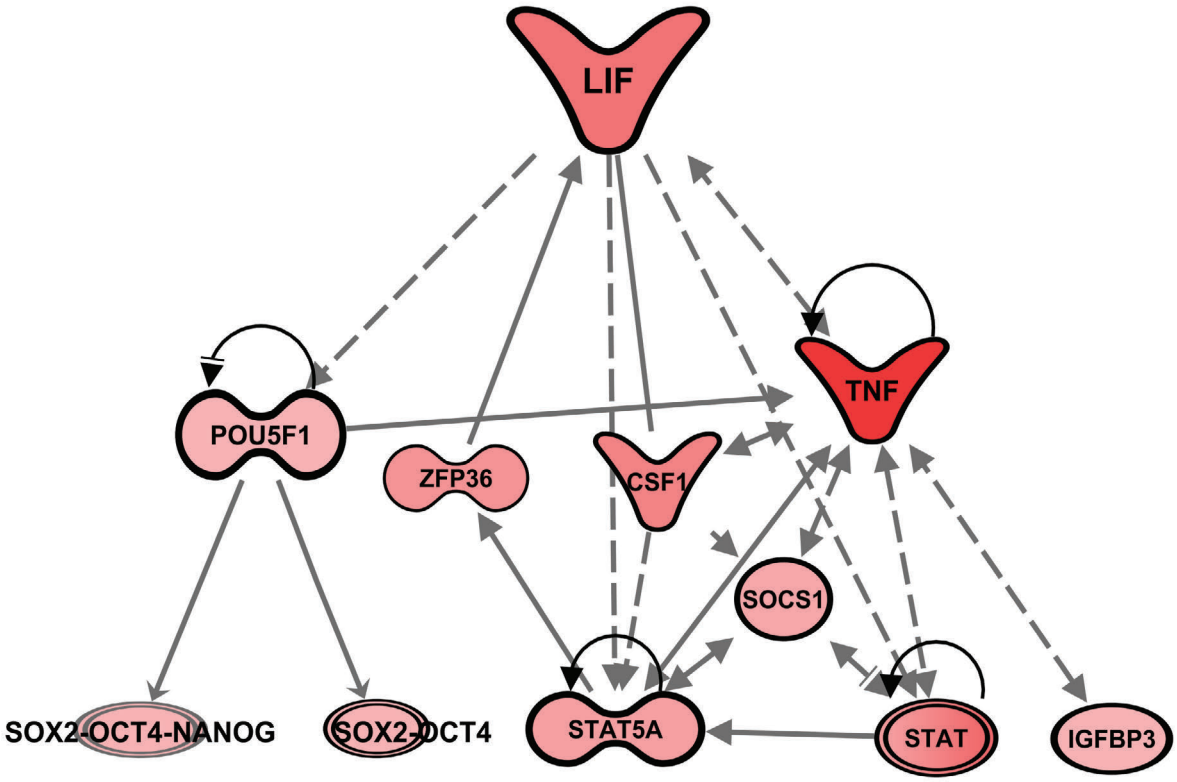

Supplementary Figure 3. Activation of the LIF pathway occurs during acute *Ctr* infection Graphical presentation of the strong upregulation of the LIF gene and associated interactors (all in red). The network was generated on the IPA^{tm} platform by pathway analysis of microarray data of all candidate genes which were consistently regulated in 3 different donors.

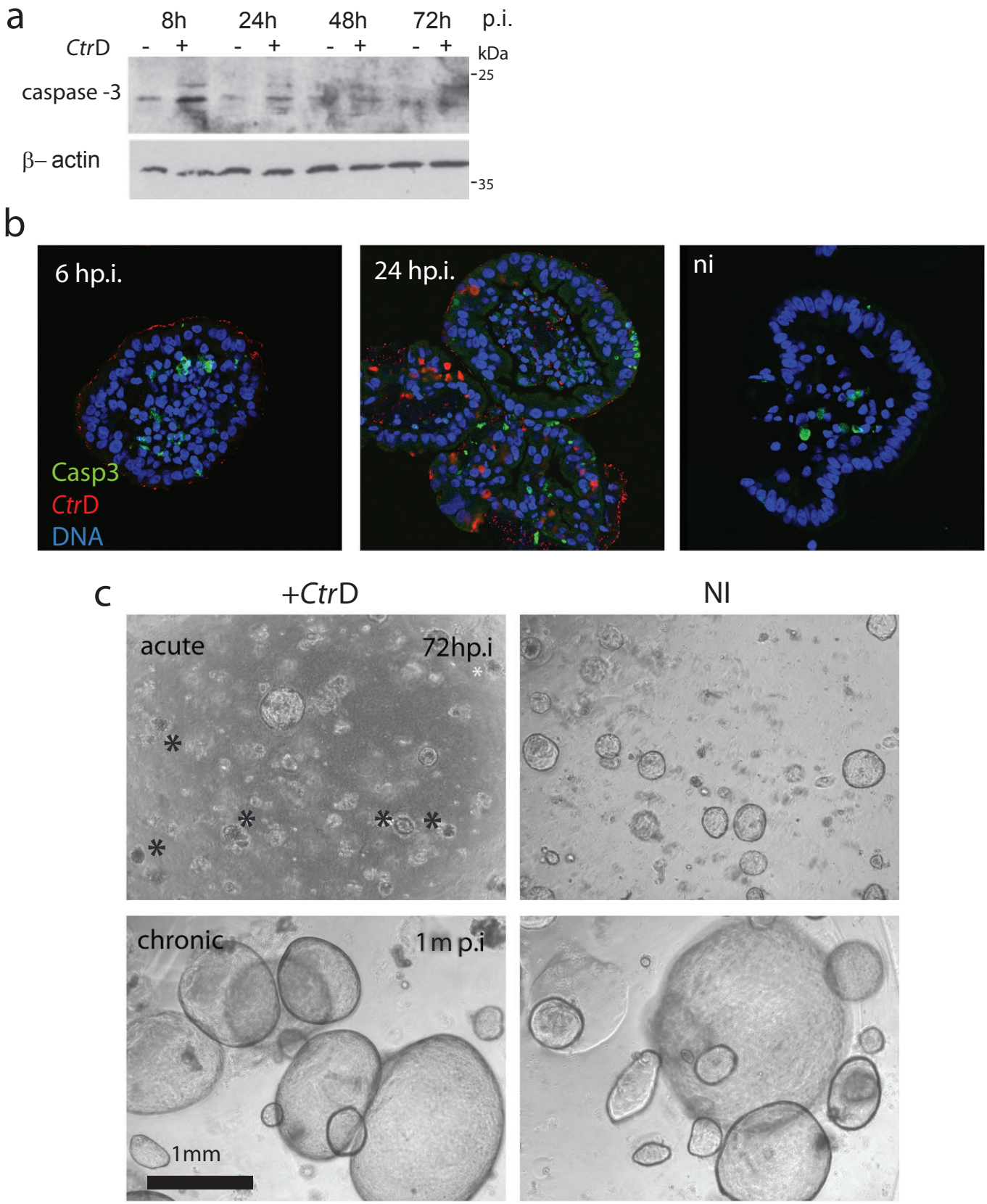

Supplementary Figure 4. Early stress response and apoptosis are compensated during chronic infection a) Western blot for active, cleaved caspase-3 showing a peak in apoptosis in infected organoids at early stages of infection (from 8 -72 h, with decreasing intensity). b) Confocal images of active caspase-3 positive cells at 6 and 24 h p.i. shows an absence of colocalization with inclusion-harboring cells *(Ctr*, red) suggesting a broader stress response and paracrine induction of apoptosis. c) While organoid culture at 72 h p.i. shows clear signs of stress (*) in comparison to control organoids, infected and non–infected cultures at 1 m p.i. have a highly similar phenotype as visible in phase contrast images.

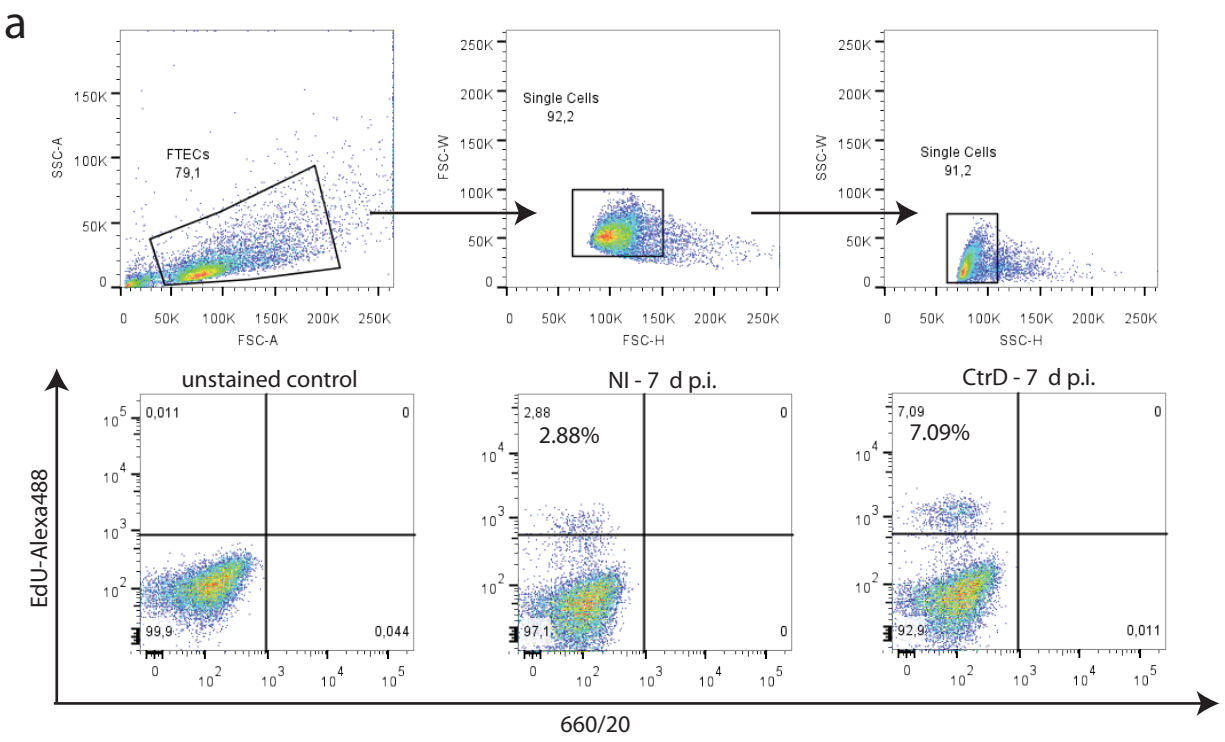

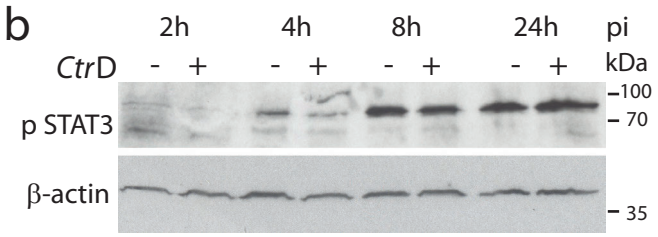

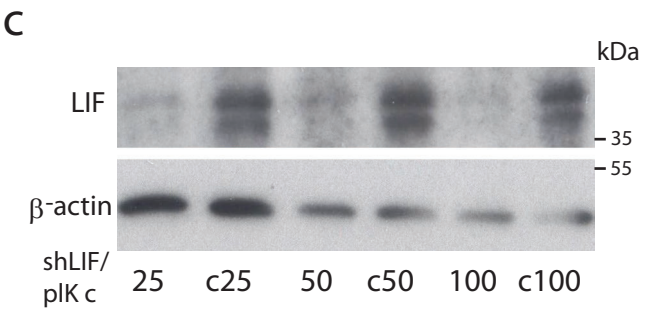

Supplementary Figure 5. LIF signaling is active in organoids independent of presence of *Ctr* a) Gating strategy to count Alexa 488+ (EdU+ proliferative cells) in infected and non-infected organoids over the course of 1 month. b) WB of the time course experiment showing that the pSTAT3 signal transiently disappears after the dissociation of organoids but recovers in both infected and non-infected cultures within a few hours after reseeding c) Depletion of LIF protein by introduction of shLIF is comparable at different virus concentrations, suggesting that a basal level of LIF is required for organoid growth.

a

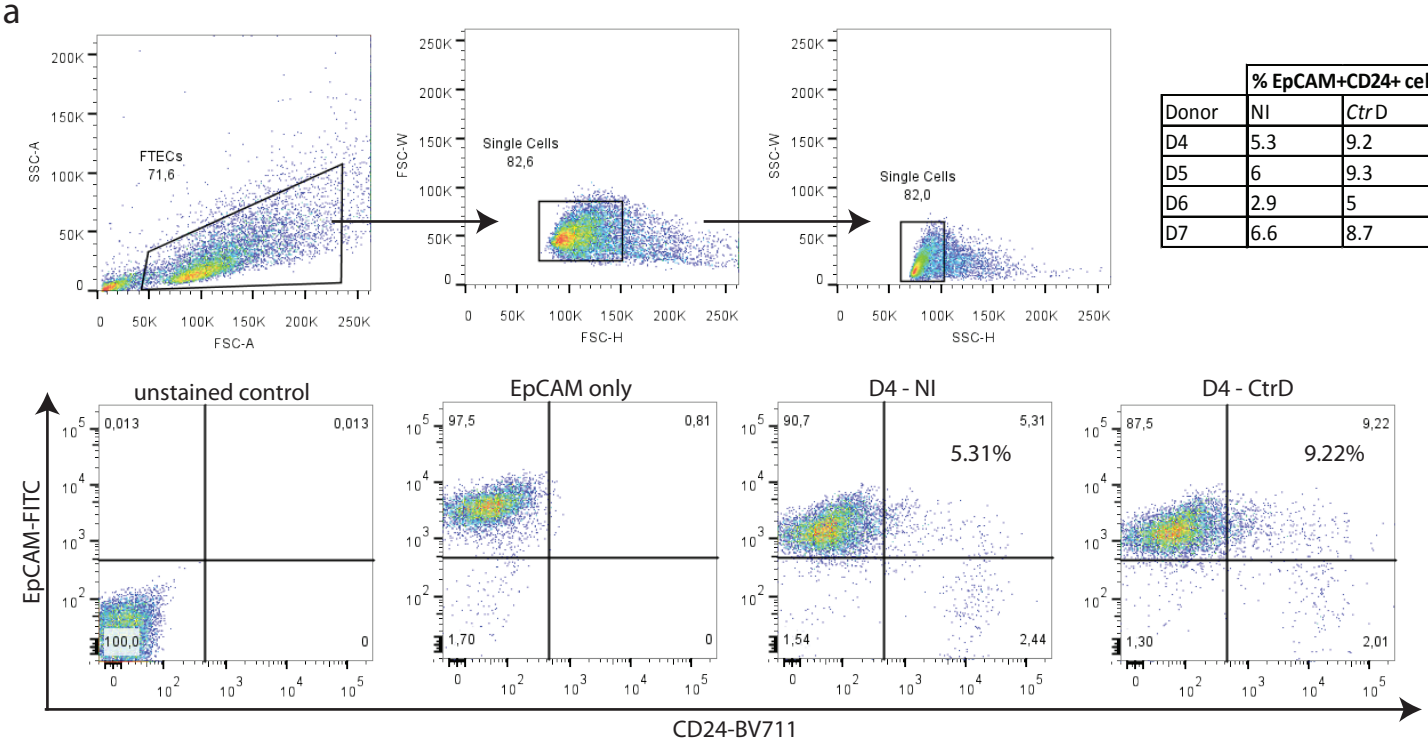

	% EpCAM+CD24+ cells	
Donor	NI	*Ctr*D
D4	5.3	9.2
D5	6	9.3
D6	2.9	5
D7	6.6	8.7

b

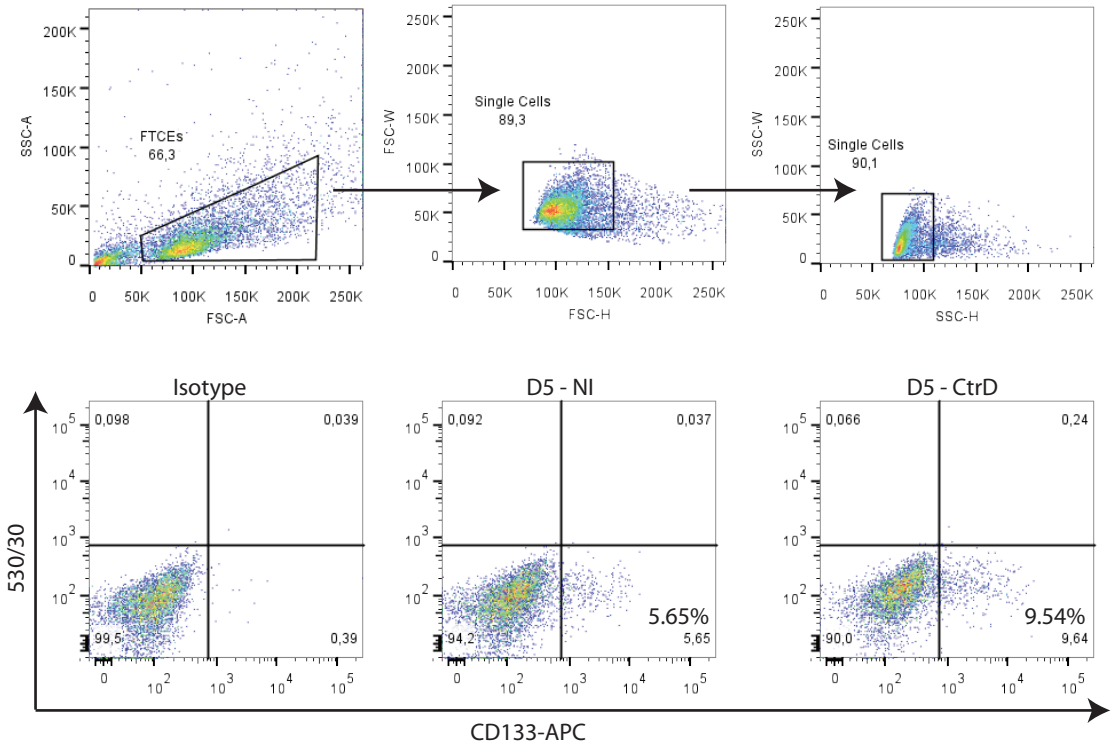

	% CD133+ cells	
Donor	NI	*Ctr*D
D4	1.0	3.7
D5	5.6	9.5
D6	5.0	5.2

Supplementary Figure 6. Chronically infected organoids show an increase in the CD24 and CD133 positive cell populations. a) Chronically infected organoids show an increase in the number of CD24+/EpCam+ cells. Depicted are representative plots from one of four independent FACS sorting experiments. b) Number of CD133+ cells acquired by FACS analysis of non-infected and infected organoid samples for three independent donors. Two out of three cultures infected with *Ctr*D for 2 months demonstrate a clear increase in the size of the CD133+ population.

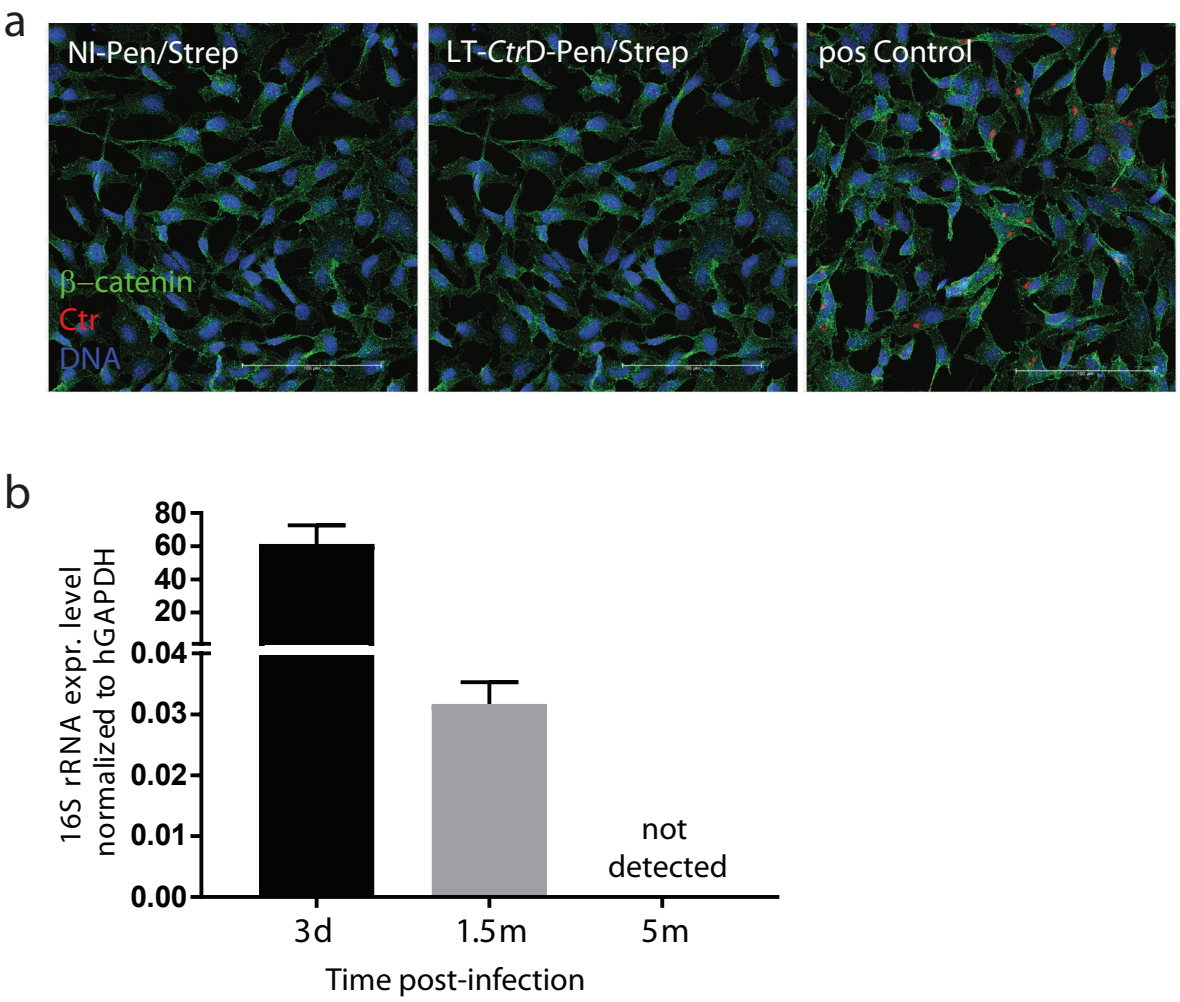

Supplementary Figure 7. Chronically infected organoids show a significantly decreased bacterial load. a) Immunofluorescence labeling of infectivity assay in Hela cells with lysate from long-term infected (LT-*Ctr*D) as well as non-infected (NI) organoids treated for 7 days with Pen/Strep. While the positive control (from 96 hp.i.) contains many inclusions, the absence of inclusions in the NI and P/S –treated chronically infected samples confirms that there were no replicative bacteria left in the culture. b) The relative expression level of bacterial 16S ribosomal RNA was determined by qPCR at different time points of the infected organoid culture and normalized to human GAPDH expression. Data is presented as mean ± sd. At 5 months p.i. the RNA content was below detection level.

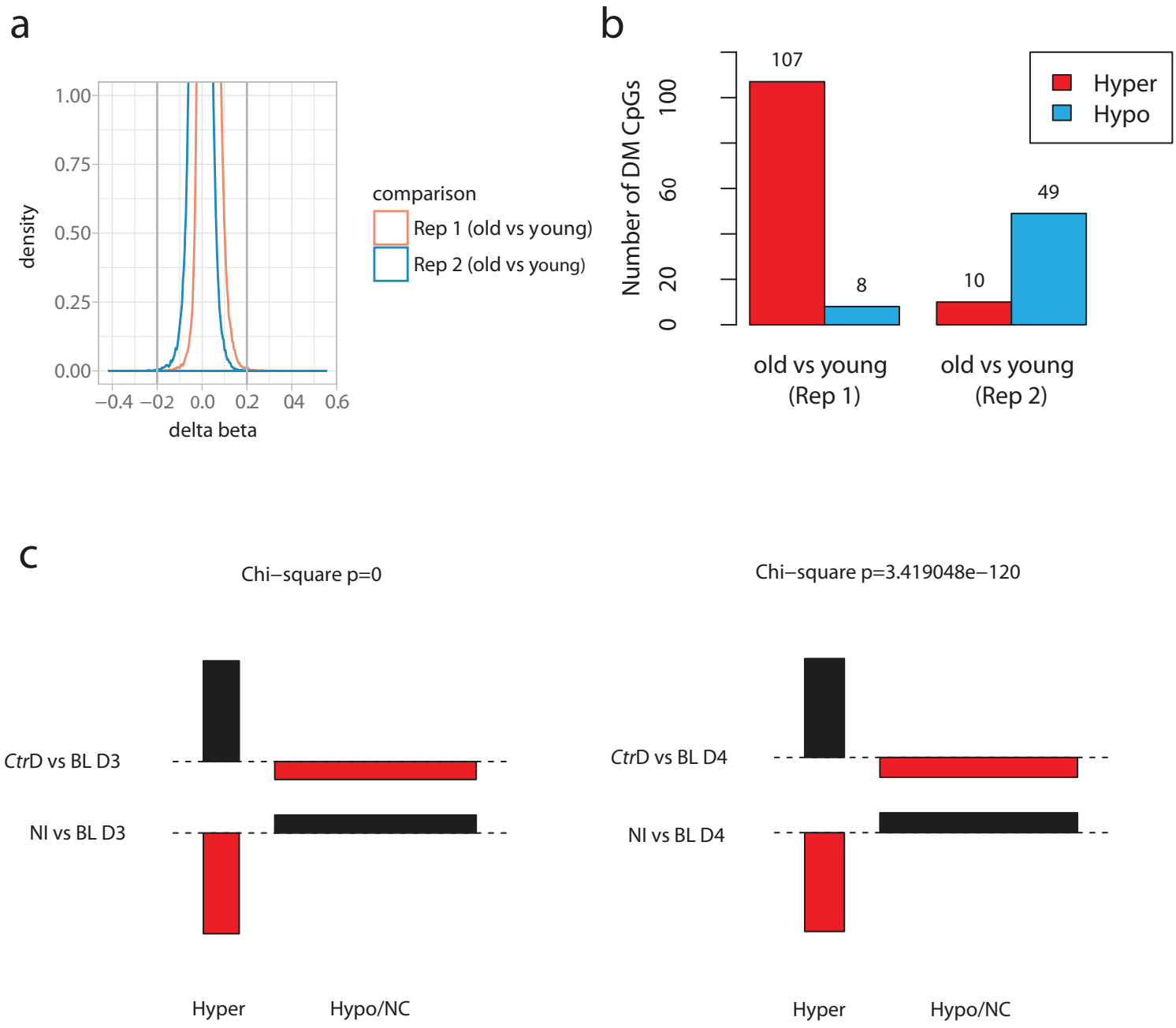

Supplementary Figure 8. Statistical analysis of methylation data in Fig. 4. a) Density plot (zoomed) of the delta beta distribution from two different donors (Rep 1 and Rep 2) comparing two different types of short-term culture. Grey vertical lines indicate the cut off of |delta beta| > 0.2. b) Barplot showing the number of differentially methylated CpGs that pass the threshold determine in a. c) Association plot of the chi-squared test applied to Fig. 4a showing the Pearson residuals ((observed-expected)/sqrt(expected)) in the height of the boxes and the expected values as width.

Fig 1a

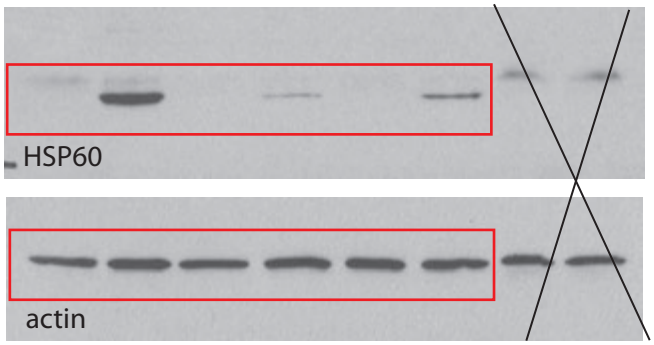

Fig1d

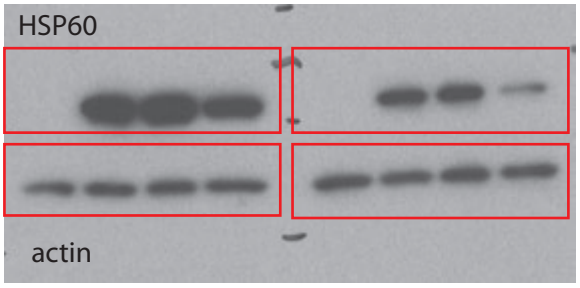

Fig1F

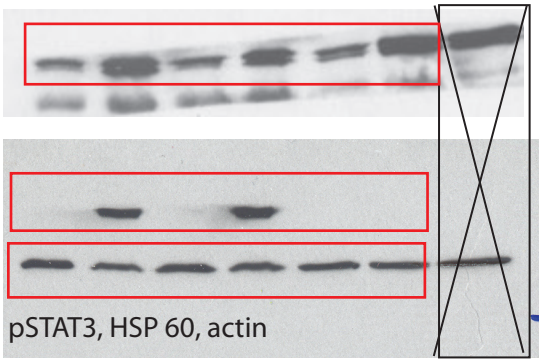

Fig2c

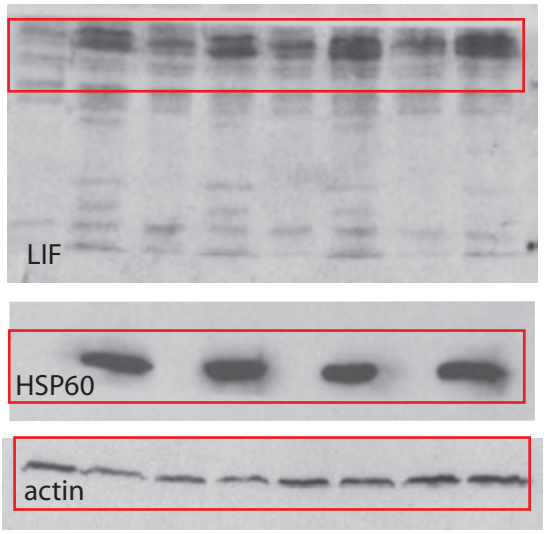

S1a

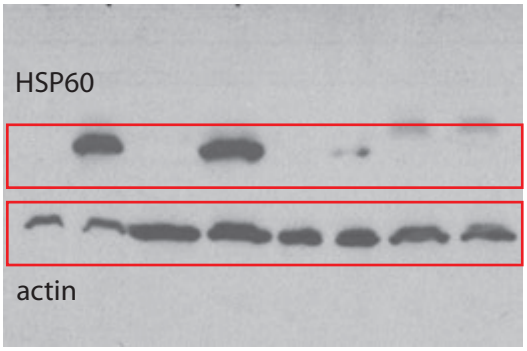

S4a

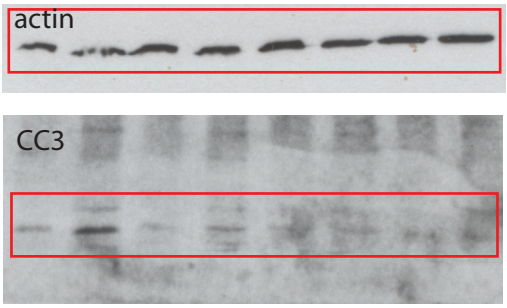

S5b

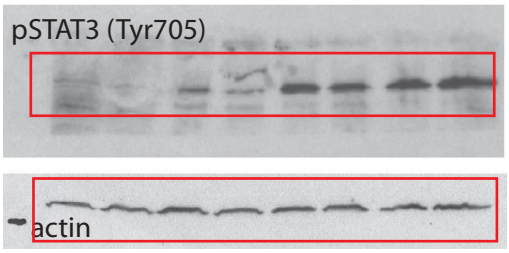

S5c

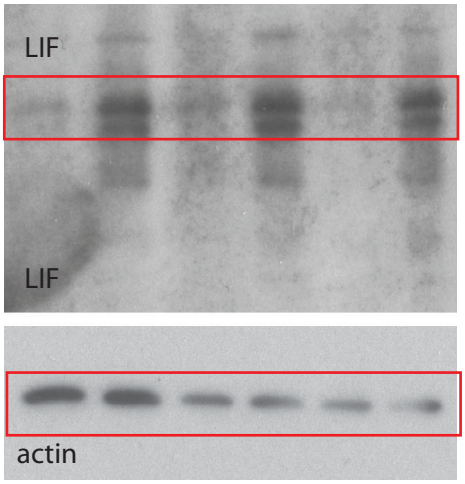

Supplementary Figure 9. Uncropped scans of blots presented in the manuscript. Cropped areas are indicated by red boxes.

Description of Additional Supplementary Files

File Name: Supplementary Data 1
Description: List of 91 genes that were significantly differentially regulated across 3 donors after curing of chronic infection.

File Name: Supplementary Data 2
Description: List of 603 CpGs that were differentially methylated across 3 different donors.

File Name: Supplementary Movie 1
Description: Live cell imaging of infected organoid showing dynamic growth of *Ctr* inclusions within an epithelial monolayer. Notably, inclusions are being expelled into the lumen, after which they burst.

ProbeName	GeneSymbol	SystematicName	GeneDescription	GencodeV25MappingStatus	GeneSymbol_Gencode	Transcript_Type	logFC	AveExpr	t	P.Value	adj.P.Val
A_23_P137484	L1TD1	NM_019079	LINE1 type transposase domain containing 1	unique gene,perfect match	L1TD1	protein_coding	1.753881568	4.124343248	7.400019239	0.00017459	0.393447114
A_33_P3599591	PAPPA	NM_002581	pappalysin 1	unique gene,perfect match	PAPPA	protein_coding	1.271083227	3.662060476	4.234897419	0.004152292	0.545118163
A_23_P156390	JAKMIP2	NM_014790	janus kinase and microtubule interacting protein 2	unique gene,perfect match	JAKMIP2	protein_coding	1.186540771	4.043196361	5.230338832	0.001339183	0.458489575
A_33_P3293049	HLA-DQA1	NM_002122	major histocompatibility complex, class II, DQ alpha 1	multiple matching genes	NA	NA	1.156223529	5.792370469	5.997402711	0.000613299	0.441891598
A_24_P852756	HLA-DQA2	NM_020056	major histocompatibility complex, class II, DQ alpha 2	unique gene,perfect match	HLA-DQA2	protein_coding	1.124361525	4.031626288	3.819857228	0.006948452	0.586899916
A_33_P3264910	NKX6-2	NM_177400	NK6 homeobox 2	unique gene,perfect match	NKX6-2	protein_coding	1.043395999	6.884438838	7.899173349	0.000116827	0.393447114
A_33_P3267375	SGCD	NM_000337	sarcoglycan delta	unique gene,perfect match	SGCD	protein_coding	0.980158017	6.113476052	4.485126568	0.003082541	0.510669229
A_33_P3243787	COL28A1	NM_001037763	collagen type XXVIII alpha 1 chain	unique gene,perfect match	COL28A1	protein_coding,nonsense_mediated_decay	0.977051816	3.789189562	4.160935612	0.004542628	0.557356491
A_24_P66780	FAM83B	NM_001010872	family with sequence similarity 83 member B	unique gene,perfect match	FAM83B	protein_coding	0.934928648	3.534132786	4.507344674	0.003003418	0.504914447
A_33_P3477521	RP11-1094H24	NR_038230	uncharacterized LOC284080	unique gene,perfect match	RP11-1094H24.4	lincRNA	0.934498627	4.226817881	4.111043352	0.004828701	0.558053468
A_23_P434398	TXLNB	NM_153235	taxilin beta	unique gene,perfect match	TXLNB	protein_coding	0.934133992	4.603021936	4.299687255	0.003840611	0.521873006
A_24_P237036	TNFSF14	NM_003807	tumor necrosis factor superfamily member 14	unique gene,perfect match	TNFSF14	protein_coding	0.881413048	6.304432327	3.690238071	0.008204209	0.609975047
A_23_P430948	ATP13A4	NM_032279	ATPase 13A4	unique gene,perfect match	ATP13A4	protein_coding,nonsense_mediated_decay,processed_transcript	0.87513634	3.26287191	3.7588693	0.007511008	0.596362749
A_23_P207507	ABCC3	NM_003786	ATP binding cassette subfamily C member 3	unique gene,perfect match	ABCC3	retained_intron,nonsense_mediated_decay,protein_coding	0.85689849	8.520092001	4.576798768	0.002770231	0.499843512
A_23_P25194	HRK	NM_003806	harakiri, BCL2 interacting protein	unique gene,perfect match	HRK	processed_transcript,protein_coding	0.823776459	8.239627844	4.559184059	0.002827411	0.499843512
A_33_P3353846	TSPO2	NM_001010873	translocator protein 2	unique gene,perfect match	TSPO2	protein_coding	0.821578364	3.88592795	3.609370628	0.009111804	0.61753414
A_32_P163739	KIAA1257	NM_020741	KIAA1257	unique gene,perfect match	KIAA1257	processed_transcript,protein_coding	0.814988361	7.975243672	4.088891377	0.004962024	0.558114085
A_33_P3407350	DBX1	NM_001029865	developing brain homeobox 1	unique gene,perfect match	DBX1	protein_coding	0.814332111	3.020204266	4.119895117	0.004776533	0.558053468
A_23_P429449	NKD1	NM_033119	naked cuticle homolog 1	unique gene,perfect match	NKD1	protein_coding	0.809186039	3.6445425	4.870517109	0.001983477	0.49050823
A_23_P7313	SPP1	NM_001040058	secreted phosphoprotein 1	unique gene,perfect match	SPP1	processed_transcript,protein_coding	0.807854449	7.805702845	10.97125629	1.45632E-05	0.373506829
A_33_P3256844	WDR49	ENST00000453925	WD repeat domain 49 [Source:HGNC Symbol;Acc:26587] [ENST00000453925]	unique gene,perfect match	WDR49	protein_coding	0.795274489	3.503853575	4.171002703	0.004487198	0.557356491
A_24_P691826	WFDC21P	ENST00000587298	Unknown	unique gene,perfect match	WFDC21P	retained_intron,lincRNA	0.79461301	5.161353643	3.804970735	0.007081386	0.59272995
A_33_P3284838	C10orf115	NR_103721	Homo sapiens chromosome 10 open reading frame 115 (C10orf115), long non-coding RNA [NR_103721]	unique gene,perfect match	C10orf67	nonsense_mediated_decay,protein_coding	0.786269496	6.01045418	6.125989976	0.00054182	0.441891598
A_33_P3424187	ARID3C	NM_001017363	AT-rich interaction domain 3C	unique gene,perfect match	ARID3C	protein_coding	0.785358796	3.038758987	3.680482338	0.008308285	0.610977
A_33_P3246418	MDFI	NM_005586	MyoD family inhibitor	unique gene,perfect match	MDFI	protein_coding	0.779447538	11.32789197	4.151794025	0.004593617	0.557356491
A_23_P121545	GPM6A	NM_201591	glycoprotein M6A	unique gene,perfect match	GPM6A	protein_coding	0.775204332	4.522707783	5.347541658	0.00118281	0.450741399
A_23_P89973	BRSK1	NM_032430	BR serine/threonine kinase 1	unique gene,perfect match	BRSK1	protein_coding	0.761469813	3.327966936	3.554917799	0.009784222	0.61753414
A_33_P3367984	ABCA12	NM_173076	ATP binding cassette subfamily A member 12	unique gene,perfect match	ABCA12	protein_coding	0.761124961	7.699783225	7.198330236	0.00020665	0.393447114
A_24_P304071	IFIT2	NM_001547	interferon induced protein with tetratricopeptide repeats 2	unique gene,perfect match	IFIT2	protein_coding	0.748858507	7.513365023	5.383543261	0.001138959	0.450741399
A_33_P3331831	LOC101928841	XM_005275740	PREDICTED: Homo sapiens collagen alpha-1(II) chain-like (LOC101928841), transcript variant X2, mRNA [XM_005275740]	unique gene,perfect match	ADPRHL1	protein_coding	0.744694906	4.186191491	4.656782008	0.002526232	0.499843512
A_33_P3311083	PHLDB3	ENST00000599242	pleckstrin homology-like domain, family B, member 3 [Source:HGNC Symbol;Acc:30499] [ENST00000599242]	unique gene,perfect match	PHLDB3	protein_coding	0.742035237	3.290824608	3.908290415	0.006212933	0.580408865
A_33_P3240492	PHYHIPL	NM_032439	phytanoyl-CoA 2-hydroxylase interacting protein like	unique gene,perfect match	PHYHIPL	protein_coding	0.740920789	5.273177616	3.680247292	0.00831081	0.610977
A_33_P3821778	LINC01021	ENST00000512067	long intergenic non-protein coding RNA 1021 [Source:HGNC Symbol;Acc:48995] [ENST00000512067]	unique gene,perfect match	LINC01021	lincRNA	0.729194584	4.915276792	4.132716643	0.004702065	0.557356491
A_33_P3396336	NA	THC2750096	NA	multiple matching genes	NA	NA	0.726734817	3.368495146	4.037472322	0.005287363	0.567593459
A_33_P3224100	CFAP47	NM_152632	cilia and flagella associated protein 47	unique gene,perfect match	CFAP47	nonsense_mediated_decay,protein_coding	0.710686313	3.953718094	3.616678038	0.009025459	0.61753414
A_24_P278747	CCND2	NM_001759	cyclin D2	unique gene,perfect match	CCND2	protein_coding	0.703533198	8.844986102	5.198406787	0.0013857	0.458489575
A_32_P351037	DNAH7	ENST00000410072	dynein, axonemal, heavy chain 7 [Source:HGNC Symbol;Acc:18661] [ENST00000410072]	unique gene,perfect match	DNAH7	protein_coding	-0.707310739	3.637823717	-5.690997598	0.000830487	0.450741399
A_24_P944588	ZNF682	NM_033196	zinc finger protein 682	unique gene,perfect match	ZNF682	protein_coding,retained_intron	-0.71133891	5.880969109	-8.79884479	5.95655E-05	0.393447114
A_23_P142830	PLA2R1	NM_007366	phospholipase A2 receptor 1	unique gene,perfect match	PLA2R1	protein_coding	-0.716709762	5.703151632	-6.172399675	0.000518363	0.441891598
A_24_P365721	SLC6A14	NM_007231	solute carrier family 6 member 14	unique gene,perfect match	SLC6A14	protein_coding	-0.721303513	8.607540933	-3.995433674	0.005570792	0.574749161
A_33_P3302260	MYRF	NM_013279	myelin regulatory factor	unique gene,perfect match	MYRF	protein_coding	-0.724478124	3.695680134	-3.599560404	0.009229137	0.61753414
A_23_P427747	M1AP	NM_138804	meiosis 1 associated protein	unique gene,perfect match	M1AP	protein_coding,processed_transcript	-0.726389752	5.517241829	-4.059618712	0.005144449	0.559821553
A_33_P3269109	GUCY1A3	ENST00000512983	guanylate cyclase 1, soluble, alpha 3 [Source:HGNC Symbol;Acc:4685] [ENST00000512983]	unique gene,perfect match	GUCY1A3	retained_intron,protein_coding,nonsense_mediated_decay	-0.727053171	6.852225153	-7.779164404	0.000128424	0.393447114
A_33_P3373960	RD3	NM_183059	retinal degeneration 3	unique gene,perfect match	RD3	protein_coding,processed_transcript	-0.731483881	4.527801058	-4.46634498	0.003151227	0.514554721
A_23_P138706	ADRA2A	NM_000681	adrenoceptor alpha 2A	unique gene,perfect match	ADRA2A	protein_coding	-0.744836385	7.422023975	-3.832726755	0.006835727	0.586034051
A_33_P3352467	SSTR2	NM_001050	somatostatin receptor 2	unique gene,perfect match	SSTR2	protein_coding	-0.745081969	4.522744435	-4.651936016	0.002540317	0.499843512
A_24_P250922	PTGS2	NM_000963	prostaglandin-endoperoxide synthase 2	unique gene,perfect match	PTGS2	protein_coding	-0.75300873	8.443208584	-4.37325968	0.003517622	0.517058911
A_23_P343398	CCR7	NM_001838	C-C motif chemokine receptor 7	unique gene,perfect match	CCR7	protein_coding	-0.753868355	5.515071853	-4.215398125	0.004251482	0.545452303
A_33_P3351416	SMOC2	NM_022138	SPARC related modular calcium binding 2	unique gene,perfect match	SMOC2	protein_coding,nonsense_mediated_decay	-0.791384734	4.889535161	-3.693855052	0.008165984	0.609975047
A_33_P3590673	SNHG18	NR_045196	small nucleolar RNA host gene 18	unique gene,perfect match	SNHG18	lincRNA	-0.792501844	7.973770072	-5.90345578	0.000672235	0.441891598
A_33_P3303309	LINC01105	NR_026832	long intergenic non-protein coding RNA 1105	unique gene,perfect match	LINC01105	processed_transcript,TEC	-0.799848495	3.802075148	-3.69412183	0.008163173	0.609975047
A_33_P3265270	SLC17A5	NM_012434	solute carrier family 17 member 5	unique gene,perfect match	SLC17A5	processed_transcript,protein_coding	-0.800602287	5.220891388	-3.558764905	0.009734987	0.61753414
A_33_P3281283	S1PR3	NM_005226	sphingosine-1-phosphate receptor 3	unique gene,perfect match	S1PR3	protein_coding	-0.80432004	6.045187706	-5.199168139	0.00138457	0.458489575
A_23_P93772	HOXA5	NM_019102	homeobox A5	unique gene,perfect match	HOXA5	processed_transcript,protein_coding	-0.816628557	5.194612128	-5.284432887	0.00126431	0.458489575
A_33_P3251856	AE000662.93		NA	unique gene,perfect match	AE000662.93	lincRNA	-0.820156049	5.143499494	-5.649443518	0.000866105	0.450741399
A_33_P3298236	DCHS2	NM_001142552	dachsous cadherin-related 2	unique gene,perfect match	DCHS2	protein_coding	-0.851836821	4.638497083	-7.190953632	0.000207943	0.393447114
A_33_P3314176	FAM46C	NM_017709	family with sequence similarity 46 member C	unique gene,perfect match	FAM46C	protein_coding	-0.875200391	10.47964326	-6.14713477	0.000530988	0.441891598
A_23_P58328	ANXA10	NM_007193	annexin A10	unique gene,perfect match	ANXA10	retained_intron,protein_coding	-0.87998759	7.079277482	-4.154193075	0.004580175	0.557356491
A_23_P13907	IGF1	NM_000618	insulin like growth factor 1	unique gene,perfect match	IGF1	protein_coding,processed_transcript	-0.883631549	7.84664476	-6.005642194	0.000608413	0.441891598
A_33_P3289296	TMEM37	NM_183240	transmembrane protein 37	unique gene,perfect match	TMEM37	protein_coding	-0.903893207	7.205389026	-5.804974478	0.000740941	0.450741399
A_24_P142503	SLC47A1	NM_018242	solute carrier family 47 member 1	unique gene,perfect match	SLC47A1	protein_coding	-0.919916487	6.656634862	-3.926316665	0.006073721	0.580408865
A_23_P69863	PCDHB5	NM_015669	protocadherin beta 5	unique gene,perfect match	PCDHB5	protein_coding	-0.925935057	3.746177752	-3.924682945	0.006086196	0.580408865
A_23_P166269	FAM3B	NM_058186	family with sequence similarity 3 member B	unique gene,perfect match	FAM3B	protein_coding,processed_transcript	-0.92841321	10.11622211	-4.072708617	0.005061978	0.558114085
A_23_P36531	TSPAN8	NM_004616	tetraspanin 8	unique gene,perfect match	TSPAN8	processed_transcript,protein_coding	-0.930478415	8.217990949	-5.04389671	0.001637825	0.462977909
A_33_P3390024	EXOC7	NM_001282314	exocyst complex component 7	unique gene,perfect match	EXOC7	protein_coding	-0.972459911	5.057861639	-4.154294363	0.004579608	0.557356491
A_33_P3298455	LINC01521	NR_120386	long intergenic non-protein coding RNA 1521	unique gene,perfect match	LINC01521	lincRNA	-0.979593468	4.52700215	-3.735972045	0.007734901	0.601296084
A_23_P24948	KCNE3	NM_005472	potassium voltage-gated channel subfamily E regulatory subunit 3	unique gene,perfect match	KCNE3	protein_coding	-1.012948093	10.91636245	-5.249255378	0.001312451	0.458489575
A_24_P366607	SERTM1	NM_203451	serine rich and transmembrane domain containing 1	unique gene,perfect match	SERTM1	protein_coding	-1.026876848	5.223940214	-5.343476574	0.001187879	0.450741399
A_24_P131580	ALPPL2	NM_031313	alkaline phosphatase, placental like 2	unique gene,perfect match	ALPPL2	protein_coding	-1.027397433	15.41707078	-4.903851955	0.001911161	0.49050823
A_32_P158966	KLRF1	NM_016523	killer cell lectin like receptor F1	unique gene,perfect match	KLRF1	processed_transcript,nonsense_mediated_decay,protein_coding	-1.032819136	5.34689851	-4.701425318	0.002400478	0.499843512

A_32_P34826	B3GALT5-AS1	NR_026543	B3GALT5 antisense RNA 1	unique gene,perfect match	B3GALT5-AS1	antisense	-1.077169613	3.853026914	-6.807559673	0.000289635	0.400099328
A_23_P47484	GLYATL2	NM_145016	glycine-N-acyltransferase like 2	multiple matching genes	NA	NA	-1.117658881	5.501195051	-7.338308784	0.00018376	0.393447114
A_23_P134237	RARRES2	NM_002889	retinoic acid receptor responder 2	unique gene,perfect match	RARRES2	protein_coding,retained_intron	-1.122419701	10.74469428	-5.742684139	0.000788456	0.450741399
A_24_P157370	IL17RB	NM_018725	interleukin 17 receptor B	unique gene,perfect match	IL17RB	protein_coding	-1.126354899	4.362118596	-4.746920007	0.002279436	0.499843512
A_33_P3377529	HOXA4	NM_002141	homeobox A4	unique gene,perfect match	HOXA4	protein_coding	-1.137867882	7.218301258	-4.702114053	0.002398594	0.499843512
A_23_P168909	ZFPM2	NM_012082	zinc finger protein, FOG family member 2	unique gene,perfect match	ZFPM2	protein_coding	-1.150681936	5.921644078	-5.757715837	0.000776685	0.450741399
A_23_P152235	IRX3	NM_024336	iroquois homeobox 3	unique gene,perfect match	IRX3	protein_coding	-1.176883106	6.225730397	-3.739519952	0.007699738	0.599929095
A_33_P3392187	CCDC85A	NM_001080433	coiled-coil domain containing 85A	multiple matching genes	NA	NA	-1.185886594	5.257356912	-3.996986698	0.00556003	0.574749161
A_23_P257231	ETNPPL	NM_031279	ethanolamine-phosphate phospho-lyase	unique gene,perfect match	ETNPPL	protein_coding	-1.209968218	6.765305049	-4.310240227	0.003792333	0.521873006
A_23_P163567	SMPD3	NM_018667	sphingomyelin phosphodiesterase 3	unique gene,perfect match	SMPD3	protein_coding	-1.230464633	10.96260124	-4.542487424	0.00288282	0.499843512
A_24_P463891	FUT9	NM_006581	fucosyltransferase 9	unique gene,perfect match	FUT9	protein_coding	-1.269212286	5.320644394	-3.850662026	0.006681953	0.586034051
A_32_P131640	SLITRK4	NM_173078	SLIT and NTRK like family member 4	unique gene,perfect match	SLITRK4	protein_coding	-1.287260568	6.484878198	-10.29857467	2.18892E-05	0.373506829
A_33_P3322519	VWA5B2	NM_138345	von Willebrand factor A domain containing 5B2	unique gene,perfect match	VWA5B2	retained_intron, protein_coding	-1.293599048	6.138965886	-5.034856269	0.00165409	0.462977909
A_23_P55616	SLC14A1	NM_001146037	solute carrier family 14 member 1 (Kidd blood group)	unique gene,perfect match	SLC14A1	protein_coding,nonsense_mediated_decay	-1.322550333	3.912503441	-3.779306256	0.00731714	0.59272995
A_23_P43164	SULF1	NM_015170	sulfatase 1	unique gene,perfect match	SULF1	nonsense_mediated_decay,protein_coding	-1.377724753	5.557053732	-6.032242335	0.000592937	0.441891598
A_23_P365412	MFSD4A	NM_181644	major facilitator superfamily domain containing 4A	unique gene,perfect match	MFSD4A	retained_intron, protein_coding	-1.411887518	5.523129819	-4.138621773	0.004668198	0.557356491
A_33_P3274501	KLRF1	NM_001291823	killer cell lectin like receptor F1	unique gene,perfect match	KLRF1	nonsense_mediated_decay,protein_coding	-1.539959277	3.802656296	-5.097484746	0.001545003	0.458489575
A_23_P417918	PENK	NM_006211	proenkephalin	unique gene,perfect match	PENK	processed_transcript,protein_coding	-1.643848653	10.3637277	-6.202312976	0.00050385	0.441891598
A_23_P427587	FGF19	NM_005117	fibroblast growth factor 19	unique gene,perfect match	FGF19	protein_coding	-1.856610333	4.03063263	-7.700718304	0.00013671	0.393447114
A_23_P349463	CHP2	NM_022097	calcineurin like EF-hand protein 2	unique gene,perfect match	CHP2	protein_coding	-1.913239383	5.014563389	-4.366658823	0.003545339	0.517058911

Row.names	logFC	AveExpr	t	P.Value	adj.P.Val	B	CHR	MAPINFO	Strand	Type	gene	feature	cgi	feat.cgi	UCSC_Islands_Name	SNP_ID	SNP_DISTANCE
cg20086286	0.287787059	0.43577583	27.88802661	3.84E-05	0.76464434	1.739205419	X	1.33E+08	F	II		IGR	shore	IGR-shore	chrX:133305678-133306936		
cg16218764	0.227835725	0.34699127	25.30889324	5.34E-05	0.76464434	1.652898507	15	47043539	F	II		IGR	opensea	IGR-opensea		rs139990316;rs569168230;rs116966886	1;25;48
cg20835412	-0.23904266	0.35601593	-25.0602735	5.52E-05	0.76464434	1.643362205	19	12460129	R	II		IGR	opensea	IGR-opensea		rs111255449;rs549733238;rs567251325;rs192090355	48;34;26;2
cg20094831	-0.2431605	0.41832476	-23.2902257	7.08E-05	0.76464434	1.567947517	10	44699412	R	II		IGR	shelf	IGR-shelf	chr10:44701884-44702149	rs189051758;rs530108998	15;13
cg15773251	0.211729749	0.28337085	22.62581812	7.81E-05	0.76464434	1.53580219	6	32078602	R	II	TNXB	TSS1500	opensea	TSS1500-opensea		rs190189438	29
cg14804729	0.201394846	0.49732904	21.16063023	9.79E-05	0.76464434	1.456071834	8	22786329	R	II	PEBP4	TSS1500	opensea	TSS1500-opensea		rs74449481;rs538045356	2;1
cg03151893	-0.22737708	0.41817364	-20.7589499	0.00010449	0.76464434	1.431821349	1	33513729	R	II		IGR	shelf	IGR-shelf	chr1:33516594-33516933	rs567271777;rs538106708;rs189518587	29;2;1
cg17110700	-0.21784673	0.38949792	-20.6235579	0.00010683	0.76464434	1.423392449	1	1.15E+08	R	II		IGR	opensea	IGR-opensea		rs374734664;rs539506012	27;26
cg21051963	-0.20587444	0.58379193	-19.7515532	0.00012364	0.76464434	1.365805038	15	36763406	F	II		IGR	opensea	IGR-opensea		rs189708343;rs182017911;rs187217980;rs149608124	1;18;20;21
cg13614083	0.23475937	0.65415033	19.73436609	0.000124	0.76464434	1.364609613	1	6085872	F	II	KCNAB2	TSS1500	shore	TSS1500-shore	chr1:6086244-6086494	rs532313666;rs76852674	17;28
cg15625392	-0.27420646	0.42849469	-19.1046625	0.00013838	0.76464434	1.319075871	5	28624261	R	II		IGR	opensea	IGR-opensea		rs190440057	2
cg21647086	-0.2488086	0.46909532	-19.0085324	0.00014076	0.76464434	1.311816079	7	34224120	R	II		IGR	opensea	IGR-opensea		rs142545188;rs77951931	2;1
cg21218195	0.216023022	0.26453503	18.56238559	0.00015252	0.76464434	1.276987169	7	98189557	R	II		IGR	opensea	IGR-opensea		rs568594771	28
cg03163469	-0.25261524	0.43633504	-18.2860826	0.00016045	0.76464434	1.254439983	1	34150850	F	II	CSMD2	Body	opensea	Body-opensea		rs537528993	0
cg20235803	0.208878575	0.66318007	18.10857948	0.00016583	0.76464434	1.239542093	2	2.02E+08	F	II	BZW1	TSS1500	shore	TSS1500-shore	chr2:201675989-201677306	rs138257745	24
cg02329994	0.255511798	0.58903159	17.63824033	0.00018124	0.76464434	1.19842645	7	1.4E+08	F	II	TBXAS1	Body	opensea	Body-opensea		rs150569322;rs73158676	7;37
cg27177112	0.356345281	0.47785804	17.13869458	0.0001997	0.76464434	1.151986866	18	58221283	F	II		IGR	opensea	IGR-opensea		rs186062109	0
cg07669309	-0.30673398	0.30369005	-16.8107158	0.00021315	0.76464434	1.119833823	16	54691248	F	II		IGR	opensea	IGR-opensea		rs569772758;rs185536251;rs4784409	9;17;25
cg17874353	-0.26545235	0.48654597	-16.4959627	0.00022718	0.76464434	1.087659423	2	1.84E+08	F	II		IGR	opensea	IGR-opensea		rs139871203;rs536949912	1;35
cg26358634	-0.31582256	0.64218455	-16.3140598	0.00023584	0.76464434	1.068449651	5	62365115	F	II		IGR	opensea	IGR-opensea		rs543041198;rs544853090;rs558761784	1;4;50
cg19972193	0.236991533	0.3830016	16.27970859	0.00023752	0.76464434	1.064769913	5	1.8E+08	R	II	FLT4	Body	shelf	Body-shelf	chr5:180075688-180076906	rs533092799;rs73812644;rs563676566	37;6;2
cg08752826	0.201198791	0.6312934	16.13790392	0.00024463	0.76464434	1.049401011	3	27956103	F	II		IGR	opensea	IGR-opensea		rs199499174	50
cg18730034	-0.24303857	0.40321892	-15.9599516	0.00025395	0.76464434	1.029699429	15	26866630	R	I	GABRB3	Body	opensea	Body-opensea			
cg16612867	-0.21116395	0.39315909	-15.8787423	0.00025835	0.76464434	1.020551597	6	37210815	F	II	TMEM217	Body	opensea	Body-opensea		rs138787824	1
cg23948537	-0.20477238	0.32020925	-15.6600931	0.0002707	0.76464434	0.995419837	15	40606171	R	II		IGR	opensea	IGR-opensea		rs147589436	30
cg01139665	-0.20399449	0.42095068	-15.3279358	0.00029097	0.76464434	0.955789977	19	4841356	F	II	PLIN3	Body	opensea	Body-opensea		rs141379398;rs146269442;rs146941045;rs533892814	1;11;29;35
cg04302628	0.264124088	0.46259507	15.0385101	0.00031025	0.76464434	0.91976217	2	2.41E+08	F	II		IGR	shelf	IGR-shelf	chr2:241097404-241097934		
cg16531665	-0.20798823	0.46969371	-14.9313976	0.00031781	0.76464434	0.906060675	13	1.12E+08	F	II		IGR	opensea	IGR-opensea		rs74128424;rs531080750;rs9555829	0;11;41
cg12480903	0.22211879	0.30009418	14.53888334	0.0003476	0.76464434	0.854073537	1	1.67E+08	F	II	CD247	Body	shore	Body-shore	chr1:167424088-167425216	rs531506334;rs549823731	2;46
cg14334652	-0.28403809	0.45633853	-14.5044326	0.00035038	0.76464434	0.849373154	3	1.65E+08	R	II		IGR	opensea	IGR-opensea		rs144248509	17
cg20251528	-0.20422324	0.22922587	-14.416944	0.00035758	0.76464434	0.837333677	6	89674094	R	II	RNGTT	TSS1500	shore	TSS1500-shore	chr6:89672884-89673579	rs142575461;rs146899019	30;12
cg10889085	0.248122181	0.49757461	14.359239	0.00036244	0.76464434	0.829311276	21	39715656	F	II	LINC01423	Body	opensea	Body-opensea		rs185488926	0
cg21581168	-0.30433095	0.33955664	-13.9011375	0.00040415	0.76464434	0.763242476	3	1.8E+08	R	II		IGR	opensea	IGR-opensea		rs549305610;rs565918019	18;12
cg05612984	0.211369508	0.51236992	13.73417825	0.00042089	0.76464434	0.73806838	4	1.73E+08	R	II	GALNTL6	Body	opensea	Body-opensea		rs112531751;rs181185765;rs539872067	29;22;1
cg06496489	-0.20031873	0.59673929	-13.7048751	0.00042392	0.76464434	0.733587366	15	39110621	R	II		IGR	opensea	IGR-opensea		rs141236750;rs550634759	13;5
cg25830548	-0.27099993	0.50344283	-13.66431	0.00042816	0.76464434	0.727352878	6	87041914	F	II		IGR	opensea	IGR-opensea		rs568817205;rs532960952;rs551205305	0;18;40
cg20618433	0.256722524	0.59366933	13.26137358	0.00047339	0.76464434	0.663393435	19	11266919	F	II	SPC24	TSS1500	shore	TSS1500-shore	chr19:11266230-11266726		
cg21765032	-0.21050699	0.67158371	-13.0704632	0.00049698	0.76464434	0.631750812	19	3293547	F	II	BRUNOL5	3'UTR	island	3'UTR-island	chr19:3293267-3293548	rs572053822;rs313784	11;46
cg19505184	-0.20397429	0.69368466	-12.7051118	0.0005465	0.76464434	0.568652931	18	66779097	F	II		IGR	opensea	IGR-opensea		rs549275073	0
cg04885756	-0.20736894	0.60882402	-12.697741	0.00054757	0.76464434	0.567344391	13	51909581	R	II		IGR	opensea	IGR-opensea		rs555648165	2
cg11507780	-0.24157377	0.48131268	-12.5241815	0.00057339	0.76464434	0.536112413	6	1.39E+08	R	II		IGR	opensea	IGR-opensea		rs149004693;rs527996503;rs187261719	46;12;1
cg01996818	-0.21825356	0.40334289	-12.4608934	0.0005832	0.76464434	0.524520148	X	1.31E+08	R	I	MST4	5'UTR	island	5'UTR-island	chrX:131156818-131157775		
cg08922347	-0.20902576	0.30806885	-12.4602026	0.0005833	0.76464434	0.524393006	11	5409945	F	II	OR51M1	TSS1500	opensea	TSS1500-opensea		rs200737360;rs574232473;rs536443958;rs150564490	1;17;26;36
cg03985452	-0.23010886	0.34453453	-12.263218	0.00061525	0.76464434	0.487593039	2	3836042	F	II		IGR	shore	IGR-shore	chr2:3833815-3834318	rs144616855;rs550729965;rs74948631;rs113593166;rs9973392;rs566676513;rs534027419;rs555	0;2;11;12;16;35;46;47
cg25711246	-0.20511314	0.62436892	-12.2615925	0.00061552	0.76464434	0.487284782	12	4917426	R	II	KCNA6	TSS1500	shore	TSS1500-shore	chr12:4918273-4919657	rs182554390;rs141063215	49;1
cg27201534	0.266040659	0.6097153	12.13322766	0.00063757	0.76464434	0.462701284	20	42379020	R	II		IGR	opensea	IGR-opensea			
cg11002686	0.244670322	0.52865276	12.06897735	0.00064899	0.76464434	0.450215325	7	55412682	F	II		IGR	island	IGR-island	chr7:55411965-55412772	rs530265982	31
cg01591405	0.208256549	0.57535516	12.04413125	0.00065348	0.76464434	0.445354053	17	18024867	F	II	MYO15A	Body	island	Body-island	chr17:18022195-18024868	rs185688918;rs201529563	37;38
cg07665542	-0.20308227	0.67602707	-11.9296915	0.00067467	0.76464434	0.42272372	16	86215740	F	II		IGR	opensea	IGR-opensea		rs78645930;rs534619492;rs554883626;rs534016771;rs537098664	5;7;12;36;49
cg06161398	0.22050275	0.70664141	11.92500262	0.00067555	0.76464434	0.421788033	9	1.17E+08	R	II		IGR	opensea	IGR-opensea		rs114999856;rs146151304	9;2
cg19866637	-0.20839868	0.417551	-11.7391339	0.00071195	0.76464434	0.384149366	1	3057893	F	II	PRDM16	Body	shore	Body-shore	chr1:3059050-3059268	rs532305565;rs551338423;rs77192050	2;14;16
cg22424764	0.2170484	0.5819861	11.71604632	0.00071665	0.76464434	0.379398522	10	16830860	R	II	RSU1	5'UTR	opensea	5'UTR-opensea		rs12358568	2
cg23161350	0.229990412	0.40789434	11.66971014	0.00072619	0.76464434	0.369812478	4	66655798	R	II		IGR	opensea	IGR-opensea		rs17086372;rs575981474;rs191031527	10;8;2
cg09811645	-0.20470855	0.2630794	-11.6488716	0.00073054	0.76464434	0.365478971	19	8840675	R	II	OR2Z1	TSS1500	opensea	TSS1500-opensea			
cg12349181	0.215133294	0.41762396	11.60056376	0.00074075	0.76464434	0.35537921	17	79057046	R	II	BAIAP2	Body	opensea	Body-opensea		rs540832891;rs559235045;rs117038010;rs147255923	31;10;9;2
cg10155058	0.20650888	0.77080825	11.36191333	0.00079394	0.76464434	0.304358036	17	37018229	R	II		IGR	opensea	IGR-opensea		rs576131835	39
cg19996406	0.20671011	0.6328471	10.98498528	0.00088843	0.76464434	0.219792934	8	8318774	F	II		IGR	opensea	IGR-opensea		rs570016507;rs535611968;rs193069989;rs572179613	0;1;5;14
cg06070970	0.244599691	0.33938428	10.95931117	0.00089538	0.76464434	0.213848087	8	1.44E+08	F	II	GLI4	3'UTR	island	3'UTR-island	chr8:144357997-144359075		
cg23328404	0.267583896	0.52447937	10.75266669	0.00095394	0.76464434	0.165107067	8	19539991	F	II	CSGALNACT1	Body	opensea	Body-opensea		rs192140590;rs544507875;rs564134731;rs533101152;rs184539647	0;3;38;43;49
cg26843612	-0.24611889	0.28993818	-10.7498974	0.00095476	0.76464434	0.164442939	6	16636157	F	II	ATXN1	5'UTR	opensea	5'UTR-opensea		rs563896454	31
cg03224627	-0.24099212	0.47388913	-10.6705906	0.00097857	0.76464434	0.145298275	1	1.78E+08	R	II		IGR	opensea	IGR-opensea		rs578065916	46
cg07078225	0.200458312	0.41978309	10.59628119	0.00100158	0.76464434	0.127138193	12	52652377	R	I		IGR	island	IGR-island	chr12:52652018-52652743	rs547361066	8
cg18994840	-0.20837899	0.47621409	-10.5940118	0.00100229	0.76464434	0.126580172	10	1.25E+08	R	II		IGR	opensea	IGR-opensea		rs192006434;rs557150580;rs147851676	38;33;2
cg01307684	-0.23100262	0.50866391	-10.5035251	0.00103128	0.76464434	0.104164083	4	80886143	F	II	ANTXR2	Body	island	Body-island	chr4:80885844-80886148		
cg07171710	0.217864032	0.39924451	10.45401067	0.0010476	0.76464434	0.091759116	3	237960	F	II	CHL1	TSS1500	shore	TSS1500-shore	chr3:238391-240140	rs185893895;rs190812100	21;49
cg08474334	0.209400561	0.46909025	10.43684178	0.00105334	0.76464434	0.087434589	1	1.57E+08	F	II	NTRK1	Body	shore	Body-shore	chr1:156814881-156815792	rs548457882	22
cg15358931	-0.23595451	0.30606437	-10.386213	0.00107049	0.76464434	0.074612126	X	1.15E+08	R	I		IGR	island	IGR-island	chrX:114546353-114546645		
cg07100798	0.214064723	0.80443098	10.38010364	0.00107259	0.76464434	0.073057747	14	20851317	F	II	TEP1	Body	opensea	Body-opensea		rs201216641;rs142149161	0;44
cg05885623	0.219915128	0.45108137	10.29625021	0.00110187	0.76464434	0.051567155	17	77247789	F	II	RBFOX3	5'UTR	opensea	5'UTR-opensea		rs143749781;rs116605820;rs117688178;rs538265573	5;6;24;28
cg09312328	0.24111878	0.50275332	10.23904988	0.00112244	0.76464434	0.036738912	6	33038766	F	II	HLA-DPA1	Body	opensea	Body-opensea		rs2301220;rs138375834;rs148836028;rs192235493;rs575057707;rs67542233;rs143577295	0;1;9;15;20;36;46
cg11176545	0.201322411	0.70888791	10.189566	0.00114063	0.76464434	0.023799381	18	42792594	R	II	SLC14A2	TSS1500	opensea	TSS1500-opensea		rs538757000	2
cg08642292	-0.24842868	0.31911092	-10.0044427	0.00121214	0.76464434	-0.02554506	15	33873247	R	II	RYR3	Body	opensea	Body-opensea		rs147192813;rs553683138	35;2
cg14153919	0.203040299	0.61673685	9.984030554	0.00122038	0.76464434	-0.03107791	15	78631963	F	II	CRABP1	TSS1500	shore	TSS1500-shore	chr15:78632669-78633108		
cg04989524	0.205222735	0.34414517	9.977569977	0.001223	0.76464434	-0.03283296	X	1.23E+08	R	II	LOC101928402	Body	island	Body-island	chrX:123093923-123094582		
cg10803922	0.228588386	0.66574997	9.853289904	0.00127486	0.76464434	-0.06695937	11	44719192	F	II		IGR	opensea	IGR-opensea		rs563119470	0
cg08876508	-0.21048968	0.53663421	-9.80770396	0.00129459	0.76464434	-0.07965302	17	34068044	R	II	RASL10B	Body	island	Body-island	chr17:34068043-34068668	rs200365146;rs199649896;rs587644033	37;30;2
cg02885259	-0.22261988	0.41248609	-9.78709217	0.00130364	0.76464434	-0.0854239	3	1.6E+08	R	II	ARL14	1stExon	opensea	1stExon-opensea			
cg08985499	0.221352549	0.39636328	9.476640609	0.00145034	0.76464434	-0.17477245	10	1.2E+08	F	II		IGR	opensea	IGR-opensea		rs10886150;rs182051485;rs567199464	7;21;29
cg22270262	-0.20729674	0.72490377	-9.29568858	0.0015457	0.76464434	-0.22902618	14	98153031	R	II	LOC100129345	TSS200	opensea	TSS200-opensea		rs148394160;rs541632711;rs561438649;rs186729962	50;11;2;1
cg05216340	-0.22743062	0.32619542	-9.2269213	0.00158405	0.76464434	-0.25008066	4	44427777	F	II	KCTD8	Body	opensea	Body-opensea		rs140027518;rs16856912;rs7691376;rs546871985	1;9;31;41
cg08603868	0.259418674	0.29387226	9.179787148	0.00161104	0.76464434	-0.26465342	11	1.08E+08	R	II		IGR	opensea	IGR-opensea		rs548781828;rs567881488	12;2
cg24392939	-0.27452332	0.54062269	-9.101141	0.0016574	0.76464434	-0.28922895	3	97591258	F	II		IGR	opensea	IGR-opensea		rs142470903	0
cg03899098	-0.20408131	0.40721041	-8.87130373	0.0018031	0.76464434	-0.36295931	15	98193650	F	II		IGR	shelf	IGR-shelf	chr15:98196021-98196391	rs184835054;rs566651132	0;22
cg23692540	-0.21755812	0.55422379	-8.78388616	0.00186281	0.76464434	-0.39177039	9	33637473	F	II		IGR	opensea	IGR-opensea		rs191007824;rs555723277	1;44
cg26211349	0.213740285	0.3707436	8.69850887	0.00192361	0.76464434	-0.42032923	17	77404555	F	II	HRNBP3	5'UTR	opensea	5'UTR-opensea		rs558652646;rs9907346;rs537992591	0;6;49
cg12710648	-0.28553067	0.34987166	-8.68327347	0.00193472	0.76464434	-0.42546973	1	7308091	R	II	CAMTA1	Body	opensea	Body-opensea		rs140576925;rs144392678	26;2
cg15474337	-0.21043728	0.46713277	-8.67851238	0.00193821	0.76464434	-0.42707892	19	50848247	R	II	NAPSB	TSS1500	opensea	TSS1500-opensea		rs73932461;rs533188427;rs545359210;rs73932462	44;39;2;1
cg01116873	0.203519983	0.75604646	8.648134539	0.00196067	0.76464434	-0.43737737	7	1.21E+08	R	II		IGR	opensea	IGR-opensea		rs566634677;rs538798698;rs559007500	40;24;1
cg04604383	-0.33312388	0.32438749	-8.61225431	0.00198763	0.76464434	-0.44961091	11	55577412	R	II		IGR	opensea	IGR-opensea		rs80137132	38
cg00774578	-0.21232698	0.63147816	-8.54805366	0.00203707	0.76464434	-0.4716906	19	54580929	F	II	TARM1	Body	opensea	Body-opensea		rs587764948;rs587644362;rs587701333	1;9;35
cg20367065	0.207686174	0.52325601	8.486937916	0.00208561	0.76464434	-0.4929386	3	97983253	R	II	OR5H6	1stExon	opensea	1stExon-opensea		rs137937308;rs577340762;rs201340537;rs113835025;rs563136835;rs201236351;rs36040433;rs1	48;46;26;24;17;6;2;1
cg20657826	0.218291264	0.50024207	8.464778464	0.00210358	0.76464434	-0.50069856	X	15928372	R	II		IGR	opensea	IGR-opensea			
cg15977716	0.206557165	0.58093884	8.430612097	0.00213167	0.76464434	-0.51272188	12	1.33E+08	F	II		IGR	shelf	IGR-shelf	chr12:132922117-132922443	rs148867669	1
cg23569180	0.204907553	0.73775517	8.322153872	0.00222408	0.76464434	-0.5513663	7	37955508	F	II	SFRP4	Body	shore	Body-shore	chr7:37955622-37956555	rs532952386;rs183186446;rs569781586	4;25;32
cg15645815	-0.20080452	0.64184529	-8.27498892	0.00226587	0.76464434	-0.56840112	21	37961337	F	II		IGR	opensea	IGR-opensea		rs536156736;rs556111623	0;1
cg18340923	0.202613251	0.33504027	8.255171495	0.00228373	0.76464434	-0.57560073	14	93896401	R	II	UNC79	5'UTR	shore	5'UTR-shore	chr14:93896736-93897466		
cg02864688	0.216879214	0.34639263	8.230279256	0.00230642	0.76464434	-0.5846795	1	11752342	R	II	MAD2L2	TSS1500	island	TSS1500-island	chr1:11750701-11752651	rs146842606	1
cg20569128	0.238688782	0.27586777	8.213781203	0.00232162	0.76464434	-0.59071858	X	1.37E+08	R	II		IGR	island	IGR-island	chrX:136655909-136657085		
cg12016495	-0.23236754	0.53055808	-8.20873846	0.00232629	0.76464434	-0.59256796	16	17162569	F	II		IGR	opensea	IGR-opensea		rs562780546;rs74012921	0;35
cg14531496	-0.21380297	0.44517716	-8.20076929	0.0023337	0.76464434	-0.59549391	5	1.48E+08	F	II		IGR	opensea	IGR-opensea		rs77208124	16
cg05549773	0.206720341	0.49684065	8.189478996	0.00234424	0.76464434	-0.59964627	5	1183037	F	II		IGR	opensea	IGR-opensea			
cg23749034	0.256049084	0.51216527	8.187744947	0.00234587	0.76464434	-0.60028474	6	35165242	R	II		IGR	opensea	IGR-opensea		rs551072334;rs569319451;rs533356658	41;38;27
cg14904299	-0.28558243	0.48955984	-8.16570677	0.00236665	0.76464434	-0.6084162	12	5330804	R	II		IGR	opensea	IGR-opensea		rs564537320;rs533472597;rs7296125	22;14;2
cg24704912	0.224581999	0.43038214	8.136660217	0.00239439	0.76464434	-0.61918179	8	1.42E+08	R	I		IGR	shore	IGR-shore	chr8:142427854-142428351	rs188620952;rs55910461	40;32
cg25274008	0.219683575	0.66450273	8.125735458	0.00240494	0.76464434	-0.62324511	1	33648648	R	II	TRIM62	TSS1500	shore	TSS1500-shore	chr1:33646613-33647878	rs547727252;rs182869484	10;2
cg24916850	-0.22515622	0.63477948	-8.05699081	0.00247267	0.76464434	-0.64899409	2	2.17E+08	R	II	MREG	TSS1500	shore	TSS1500-shore	chr2:216877899-216878352		
cg16867568	0.270309097	0.44085434	7.967188485	0.00256487	0.76464434	-0.68310481	19	42471655	R	II	ATP1A3	Body	opensea	Body-opensea		rs371698093;rs577933395	12;11
cg07122460	-0.22941931	0.48061348	-7.90715781	0.00262897	0.76464434	-0.70621147	12	4287879	F	II		IGR	opensea	IGR-opensea		rs147659431;rs183753536	1;48
cg14196261	0.20410779	0.41651991	7.898811685	0.00263805	0.76464434	-0.70944355	X	23761469	F	II	ACOT9	TSS200	island	TSS200-island	chrX:23761070-23761610		
cg24176731	0.215818964	0.55304063	7.858783798	0.00268213	0.76464434	-0.72501139	11	73357164	R	II	PLEKHB1	TSS200	opensea	TSS200-opensea		rs542511379;rs189338957	34;2
cg12615982	0.226327192	0.26275651	7.849044828	0.00269299	0.76464434	-0.72881592	3	1.69E+08	R	II	TERC	TSS1500	shore	TSS1500-shore	chr3:169482338-169483052	rs546654815	12
cg09608709	-0.21889224	0.50737737	-7.84052824	0.00270254	0.76464434	-0.73214834	20	34949883	R	II	DLGAP4	5'UTR	opensea	5'UTR-opensea		rs559400036;rs529627903;rs144487595	33;2;1
cg26345912	-0.22491782	0.4483791	-7.8036842	0.00274436	0.76464434	-0.74662327	5	1.65E+08	R	II		IGR	opensea	IGR-opensea		rs10064661;rs561269436;rs531718922;rs549876827;rs571321298;rs532625274	34;30;21;20;19;10
cg23594656	-0.22703987	0.53166829	-7.78242197	0.00276887	0.76464434	-0.75501995	7	65796392	R	II	TPST1	Body	opensea	Body-opensea			
cg02651643	-0.28527059	0.40179846	-7.78036045	0.00277126	0.76464434	-0.75583577	10	26461882	F	II	MYO3A	Body	opensea	Body-opensea			
cg01225622	-0.2060614	0.4184802	-7.76176849	0.00279294	0.76464434	-0.76320681	14	75555285	R	II	NEK9	Body	opensea	Body-opensea		rs555962390	45
cg02834433	-0.24173168	0.63359261	-7.72400071	0.00283767	0.76464434	-0.77825601	15	28017186	R	II	OCA2	Body	shore	Body-shore	chr15:28015346-28015795	rs148482689;rs370650196	40;18
cg05725721	-0.22038728	0.45580846	-7.69765145	0.00286942	0.76464434	-0.78881571	3	1.61E+08	F	II	B3GALNT1	TSS1500	shore	TSS1500-shore	chr3:160822494-160823260		
cg26189637	-0.25296213	0.58266366	-7.69324442	0.00287477	0.76464434	-0.79058673	19	20214032	F	II	ZNF90	Body	opensea	Body-opensea		rs554879541;rs567947553;rs537016945;rs1725924;rs62107004;rs188657413	1;15;21;44;45;49
cg04903930	-0.20956896	0.57731849	-7.69037612	0.00287826	0.76464434	-0.79174015	4	78352562	R	II		IGR	opensea	IGR-opensea		rs145520232;rs551636641;rs571432298	47;17;2
cg09179637	0.237248797	0.5639564	7.658638224	0.00291726	0.76464434	-0.80454244	6	40492307	R	II	LRFN2	5'UTR	opensea	5'UTR-opensea		rs679821;rs574130059	42;1
cg23424136	0.213770607	0.30979674	7.624279732	0.00296025	0.76464434	-0.81848426	7	25765894	F	II		IGR	opensea	IGR-opensea		rs565381606	0
cg18686270	-0.23160168	0.66011221	-7.54184604	0.00306673	0.76464434	-0.85228716	3	1.46E+08	F	II	PLSCR1	5'UTR	shelf	5'UTR-shelf	chr3:146262126-146262505	rs545677412;rs16858468	0;43
cg07079560	-0.22595633	0.6573995	-7.49655873	0.00312732	0.76464434	-0.87107259	5	53735028	F	II		IGR	opensea	IGR-opensea		rs188654175;rs139687029;rs7727143	1;16;28
cg01882539	0.201634618	0.64899518	7.434514549	0.00321284	0.76464434	-0.89705972	17	32481208	R	II	ACCN1	Body	shelf	Body-shelf	chr17:32484007-32484280	rs28592640;rs148777665;rs144806363	27;20;1
cg27312789	-0.20470696	0.38256016	-7.4298669	0.00321937	0.76464434	-0.89901815	11	11809714	F	II		IGR	opensea	IGR-opensea		rs574849290;rs558205679	6;51
cg10514207	0.200767273	0.52232828	7.424363496	0.00322712	0.76464434	-0.90133932	13	49384181	F	II		IGR	opensea	IGR-opensea		rs553339499;rs185069149	1;43
cg09496161	-0.20941493	0.43897947	-7.39023961	0.0032757	0.76464434	-0.91578354	19	54155607	F	II		IGR	shelf	IGR-shelf	chr19:54151076-54152241	rs575844374	0
cg09023235	-0.20528135	0.46966197	-7.36441576	0.0033131	0.76464434	-0.92677406	18	49922133	R	II	DCC	Body	opensea	Body-opensea		rs546401995;rs137929648;rs117572729;rs188671830	29;19;17;13
cg25051970	0.201818105	0.62866083	7.334849151	0.00335658	0.76464434	-0.93942095	10	1.35E+08	R	II	SCART1	Body	shelf	Body-shelf	chr10:135270783-135271061	rs2253522	24
cg17597740	-0.2155002	0.27712826	-7.32309181	0.00337408	0.76464434	-0.94446898	4	1.89E+08	R	II	TRIML1	TSS1500	opensea	TSS1500-opensea		rs566580703	38
cg25959317	0.242921299	0.65352028	7.28172571	0.00343656	0.76464434	-0.96231572	2	2.09E+08	F	II		IGR	opensea	IGR-opensea		rs542717212	11
cg25083484	-0.23178951	0.35514353	-7.27801016	0.00344225	0.76464434	-0.96392532	5	23384883	R	II		IGR	opensea	IGR-opensea		rs527672382	13
cg02408697	0.213791796	0.71131262	7.255100101	0.00347757	0.76464434	-0.97387428	10	1416920	F	I	ADARB2	Body	shore	Body-shore	chr10:1415976-1416249	rs189357386;rs549665260;rs568882738;rs11250483	1;19;39;42
cg23839338	0.202015206	0.56136748	7.249456856	0.00348634	0.76464434	-0.97633132	14	24834668	F	II	NFATC4	TSS1500	shore	TSS1500-shore	chr14:24835810-24836220	rs142887365;rs557642574	18;32
cg19749975	0.229977262	0.57524935	7.211142012	0.00354664	0.76464434	-0.99308048	1	71547563	F	II	ZRANB2	TSS1500	shore	TSS1500-shore	chr1:71546486-71546783	rs184816736;rs574415326;rs189240599	1;9;14
cg00011225	-0.23026018	0.45456707	-7.20522911	0.00355607	0.76464434	-0.99567574	2	2.2E+08	F	I	WNT6	Body	island	Body-island	chr2:219738081-219738788		
cg09249159	-0.23191924	0.43985857	-7.08116243	0.00376142	0.76464434	-1.05078374	3	1.79E+08	R	II		IGR	opensea	IGR-opensea		rs568380684	12
cg15424233	-0.20291355	0.61877663	-7.07646123	0.0037695	0.76464434	-1.05289669	2	9865477	R	II		IGR	opensea	IGR-opensea		rs545032306;rs577601158;rs9789690;rs560113583;rs528665051;rs548801633;rs143229290	35;33;31;30;23;9;1
cg12945378	-0.2098917	0.73425358	-7.05130385	0.00381309	0.76464434	-1.06423478	12	1.18E+08	R	II	KSR2	Body	shore	Body-shore	chr12:118198767-118199287	rs577461650	1
cg18217594	0.226708658	0.53808458	7.005908161	0.0038934	0.76464434	-1.08482734	12	9293085	R	II		IGR	opensea	IGR-opensea			
cg08171505	-0.20671556	0.48251767	-7.00581673	0.00389356	0.76464434	-1.08486899	X	70883292	F	II	BCYRN1	Body	opensea	Body-opensea			
cg08303110	-0.21215111	0.47102354	-6.97444963	0.00395032	0.76464434	-1.09919912	4	68033903	R	II		IGR	opensea	IGR-opensea		rs111352377	9
cg09839120	-0.22982956	0.56573469	-6.93507468	0.00402307	0.76464434	-1.11730556	7	1.5E+08	F	II		IGR	opensea	IGR-opensea		rs569647745	28
cg11761627	-0.20550741	0.27509262	-6.93238607	0.0040281	0.76464434	-1.11854672	5	62283805	R	II		IGR	opensea	IGR-opensea		rs148964414;rs550835574;rs113959715	32;23;21
cg21396956	-0.26783899	0.33049231	-6.88481979	0.00411843	0.76464434	-1.14060752	18	56340167	F	II	MALT1	Body	shore	Body-shore	chr18:56338211-56339277		
cg12490910	-0.22602614	0.41409715	-6.85418813	0.00417797	0.76464434	-1.15491749	7	6712945	F	II		IGR	opensea	IGR-opensea		rs148303978	1
cg04328144	0.234489788	0.32097569	6.852772779	0.00418075	0.76464434	-1.15558065	6	70468286	R	II	LMBRD1	Body	opensea	Body-opensea		rs534853428;rs73486006;rs146968588;rs568212006;rs537352504	41;30;24;24;1
cg24000300	0.238826665	0.55151053	6.849993905	0.00418621	0.76464434	-1.15688321	8	49014558	R	II		IGR	opensea	IGR-opensea		rs143743819;rs541530138	18;2
cg24208650	-0.2017739	0.52899279	-6.81360105	0.00425857	0.76464434	-1.17400402	3	50515965	F	II	CACNA2D2	5'UTR	opensea	5'UTR-opensea		rs528777980	15
cg04169075	-0.21022911	0.3762505	-6.73212042	0.00442646	0.76464434	-1.21275903	15	67215905	R	II		IGR	opensea	IGR-opensea		rs561533516	35
cg01188753	0.208623793	0.58950092	6.728902472	0.00443326	0.76464434	-1.2143017	20	47897068	R	II	C20orf199	Body	shore	Body-shore	chr20:47894197-47895199		
cg03468480	-0.23195083	0.54869577	-6.69971524	0.00449557	0.76464434	-1.22833643	22	37386714	R	II		IGR	opensea	IGR-opensea		rs557751028;rs144045154	47;37
cg24366564	0.2435185	0.43205139	6.697044299	0.00450133	0.76464434	-1.22962458	17	2843149	R	I	RAP1GAP2	Body	opensea	Body-opensea		rs139091470;rs538011045	44;29
cg03100209	0.20476162	0.66072005	6.69650096	0.0045025	0.76464434	-1.2298867	19	49921142	R	II	CCDC155	3'UTR	opensea	3'UTR-opensea		rs565287530	2
cg11050156	-0.20283308	0.56778945	-6.69363762	0.00450868	0.76464434	-1.2312685	3	1.24E+08	R	II	CCDC14	5'UTR	shore	5'UTR-shore	chr3:123679785-123680481	rs547849626;rs372873046	2;1
cg19858756	-0.21290004	0.43120255	-6.6772445	0.00454431	0.76464434	-1.23919377	5	1.56E+08	F	II	SGCD	Body	opensea	Body-opensea		rs571004672;rs537274047;rs145838921;rs150942951	0;38;39;49
cg22328256	-0.26974728	0.39649322	-6.6717958	0.00455622	0.76464434	-1.24183333	6	28757381	F	II		IGR	shelf	IGR-shelf	chr6:28753869-28754138	rs115750861	27
cg26969102	-0.27237019	0.39954371	-6.63698288	0.00463333	0.76464434	-1.25876176	19	56954002	R	II	ZNF667	Body	opensea	Body-opensea		rs35914474;rs149168669	41;2
cg12778228	0.224611478	0.54794396	6.614799355	0.00468333	0.76464434	-1.26960664	17	16341601	R	II	NCRNA00188	TSS1500	shore	TSS1500-shore	chr17:16342504-16342897		
cg26847392	-0.25095446	0.41130279	-6.60551375	0.00470446	0.76464434	-1.2741595	11	55762735	R	II	OR5F1	TSS1500	opensea	TSS1500-opensea		rs183027316;rs529218163	2;1
cg03354203	0.279180911	0.3883633	6.586182647	0.00474885	0.76464434	-1.2836633	1	30128888	F	II		IGR	opensea	IGR-opensea		rs527869828;rs548048721;rs564205068;rs193224152	1;17;19;33
cg10791959	-0.21885732	0.40207824	-6.58448446	0.00475277	0.76464434	-1.28449983	3	1.35E+08	R	I	EPHB1	Body	shore	Body-shore	chr3:134514085-134515980		
cg04318989	0.226369572	0.65712598	6.566296067	0.00479507	0.76464434	-1.29347625	1	2.19E+08	R	II	LYPLAL1	TSS1500	island	TSS1500-island	chr1:219347109-219347572	rs187690958;rs552191147;rs569218807;rs146324348	40;26;16;13
cg01999908	0.2011014	0.74017242	6.561076165	0.0048073	0.76464434	-1.29605807	7	1.27E+08	F	II	PAX4	TSS1500	opensea	TSS1500-opensea		rs538255526;rs327513;rs565689557	1;14;39
cg08514779	0.216565582	0.67212977	6.502519698	0.00494723	0.76464434	-1.32519509	13	1.12E+08	R	II		IGR	opensea	IGR-opensea		rs564359049	17
cg03545757	0.20884087	0.61569677	6.467361215	0.00503374	0.76464434	-1.34284458	16	1366304	F	II	UBE2I	Body	shore	Body-shore	chr16:1363813-1364496	rs551003222;rs4638578;rs4017714;rs144204134;rs566948700;rs76747201;rs111956252	3;4;13;29;31;40;42
cg22404419	-0.20417013	0.55531401	-6.44291392	0.00509504	0.76464434	-1.35518625	9	79785806	R	II		IGR	opensea	IGR-opensea		rs549273205;rs531773966	9;2
cg14551114	-0.21015716	0.51392138	-6.40345739	0.005196	0.76464434	-1.37522565	13	52368022	F	II	DHRS12	Body	opensea	Body-opensea		rs139361426;rs570042307	0;32
cg08904591	-0.21369349	0.48336631	-6.38494333	0.00524425	0.76464434	-1.38468034	15	96855873	F	II	NR2F2-AS1	Body	opensea	Body-opensea		rs531745232;rs548384719;rs568381155;rs534247714;rs77736520	0;1;5;34;44
cg10055165	-0.24445935	0.530922	-6.38206693	0.00525179	0.76464434	-1.38615223	11	1.26E+08	F	II	PATE2	TSS1500	opensea	TSS1500-opensea		rs548717091;rs540100153	1;16
cg03259333	-0.26027978	0.58206524	-6.35378055	0.00532675	0.76464434	-1.4006695	5	1.79E+08	R	II	ADAMTS2	Body	shore	Body-shore	chr5:178593903-178594656	rs549634977	1
cg15636519	0.205315503	0.57242489	6.335688763	0.00537541	0.76464434	-1.40999556	2	1.92E+08	F	II	STAT4	3'UTR	opensea	3'UTR-opensea		rs3024907	24

cg24593093	-0.24017359	0.55521425	-6.3337964	0.00538054	0.76464434	-1.4109729	15	32954373	R	II	SCG5	Body	opensea	Body-opensea		rs180896699;rs529718089	2;1	
cg07894663	0.201215624	0.44027879	6.306174717	0.00545602	0.76464434	-1.42527853	16	4338268	R	II		IGR	opensea	IGR-opensea		rs111517284		29
cg06266516	-0.26889318	0.38612641	-6.28948936	0.00550227	0.76464434	-1.43395653	7	79609099	F	II		IGR	opensea	IGR-opensea		rs140649679;rs185125452;rs145814385;rs137929049	13;25;41;45	
cg07956003	-0.22989657	0.66203088	-6.26318258	0.00557621	0.76464434	-1.44769466	7	95433460	F	II	DYNC1I1	5'UTR	opensea	5'UTR-opensea		rs533590111;rs553311278;rs191225692;rs112429640	18;22;33;42	
cg18316031	0.237012953	0.50268557	6.260392142	0.00558413	0.76464434	-1.44915594	11	30147451	F	II		IGR	opensea	IGR-opensea		rs78503251;rs542132807;rs144907806;rs530976001	0;5;27;31	
cg18751141	-0.24286852	0.32914905	-6.25043225	0.0056125	0.76464434	-1.45437802	7	27138173	F	II		IGR	shore	IGR-shore	chr7:27135342-27136736	rs373259447;rs6668	2;10	
cg16620039	-0.21842999	0.47931446	-6.2408711	0.00563991	0.76464434	-1.45940036	14	1.02E+08	R	II		IGR	opensea	IGR-opensea		rs117159770;rs370598031;rs182489377	10;2;1	
cg26312935	0.206493409	0.48949059	6.195070319	0.00577362	0.76464434	-1.48358624	15	59279406	F	II	RNF111	TSS1500	shore	TSS1500-shore	chr15:59279741-59280720	rs529901828;rs62002482	19;35	
cg02552189	0.207852543	0.52877148	6.193364399	0.00577867	0.76464434	-1.48449117	2	2.24E+08	F	II		IGR	opensea	IGR-opensea		rs556525151;rs1440073	1;40	
cg05672337	-0.20406916	0.42716491	-6.19054788	0.00578704	0.76464434	-1.48598588	12	86580421	F	II	MGAT4C	5'UTR	opensea	5'UTR-opensea		rs570043794		50
cg22435568	-0.32360664	0.33210039	-6.19015428	0.00578821	0.76464434	-1.48619482	19	35849287	F	I	FFAR3	TSS200	opensea	TSS200-opensea		rs555975639		19
cg05334656	0.230778238	0.62739696	6.162738464	0.00587044	0.76464434	-1.50078738	4	4866047	R	II		IGR	shore	IGR-shore	chr4:4866438-4866813	rs186128404		20
cg07388775	0.244612429	0.56956717	6.151028746	0.00590601	0.76464434	-1.50704343	4	88529234	F	II	DSPP	TSS1500	opensea	TSS1500-opensea		rs530655012		48
cg20995564	-0.29824085	0.49851915	-6.13056671	0.00596884	0.76464434	-1.5180092	2	1.45E+08	R	II	ZEB2	Body	opensea	Body-opensea		rs549658388;rs139922284	48;11	
cg15743533	0.216659021	0.52401727	6.108274461	0.00603826	0.76464434	-1.53000478	20	815345	F	II	FAM110A	TSS1500	shore	TSS1500-shore	chr20:814120-814755	rs149423152		26
cg02831700	0.300191923	0.36090181	6.106193417	0.00604479	0.76464434	-1.53112721	2	1.56E+08	R	II		IGR	opensea	IGR-opensea				
cg10950266	-0.23563261	0.24846149	-6.08847496	0.00610077	0.76464434	-1.54070204	X	1.01E+08	F	I	ARMCX4	TSS200	island	TSS200-island	chrX:100673191-100673673			
cg08678202	0.224353053	0.68092217	6.084428027	0.00611365	0.76464434	-1.54289352	10	1546680	F	II	ADARB2	Body	opensea	Body-opensea		rs188283866;rs111888230	38;48	
cg25361961	0.228875351	0.48163396	6.065882403	0.00617312	0.76464434	-1.55295806	19	58070048	F	II		IGR	shore	IGR-shore	chr19:58070553-58071273	rs10221464		16
cg17389351	0.255085279	0.76625022	6.053597469	0.00621292	0.76464434	-1.55964473	15	72552964	F	II	PARP6	Body	opensea	Body-opensea		rs576673720;rs368305146;rs201870693	8;34;49	
cg06787637	-0.20682356	0.62966079	-6.02889394	0.00629394	0.76464434	-1.57313868	8	86347111	F	II		IGR	shelf	IGR-shelf	chr8:86350765-86351196	rs11985029		5
cg21262776	-0.23070879	0.54197565	-6.00973338	0.00635771	0.76464434	-1.58364908	1	3144113	F	I	PRDM16	Body	shelf	Body-shelf	chr1:3147845-3148081	rs552137951;rs571241659	13;35	
cg04351586	0.239311955	0.57343949	5.970237122	0.00649178	0.76464434	-1.60543717	7	92483047	R	II	LOC101927497	Body	opensea	Body-opensea		rs530111990;rs532734448;rs546175832	29;27;2	
cg10105501	-0.20458819	0.52871546	-5.94928094	0.00656437	0.76464434	-1.61706514	1	42836436	F	II		IGR	opensea	IGR-opensea				
cg15505944	-0.20021142	0.64900129	-5.94454468	0.00658092	0.76464434	-1.61969967	19	23298818	F	II	ZNF730	TSS1500	shore	TSS1500-shore	chr19:23299727-23300167	rs76964790;rs192350760;rs560489421;rs527722952;rs2085999	26;31;38;39;48	
cg12545533	0.200320975	0.65428925	5.907603107	0.00671184	0.76464434	-1.64033114	1	1.14E+08	R	II	PTPN22	Body	opensea	Body-opensea		rs79773973		20
cg23624705	-0.22958896	0.38327419	-5.8985681	0.00674436	0.76464434	-1.64539954	1	92952655	R	II	GFI1	TSS1500	shore	TSS1500-shore	chr1:92945907-92952609			
cg24559073	-0.20461211	0.40930942	-5.87258364	0.00683902	0.76464434	-1.66002558	X	47342471	F	I	ZNF41	TSS200	island	TSS200-island	chrX:47341887-47342697			
cg22583415	-0.21119016	0.68459014	-5.8646166	0.00686838	0.76464434	-1.66452479	6	1.57E+08	R	II		IGR	opensea	IGR-opensea		rs138226527		2
cg01441501	-0.2117503	0.50919455	-5.83259532	0.00698801	0.76464434	-1.68267826	9	73051063	R	II		IGR	opensea	IGR-opensea				
cg22549339	-0.21371388	0.34311369	-5.82906286	0.00700137	0.76464434	-1.68468778	15	27891472	F	II		IGR	opensea	IGR-opensea		rs141584988;rs188257383	10;48	
cg18279094	-0.22588932	0.28564465	-5.80802972	0.00708159	0.76464434	-1.69668153	1	63790044	F	I	FOXD3	1stExon	island	1stExon-island	chr1:63782394-63790471			
cg20630344	0.215846151	0.39350856	5.780458193	0.00718852	0.76464434	-1.71247799	16	80604078	F	II	LINC01227	Body	opensea	Body-opensea		rs555389923;rs573648009	6;38	
cg23049120	0.232578478	0.54619949	5.764968985	0.0072495	0.76464434	-1.72138934	6	17290089	R	II	RBM24	Body	opensea	Body-opensea		rs538542390		11
cg20495964	0.208326359	0.37950815	5.724891855	0.00741034	0.76464434	-1.74457172	6	36744880	F	II	CPNE5	Body	opensea	Body-opensea		rs186890		39
cg16283208	-0.23843885	0.51505628	-5.70020789	0.00751166	0.76464434	-1.75894027	11	59323398	F	I		IGR	opensea	IGR-opensea		rs200096245;rs531259608	33;41	
cg12788111	0.226427427	0.55610796	5.687394133	0.00756495	0.76464434	-1.76642645	15	59279393	F	II	RNF111	TSS1500	shore	TSS1500-shore	chr15:59279741-59280720	rs529901828;rs62002482	32;48	
cg18395637	-0.21558514	0.32310698	-5.68245407	0.00758562	0.76464434	-1.76931759	4	1.13E+08	F	II		IGR	opensea	IGR-opensea		rs190457554		12
cg11902941	-0.20274226	0.70259763	-5.67510005	0.00761653	0.76464434	-1.77362663	2	741806	F	II		IGR	opensea	IGR-opensea		rs114124028		1
cg00576773	0.204788738	0.50634111	5.66167251	0.00767338	0.76464434	-1.78151039	15	89909904	R	II	MIR9-3	TSS1500	shore	TSS1500-shore	chr15:89910521-89912177	rs560153254		2
cg16454924	-0.20584204	0.3406192	-5.64993053	0.00772354	0.76464434	-1.78842145	1	79114951	F	II	IFI44	TSS1500	opensea	TSS1500-opensea		rs147022952		26
cg21456399	0.228107917	0.63561721	5.6335584	0.00779416	0.76464434	-1.79808421	2	2.3E+08	F	II	DNER	Body	opensea	Body-opensea		rs535542649;rs535615458;rs72987944;rs572255645	17;18;38;39	
cg04512966	-0.22543361	0.65207509	-5.63017695	0.00780885	0.76464434	-1.80008378	2	1.63E+08	F	II	DPP4	Body	opensea	Body-opensea				
cg21082141	0.235457876	0.41744955	5.629721072	0.00781084	0.76464434	-1.80035346	4	81111985	F	II	PRDM8	5'UTR	shore	5'UTR-shore	chr4:81109887-81110460	rs72656526		25
cg04109543	0.262706781	0.61974662	5.625547454	0.00782902	0.76464434	-1.80282351	6	10422874	F	II		IGR	shore	IGR-shore	chr6:10422321-10422648	rs529375746;rs551015906	45;51	
cg10973881	0.227816966	0.54366636	5.622639257	0.00784172	0.76464434	-1.80454584	1	1.51E+08	R	II	TMOD4	TSS200	opensea	TSS200-opensea		rs587691427;rs58442766;rs189902209	38;11;7	
cg24786671	-0.2109805	0.43899635	-5.58550838	0.00800623	0.76464434	-1.82662234	21	31722001	R	II	KRTAP23-1	TSS1500	opensea	TSS1500-opensea		rs78545747		32
cg07180125	0.204020912	0.39853395	5.561248462	0.00811609	0.76464434	-1.84113319	10	1.14E+08	F	II		IGR	opensea	IGR-opensea		rs185522989		39
cg17259303	0.232210241	0.48817256	5.555450769	0.00814262	0.76464434	-1.84461125	3	1.57E+08	R	II		IGR	opensea	IGR-opensea		rs530570534		2
cg09873379	0.22109057	0.40433942	5.543948136	0.0081956	0.76464434	-1.85152345	12	1.09E+08	R	II		IGR	opensea	IGR-opensea		rs79449355;rs537990518;rs148555886	14;12;2	
cg24827217	-0.20659891	0.32579733	-5.52889418	0.00826559	0.76464434	-1.8605933	3	1.68E+08	R	II	EGFEM1P	Body	opensea	Body-opensea		rs540969636;rs143895222	11;1	
cg12347792	0.206434098	0.52254596	5.472289343	0.00853564	0.76464434	-1.89493801	4	1.86E+08	F	I	CCDC110	TSS1500	shore	TSS1500-shore	chr4:186392574-186393184	rs28429774		49
cg01131388	0.207614945	0.72849336	5.470156583	0.00854604	0.76464434	-1.89623954	3	1.58E+08	R	II		IGR	opensea	IGR-opensea		rs186205512;rs376134667;rs552206097	42;15;1	
cg21498923	0.20203871	0.41722138	5.469838875	0.00854759	0.76464434	-1.89643347	20	2187540	R	II	LOC388780	TSS200	island	TSS200-island	chr20:2187532-2188576	rs556981361;rs148299112	47;27	
cg24847427	0.20724516	0.51148342	5.461729875	0.00858725	0.76464434	-1.90138731	7	1.01E+08	R	II		IGR	shelf	IGR-shelf	chr7:100964790-100965201	rs7799285;rs560135184	22;1	
cg07820966	0.200907943	0.48518552	5.450551382	0.00864232	0.76464434	-1.9082293	4	1.86E+08	R	II		IGR	opensea	IGR-opensea		rs555561029;rs572260369;rs534860733;rs75748238;rs73873171	51;40;16;15;2	
cg27441138	0.201202929	0.69103752	5.448029837	0.0086548	0.76464434	-1.90977474	1	2.28E+08	R	II	WNT3A	Body	shelf	Body-shelf	chr1:228246631-228247197	rs150517928		44
cg06445384	0.244576156	0.60898635	5.43104538	0.00873949	0.76464434	-1.9202044	6	1.59E+08	F	II		IGR	opensea	IGR-opensea		rs376841394		24
cg09675542	0.21548971	0.54178282	5.412317842	0.00883408	0.76464434	-1.93174495	7	19548878	R	II		IGR	opensea	IGR-opensea		rs4721778;rs116670532;rs540808487;rs561660382	38;37;8;1	
cg05551587	-0.2610062	0.48622184	-5.39282359	0.00893393	0.76464434	-1.94380332	2	1.08E+08	R	II		IGR	opensea	IGR-opensea		rs554222398		1
cg11845620	-0.20058567	0.56977967	-5.39194415	0.00893847	0.76464434	-1.9443484	17	37197733	F	II		IGR	opensea	IGR-opensea		rs117807470		5
cg07027512	-0.21072857	0.7706989	-5.3916456	0.00894001	0.76464434	-1.94453346	19	56123563	R	II	ZNF865	TSS1500	shore	TSS1500-shore	chr19:56125349-56128167	rs545336582;rs537630538	45;1	
cg10236447	-0.24687395	0.40363771	-5.38633021	0.00896751	0.76464434	-1.94783017	X	53077495	F	II	GPR173	TSS1500	opensea	TSS1500-opensea				
cg26654775	0.212813929	0.6534427	5.384907583	0.00897488	0.76464434	-1.94871309	13	47971330	R	II		IGR	opensea	IGR-opensea		rs192962374;rs569130173	25;18	
cg16247474	0.225793136	0.71516313	5.38265361	0.00898659	0.76464434	-1.95011249	5	1.74E+08	R	II	LINC01411	Body	opensea	Body-opensea		rs139415988;rs149628702	36;2	
cg17391194	0.202859714	0.32479956	5.381475833	0.00899271	0.76464434	-1.95084397	11	82401662	R	II		IGR	shore	IGR-shore	chr11:82400585-82400858	rs572306886		23
cg19439713	-0.28267837	0.56139355	-5.36347315	0.00908698	0.76464434	-1.96204602	11	15062810	F	II		IGR	opensea	IGR-opensea		rs551674680;rs562974851;rs530309151;rs145090638	10;11;16;40	
cg23552876	0.205009123	0.31381429	5.345531592	0.00918217	0.76464434	-1.97324972	17	26697752	R	II	SARM1	TSS1500	shore	TSS1500-shore	chr17:26698359-26699557	rs16964236		21
cg19805208	0.255617005	0.59231883	5.339447245	0.00921474	0.76464434	-1.97705815	16	89050256	F	II		IGR	opensea	IGR-opensea		rs553342852		14
cg12806613	0.213013738	0.23800882	5.31792638	0.00933111	0.76464434	-1.99056572	1	63540205	F	I		IGR	opensea	IGR-opensea				
cg03207868	-0.22726584	0.56070289	-5.30602956	0.00939625	0.76464434	-1.99805747	20	56778561	F	II		IGR	shelf	IGR-shelf	chr20:56780583-56781118	rs6099989;rs115355912;rs6026129	1;11;43	
cg24759795	-0.26055389	0.5503056	-5.28935584	0.0094885	0.76464434	-2.00858708	8	1.14E+08	R	II	CSMD3	Body	shore	Body-shore	chr8:114444826-114445085	rs114251401;rs1478675;rs187400358;rs551518133	51;18;8;3	
cg07674312	0.253501335	0.68383657	5.282975481	0.00952411	0.76464434	-2.01262554	10	1.27E+08	F	II		IGR	opensea	IGR-opensea		rs370912039;rs545536444	21;38	
cg25733888	0.273358024	0.64971922	5.281396946	0.00953294	0.76464434	-2.01362547	14	35682442	R	II	KIAA0391	Body	opensea	Body-opensea		rs181284369		2
cg10595547	0.257800558	0.33859158	5.27261188	0.0095823	0.76464434	-2.01919609	10	1.19E+08	F	I		IGR	shore	IGR-shore	chr10:119311204-119312104	rs71475030;rs371459821	20;47	
cg21757338	-0.20595582	0.22847651	-5.27146786	0.00958876	0.76464434	-2.01992223	5	57751006	F	II	PLK2	Body	opensea	Body-opensea		rs148634317;rs192767656	10;13	
cg21482921	0.226252998	0.40745822	5.251172735	0.00970413	0.76464434	-2.03283147	10	5084043	F	II		IGR	opensea	IGR-opensea		rs552389111;rs144104296;rs114115777;rs184467508;rs568378496	0;1;28;35;46	
cg17124408	-0.20972148	0.45792068	-5.24675457	0.00972948	0.76464434	-2.03564865	11	63137398	F	II	SLC22A9	5'UTR	opensea	5'UTR-opensea		rs558847894;rs572671944;rs561550129	0;1;8	
cg18861197	-0.2214465	0.52924505	-5.23014502	0.00982553	0.76464434	-2.0462616	8	27209336	R	II	PTK2B	5'UTR	opensea	5'UTR-opensea				
cg21335376	-0.20809441	0.53339187	-5.17669546	0.01014286	0.76464434	-2.08065255	7	1.33E+08	R	II	CHCHD3	Body	opensea	Body-opensea		rs538490940		43
cg04490079	0.295873804	0.61188059	5.149664995	0.01030829	0.76464434	-2.09818428	3	98216207	R	II	OR5K2	TSS1500	opensea	TSS1500-opensea		rs191372428;rs573187805	11;10	
cg16203262	0.271322115	0.4670498	5.139279076	0.01037275	0.76464434	-2.10494561	13	78495961	F	II	EDNRB	5'UTR	shelf	5'UTR-shelf	chr13:78492425-78493382	rs147843823;rs533251846	0;22	
cg21434954	-0.20146865	0.58055369	-5.13422129	0.01040433	0.76464434	-2.10824335	1	1.53E+08	R	II	LCE1B	TSS1500	opensea	TSS1500-opensea		rs141569525		2
cg06477065	-0.21440166	0.69755451	-5.13355004	0.01040853	0.76464434	-2.10868126	11	46406856	R	II	CHRM4	1stExon	shore	1stExon-shore	chr11:46406904-46407441	rs200378895;rs2229163	49;1	
cg08227888	0.2148812	0.54317293	5.110943127	0.01055125	0.76464434	-2.12346385	17	58756766	R	II	BCAS3	5'UTR	shore	5'UTR-shore	chr17:58754625-58755480	rs555003474		42
cg04017943	-0.24133938	0.34745605	-5.10278158	0.01060338	0.76464434	-2.12881704	2	53437876	F	II		IGR	opensea	IGR-opensea		rs532294671		48
cg13224197	0.205307076	0.35335891	5.101096139	0.01061418	0.76464434	-2.12992361	1	4193192	R	II		IGR	island	IGR-island	chr1:4192633-4193243	rs561979268;rs572242448	44;19	
cg17914442	0.202838819	0.50471986	5.098720899	0.01062944	0.76464434	-2.1314837	2	2.17E+08	F	II	MARCH4	Body	opensea	Body-opensea		rs560746535;rs371338919	0;1	
cg13516479	0.208810791	0.5453429	5.07786752	0.01076454	0.76464434	-2.14521223	6	1.22E+08	F	II		IGR	opensea	IGR-opensea		rs149391054		17
cg00511932	-0.22102644	0.60921133	-5.07408674	0.01078926	0.76464434	-2.14770738	1	14451215	R	II		IGR	opensea	IGR-opensea		rs558514962;rs5772563;rs113398528;rs574407600;rs543065823	41;12;10;7;2	
cg00407329	0.209192682	0.53201249	5.07311086	0.01079566	0.76464434	-2.14835172	6	1.01E+08	R	II	SIM1	Body	shore	Body-shore	chr6:100895007-100895246			
cg17334359	0.252469013	0.44218635	5.049584076	0.01095126	0.76464434	-2.16392374	5	1.63E+08	R	II	MAT2B	TSS1500	shelf	TSS1500-shelf	chr5:162932454-162932946			
cg05833905	-0.21669216	0.38169653	-5.04179079	0.01100343	0.76464434	-2.16909814	6	1.24E+08	R	II	TRDN	Body	opensea	Body-opensea				
cg18741768	0.206197833	0.57025447	5.038508403	0.0110255	0.76464434	-2.17127991	12	1.1E+08	F	II	MYO1H	TSS1500	opensea	TSS1500-opensea		rs78015108;rs183156059;rs570100567;rs79127498	12;21;26;46	
cg24536007	0.221514624	0.59669988	5.023201264	0.01112914	0.76464434	-2.18147333	17	32309520	F	II	ASIC2	Body	opensea	Body-opensea		rs550156246;rs570015025	1;26	
cg03398194	-0.26978119	0.37823376	-5.02052679	0.01114738	0.76464434	-2.18325754	2	51848103	F	II		IGR	opensea	IGR-opensea		rs1516171		11
cg13921062	0.237805164	0.4692321	4.986766462	0.01138084	0.76680115	-2.20586204	16	80648264	F	II	CDYL2	Body	opensea	Body-opensea		rs7500067		32
cg10125277	0.260572624	0.62988622	4.964199491	0.01154035	0.76757652	-2.22105727	11	1.18E+08	R	II	TMPRSS4-AS1	Body	opensea	Body-opensea		rs549952198		15
cg12097011	-0.24971853	0.52972047	-4.96386536	0.01154273	0.76757652	-2.22128278	10	7145290	R	II		IGR	opensea	IGR-opensea		rs576358838;rs114697986	21;2	
cg03425812	-0.26624504	0.58735298	-4.93881353	0.01172317	0.76802395	-2.23823289	15	45005363	R	II	B2M	Body	shore	Body-shore	chr15:45003460-45004345			
cg16727243	0.236344812	0.47628111	4.930640145	0.01178281	0.76802395	-2.24378145	2	20441905	R	II		IGR	opensea	IGR-opensea				
cg03230989	-0.25959774	0.36196258	-4.9257549	0.01181864	0.76802395	-2.24710217	9	26066126	F	II	LOC100506422	TSS1500	opensea	TSS1500-opensea		rs540431674;rs565111661	0;48	
cg24910616	-0.22639765	0.44211062	-4.9247786	0.01182581	0.76802395	-2.24776619	14	65886630	R	II	FUT8	5'UTR	opensea	5'UTR-opensea		rs549615519;rs569456109	46;2	
cg04186268	-0.23013748	0.38658213	-4.92423601	0.0118298	0.76802395	-2.24813529	1	85557733	R	II	WDR63	Body	opensea	Body-opensea		rs568344436;rs191619929;rs536880749	46;2;1	
cg07189394	-0.21379242	0.44192695	-4.91806483	0.01187531	0.76802395	-2.25233604	3	1.32E+08	F	II		IGR	opensea	IGR-opensea		rs77034109;rs545710267;rs560643538	18;24;41	
cg11228388	0.201980332	0.59204776	4.898965355	0.01201757	0.76802395	-2.26537015	1	62625859	R	II	INADL	Body	opensea	Body-opensea		rs192085589;rs150650432	48;1	
cg24018963	-0.2094569	0.34418282	-4.89782736	0.01202612	0.76802395	-2.26614833	15	83226022	F	II	CPEB1	Body	opensea	Body-opensea		rs548832200		15
cg02012327	0.202862439	0.62047502	4.896262015	0.01203788	0.76802395	-2.26721903	13	20676694	F	II	LINC01072	TSS200	opensea	TSS200-opensea		rs116651615		13
cg23008023	-0.20771572	0.74090856	-4.85632451	0.01234302	0.76802395	-2.29465049	10	1.25E+08	R	II		IGR	opensea	IGR-opensea		rs190540013;rs551970092;rs138074324;rs180695528	48;43;32;1	
cg22666555	0.221235617	0.52157379	4.855560272	0.01234895	0.76802395	-2.29517756	6	34114320	F	II	GRM4	TSS1500	shore	TSS1500-shore	chr6:34111735-34113944			
cg11830692	0.25849713	0.68357765	4.848872822	0.01240103	0.76806503	-2.29979314	18	10856494	F	II	PIEZO2	Body	opensea	Body-opensea		rs143191022;rs566632765	0;23	
cg21803548	-0.20124681	0.4328035	-4.84042626	0.0124672	0.76806503	-2.3056317	3	1.44E+08	R	II		IGR	opensea	IGR-opensea		rs58537913		26
cg10920646	-0.21868851	0.44838686	-4.84028169	0.01246833	0.76806503	-2.30573172	13	1.13E+08	R	II	LINC00354	Body	opensea	Body-opensea		rs189077678;rs4465505;rs148735910	47;26;16	
cg04786038	0.206477557	0.32669607	4.838419962	0.01248298	0.76806503	-2.30701998	18	2147655	F	II		IGR	opensea	IGR-opensea		rs186430926		1
cg09573795	0.230804094	0.64361046	4.826053593	0.01258082	0.76806503	-2.3155894	4	4863874	F	II	MSX1	Body	shore	Body-shore	chr4:4864456-4864834			
cg08869206	-0.23796598	0.55563303	-4.82123473	0.01261921	0.76806503	-2.31893445	7	57521583	R	II	ZNF716	Body	opensea	Body-opensea		rs11972967;rs117553144;rs184915495;rs35357268	33;25;13;2	
cg17463271	-0.3264596	0.57939285	-4.81699703	0.01265309	0.76806503	-2.32187877	9	1.4E+08	F	II		IGR	shelf	IGR-shelf	chr9:140033235-140034176	rs189965512;rs9411251	20;27	
cg10277551	0.235196104	0.46261275	4.808429101	0.01272194	0.76806503	-2.32783935	6	99871388	F	II	PNISR	5'UTR	shore	5'UTR-shore	chr6:99872726-99873206			
cg19744045	-0.20856726	0.34504745	-4.80464615	0.01275248	0.76806503	-2.33047437	4	22457802	R	II	ADGRA3	Body	opensea	Body-opensea		rs188405945		17
cg15905075	0.285600143	0.47105875	4.800775394	0.01278384	0.76806503	-2.33317262	11	66060288	R	II	TMEM151A	Body	shore	Body-shore	chr11:66059287-66059935	rs202175630;rs113399864;rs559290204	47;46;5	
cg06606091	0.201249784	0.50620744	4.792208608	0.01285358	0.76806503	-2.33915188	16	3082291	F	II	LOC100128770	TSS200	shelf	TSS200-shelf	chr16:3078141-3078553	rs552611889;rs2717713;rs2717712	4;36;48	
cg24366429	0.221328231	0.35228083	4.785204602	0.01291095	0.76806503	-2.34404804	17	77207424	F	I	HRNBP3	5'UTR	opensea	5'UTR-opensea		rs574333698;rs184016813	29;39	
cg26112621	-0.20708602	0.48691423	-4.78472302	0.01291491	0.76806503	-2.34438495	6	1.61E+08	F	II		IGR	opensea	IGR-opensea		rs139127244;rs560243394;rs368059805	0;27;31	
cg03788849	0.24897775	0.36287702	4.752527762	0.01318293	0.76806503	-2.36698228	X	10587190	F	II	MID1	5'UTR	shore	5'UTR-shore	chrX:10588199-10588486			
cg23452259	0.201026615	0.61979376	4.745384776	0.01324334	0.76806503	-2.37201571	2	2.2E+08	R	II	CDK5R2	TSS1500	shore	TSS1500-shore	chr2:219824151-219825864	rs531044448		3
cg06877840	-0.22939844	0.57739617	-4.74494927	0.01324703	0.76806503	-2.37232283	10	95362344	F	II	RBP4	TSS1500	shore	TSS1500-shore	chr10:95360389-95361387	rs553956647		35
cg21854896	-0.2057861	0.36599502	-4.7433848	0.01326031	0.76806503	-2.37342633	11	66704070	R	II	PC	5'UTR	opensea	5'UTR-opensea		rs374068080		45
cg07205796	-0.20094464	0.37852209	-4.74080352	0.01328227	0.76806503	-2.37524778	16	1187722	F	I		IGR	opensea	IGR-opensea		rs574367637;rs117540024;rs563244406;rs577073237;rs534277377	9;11;14;36;47	
cg18072492	0.21006526	0.29984307	4.738421394	0.01330257	0.76806503	-2.37692956	12	40944308	F	II	MUC19	Body	opensea	Body-opensea				
cg03735233	0.219928734	0.69906867	4.73013207	0.01337351	0.76807709	-2.38278807	16	68318873	R	II	SLC7A6	Body	opensea	Body-opensea		rs74534997;rs554771451	47;15	
cg05832246	-0.25928617	0.50055443	-4.7285949	0.01338671	0.76825146	-2.38387554	11	1.12E+08	R	II	ALG9	TSS1500	shore	TSS1500-shore	chr11:111741953-111742292	rs527550469;rs140164262	15;27	
cg25662013	0.251900302	0.43761187	4.726595298	0.01340392	0.76853595	-2.38529067	2	1.79E+08	R	II		IGR	opensea	IGR-opensea		rs564396134;rs181853991;rs550203734	29;2;1	
cg01940576	0.214355696	0.70252681	4.721465183	0.01344819	0.76903666	-2.38892389	14	36946996	F	II	SFTA3	Body	opensea	Body-opensea		rs561831615		10
cg22211164	-0.22168339	0.44378608	-4.71827099	0.01347585	0.76931533	-2.39118796	2	68615001	R	II	PLEK	Body	opensea	Body-opensea		rs143954783;rs371615644;rs570763729	45;18;10	
cg02146412	-0.24502264	0.51403354	-4.7046321	0.01359475	0.77029122	-2.40087174	11	83501743	R	II	DLG2	Body	opensea	Body-opensea		rs537572890		29
cg12415917	-0.22558597	0.35014159	-4.70381499	0.01360191	0.77029122	-2.40145274	11	6047917	R	II	OR56A1	3'UTR	opensea	3'UTR-opensea		rs577314841;rs541406967;rs146178966	51;47;35	
cg07462756	0.214558438	0.28441206	4.703239211	0.01360697	0.77029523	-2.4018622	4	4859985	R	II	MSX1	TSS1500	island	TSS1500-island	chr4:4859632-4860191	rs139913705;rs528852346	51;49	
cg27216575	-0.2693507	0.39434493	-4.69697044	0.01366212	0.77039258	-2.4063233	8	15935536	R	II		IGR	opensea	IGR-opensea		rs535747759;rs56714723;rs6980732	11;4;3	
cg26579578	0.222151802	0.54028224	4.676442019	0.01384472	0.77039258	-2.42097162	11	69707303	R	I		IGR	shore	IGR-shore	chr11:69706778-69707017	rs553544925;rs147472258;rs539088862;rs60065093;rs575558742;rs543386389;rs555611829	51;46;39;29;21;5;3	
cg19870626	0.251850607	0.62791019	4.670321315	0.01389976	0.77088228	-2.42535087	1	1.76E+08	F	II		IGR	opensea	IGR-opensea		rs112615490		1
cg24725789	0.254720692	0.44633847	4.659715111	0.01399578	0.77088228	-2.43295224	10	1.19E+08	R	I		IGR	shore	IGR-shore	chr10:119311204-119312104	rs540990381;rs139987854;rs55864149	43;39;19	
cg19231141	0.2070927	0.68647567	4.624997104	0.01431599	0.77088228	-2.45794842	5	1.7E+08	F	II	KCNMB1	5'UTR	opensea	5'UTR-opensea		rs542650098		0
cg15084405	0.215985277	0.63956108	4.623704877	0.01432809	0.77088228	-2.45888218	3	1.79E+08	F	II		IGR	opensea	IGR-opensea		rs550233552;rs148372811;rs74656452;rs114040335	0;8;9;37	
cg00761644	-0.25097029	0.57508507	-4.61891198	0.01437307	0.77088228	-2.46234765	7	1.39E+08	R	II	ZC3HAV1	Body	shore	Body-shore	chr7:138793113-138794608	rs143494441		35
cg21941611	-0.20879707	0.59455423	-4.61873326	0.01437475	0.77088228	-2.46247693	17	3378804	F	II	ASPA	TSS1500	shelf	TSS1500-shelf	chr17:3375006-3375237	rs574887439;rs139039478;rs141502166	0;4;10	
cg16678267	-0.21923085	0.30675877	-4.61838395	0.01437803	0.77088228	-2.46272964	8	31896371	F	II	NRG1-IT1	Body	opensea	Body-opensea		rs550425484;rs567132630;rs368427001	6;9;18	
cg08013396	0.247894586	0.58205056	4.598570329	0.01456593	0.7722674	-2.4770929	10	1.34E+08	F	II		IGR	shelf	IGR-shelf	chr10:133849676-133850826	rs540039405;rs74161713;rs576650144	1;30;31	
cg17381970	-0.22270111	0.8067869	-4.59679731	0.0145829	0.7722674	-2.478381	3	1.79E+08	F	II	MFN1	Body	opensea	Body-opensea		rs9834493		8
cg00600521	-0.22712794	0.69905259	-4.58992042	0.01464893	0.77239126	-2.48338143	7	1.22E+08	R	II	AASS	TSS1500	shore	TSS1500-shore	chr7:121783946-121784663	rs549827662		47
cg10935498	0.301594211	0.52323705	4.582674051	0.01471892	0.77239126	-2.48865804	6	79898777	R	II		IGR	opensea	IGR-opensea		rs536071061;rs545390293	13;2	
cg23447131	0.228801726	0.33442378	4.571371202	0.01482893	0.77239126	-2.49690392	2	70312835	F	II	PCBP1-AS1	Body	shore	Body-shore	chr2:70313200-70315490	rs527812602;rs541390747;rs11884681;rs533020241	22;29;45;49	
cg21346855	-0.26361988	0.5529822	-4.54175059	0.01512217	0.77305885	-2.51860292	14	1.02E+08	R	II	MIR544A	TSS200	opensea	TSS200-opensea		rs539086957;rs559112867	30;25	
cg09179973	0.256660315	0.3065644	4.539452483	0.01514523	0.77305885	-2.52029187	11	33843608	F	II		IGR	opensea	IGR-opensea		rs12276001		1
cg27241753	-0.21631349	0.54461651	-4.5154617	0.01538856	0.77438217	-2.5379704	8	53205926	F	II	ST18	5'UTR	opensea	5'UTR-opensea		rs564238967;rs531528800;rs183859637	0;11;15	
cg23949067	0.202789652	0.33129226	4.505924958	0.01548665	0.77438217	-2.54502178	9	88023575	F	II		IGR	opensea	IGR-opensea				
cg00209050	-0.20379916	0.79283987	-4.50335916	0.01551317	0.77438217	-2.54692123	20	16801919	R	II		IGR	opensea	IGR-opensea		rs533504157;rs147601762	48;2	
cg27473053	-0.20899481	0.50506701	-4.49506579	0.0155993	0.77492141	-2.55306753	19	50472464	R	II	SIGLEC16	TSS1500	opensea	TSS1500-opensea		rs7246244;rs181738861	50;49	
cg20013963	0.207142646	0.61449784	4.493192506	0.01561883	0.77492141	-2.55445727	7	34978959	R	II	DPY19L1	Body	opensea	Body-opensea				
cg05094970	-0.24635835	0.45956627	-4.49198478	0.01563145	0.77492141	-2.55535353	16	26799507	R	II		IGR	opensea	IGR-opensea		rs574775946;rs543765668	23;18	
cg01233015	-0.28879803	0.48523001	-4.48696174	0.01568404	0.77498654	-2.5590835	7	1.53E+08	R	II		IGR	shore	IGR-shore	chr7:152591458-152591706			
cg14997132	0.291443568	0.43057201	4.475632137	0.01580348	0.77521251	-2.56751049	5	82771274	R	II	VCAN	5'UTR	shore	5'UTR-shore	chr5:82770148-82770599			
cg18935575	-0.21625845	0.47310361	-4.4616169	0.01595281	0.7754526	-2.57796183	7	1.14E+08	F	II		IGR	opensea	IGR-opensea				
cg00637744	-0.2087027	0.39632561	-4.45351325	0.01603997	0.7754526	-2.58401837	2	59239404	R	II	LINC01122	Body	opensea	Body-opensea		rs11687358;rs113060170;rs549098507	38;30;20	
cg13987192	0.235902646	0.4332114	4.452428575	0.01605168	0.7754526	-2.5848298	12	6933322	F	II	GPR162	Body	island	Body-island	chr12:6933276-6933605			
cg00626846	0.221546147	0.53493353	4.447316276	0.01610702	0.7756896	-2.58865661	20	58028119	R	II		IGR	opensea	IGR-opensea		rs544606310;rs559688884;rs527597093	35;22;2	
cg17119907	0.232624266	0.62190521	4.445065319	0.01613147	0.7756896	-2.59034281	12	1.18E+08	R	I	NOS1	5'UTR	shore	5'UTR-shore	chr12:117798076-117799448	rs573218123;rs368185075;rs555630934	42;29;2	
cg08592304	-0.23924644	0.28577128	-4.43015478	0.01629456	0.77617979	-2.60153185	15	35060564	R	II	LOC101928174	Body	opensea	Body-opensea		rs187576245;rs112428392	49;13	
cg00495320	0.215961342	0.4661852	4.428681769	0.01631078	0.77617979	-2.60263904	8	73454968	F	II	KCNB2	5'UTR	opensea	5'UTR-opensea		rs560702797		0
cg17188793	0.204206593	0.35909316	4.42482835	0.01635332	0.77633497	-2.60553705	10	21806896	R	II	SKIDA1	5'UTR	shore	5'UTR-shore	chr10:21805879-21806630	rs41277378		40
cg21397540	0.243735115	0.57363923	4.383367398	0.01681994	0.77709472	-2.6368618	1	2.48E+08	R	II		IGR	opensea	IGR-opensea		rs10925000;rs533876990;rs12043526	35;18;15	
cg07674459	-0.23763963	0.60824858	-4.38195477	0.01683613	0.77712188	-2.63793372	15	1.01E+08	R	II	FLJ42289	TSS1500	shore	TSS1500-shore	chr15:100890242-100890494	rs73485998;rs189836683	17;1	
cg21930362	-0.21120233	0.59682514	-4.37574712	0.01690751	0.77715927	-2.64264779	3	1.51E+08	R	II	IGSF10	Body	opensea	Body-opensea		rs181702818		48
cg02483554	0.205872917	0.66152133	4.369736324	0.01697699	0.77743017	-2.64721802	10	35894194	F	II	GJD4	TSS200	shelf	TSS200-shelf	chr10:35896518-35897461	rs138770920;rs189212984;rs2384382;rs141709498;rs367741033;rs146254090	0;13;17;38;45;47	
cg02946570	-0.20190546	0.32993658	-4.36341954	0.01705039	0.77774378	-2.65202691	2	21023387	R	II	C2orf43	TSS1500	shore	TSS1500-shore	chr2:21022564-21022934	rs555123916;rs574968165	43;14	

cg00761160	0.245474412	0.51126232	4.347562005	0.01723641	0.77890514	-2.66412622	2	2.37E+08	R	II		IGR	opensea	IGR-opensea		rs529891862;rs187393350;rs192287729	42;41;30	
cg14010852	0.227269799	0.40269572	4.344924899	0.01726759	0.77890514	-2.6661421	4	72903914	F	II	NPFFR2	Body	opensea	Body-opensea		rs188528011		34
cg09564946	0.260523892	0.41798346	4.336018471	0.01737343	0.77890514	-2.67295843	20	18834994	F	II		IGR	opensea	IGR-opensea		rs140525862;rs563261530	0;20	
cg00232772	0.26641349	0.25440637	4.331823364	0.01742356	0.77890514	-2.67617332	20	1612808	F	II	SIRPG-AS1	TSS1500	opensea	TSS1500-opensea		rs143750401;rs1535883;rs183513542	8;11;33	
cg23501439	0.207415455	0.76642411	4.310665796	0.01767918	0.77890514	-2.69242901	7	819747	R	II	HEATR2	Body	shore	Body-shore	chr7:821689-822634	rs545458312;rs140641290;rs113906181	41;38;12	
cg02380180	-0.21356112	0.40275302	-4.30496627	0.01774885	0.77890514	-2.69681998	18	21417764	F	II	LAMA3	Body	opensea	Body-opensea				
cg16686789	-0.24892623	0.34738788	-4.29508951	0.01787038	0.77890514	-2.70444116	10	1.33E+08	R	II		IGR	shore	IGR-shore	chr10:132583720-132584164	rs569567690;rs146218562	46;2	
cg21565690	-0.2496693	0.69363017	-4.29235673	0.01790419	0.77890514	-2.70655254	14	78720727	R	II	NRXN3	Body	opensea	Body-opensea		rs191472210;rs74065956;rs549181868	49;48;2	
cg09481000	-0.23006194	0.52511409	-4.29198531	0.01790879	0.77890514	-2.7068396	8	35401713	R	II	UNC5D	Body	opensea	Body-opensea		rs548457401;rs569799232;rs7002972	51;17;14	
cg13987498	-0.24752302	0.45612469	-4.2915284	0.01791446	0.77890514	-2.70719275	12	1.03E+08	F	II	PAH	ExonBnd	opensea	ExonBnd-opensea		rs187133779;rs191142120;rs140175796;rs200366386	1;19;23;37	
cg23384326	0.205303397	0.3439132	4.282384953	0.01802825	0.77890514	-2.7142668	22	24912201	F	II	UPB1	Body	opensea	Body-opensea		rs184265454;rs6004171;rs566830509;rs11704820	19;31;46;47	
cg08815515	0.208889577	0.60499521	4.276262132	0.01810495	0.77890514	-2.71901121	2	1.2E+08	R	II	CFAP221	Body	opensea	Body-opensea		rs12999064;rs59301232	17;13	
cg23897667	0.200880734	0.60652732	4.27414147	0.01813162	0.77890514	-2.72065583	8	98572582	F	II		IGR	opensea	IGR-opensea		rs554126070;rs115542777	29;32	
cg27204474	0.209342089	0.43109888	4.273951147	0.01813401	0.77890514	-2.72080346	X	1.3E+08	F	II	FLJ30058	TSS1500	shore	TSS1500-shore	chrX:130192131-130192735			
cg26170191	-0.2030953	0.55553736	-4.26806185	0.01820833	0.77890514	-2.72537462	14	23763073	R	II		IGR	opensea	IGR-opensea		rs534196352;rs74793897	34;17	
cg14776612	-0.25872667	0.28591446	-4.2531894	0.0183977	0.77890514	-2.73694265	2	1.16E+08	R	II	DPP10-AS3	TSS1500	opensea	TSS1500-opensea		rs185033505		49
cg07462594	-0.22059609	0.50467541	-4.24784016	0.01846642	0.77890514	-2.74111191	5	27110547	F	II		IGR	opensea	IGR-opensea		rs181966226;rs535157011	0;40	
cg08979000	-0.20365174	0.37354972	-4.23939036	0.01857562	0.77922935	-2.74770701	4	19384884	F	II		IGR	opensea	IGR-opensea				
cg11050858	-0.20894057	0.65045622	-4.23920779	0.01857799	0.77922935	-2.74784964	9	1.16E+08	R	II	ZNF883	Body	opensea	Body-opensea		rs116612685		2
cg00899400	0.261798114	0.51967355	4.233849502	0.01864767	0.77922935	-2.75203781	7	27154537	F	II	HOXA3	5'UTR	shore	5'UTR-shore	chr7:27154999-27155426	rs569887316		1
cg17898737	0.213356926	0.69739903	4.233215985	0.01865593	0.77922935	-2.75253328	7	69459947	R	II	AUTS2	Body	opensea	Body-opensea		rs542338290;rs145453170	22;1	
cg00868652	-0.2369163	0.47695086	-4.22563728	0.01875509	0.77922935	-2.75846553	15	50411535	F	II	ATP8B4	TSS200	opensea	TSS200-opensea		rs533592730		10
cg23769249	0.216098635	0.54305502	4.223947608	0.01877729	0.77922935	-2.75978937	13	67957902	F	II		IGR	opensea	IGR-opensea		rs573943115		33
cg13605674	-0.24547615	0.39605328	-4.22266955	0.0187941	0.77922935	-2.76079101	3	1.96E+08	F	II	TM4SF19	TSS200	opensea	TSS200-opensea				
cg00962459	0.254574616	0.63494346	4.205936303	0.01901598	0.77922935	-2.77392922	2	68871642	F	II	PROKR1	TSS1500	shore	TSS1500-shore	chr2:68870351-68871055			
cg04978236	0.269429808	0.61395334	4.204454217	0.01903579	0.77922935	-2.77509504	11	65802195	R	II		IGR	opensea	IGR-opensea		rs373871707;rs549282848	47;13	
cg13161013	-0.22234659	0.51459979	-4.20205409	0.01906792	0.77922935	-2.77698374	6	84567967	F	II	CYB5R4	TSS1500	shore	TSS1500-shore	chr6:84569263-84569619	rs576036878		3
cg26690742	0.213638275	0.34386837	4.198960891	0.01910943	0.77931086	-2.77941919	11	2889602	R	II		IGR	shore	IGR-shore	chr11:2890388-2891337			
cg04260375	-0.20085643	0.33931399	-4.17700467	0.01940738	0.77973473	-2.79675049	4	16828308	R	II	LDB2	Body	opensea	Body-opensea		rs149925594;rs550041173;rs182299256	34;9;1	
cg26605476	-0.20809108	0.54894839	-4.16377972	0.01958965	0.77973473	-2.80722699	16	1214867	R	I	CACNA1H	Body	shelf	Body-shelf	chr16:1217128-1217336	rs545001665;rs564923919;rs527401151	36;29;1	
cg03278568	-0.2032188	0.33395984	-4.16185602	0.01961634	0.77973473	-2.80875324	5	5166415	F	II	ADAMTS16	Body	opensea	Body-opensea		rs34627029;rs551430566	0;3	
cg15763498	0.20205714	0.43602297	4.1565577	0.01969009	0.77973473	-2.81295998	10	50588096	F	II	DRGX	Body	opensea	Body-opensea		rs147934589;rs536450334	2;21	
cg15212549	-0.23410684	0.43881843	-4.14981784	0.0197844	0.77973473	-2.81831779	6	68606787	R	II		IGR	opensea	IGR-opensea		rs558552483		1
cg04713176	0.221851004	0.62083515	4.137777522	0.0199543	0.77973473	-2.82790742	12	4497426	F	II		IGR	opensea	IGR-opensea		rs115661923		21
cg06524362	0.204356707	0.4393252	4.132125923	0.02003467	0.78005694	-2.83241676	4	1.77E+08	R	II	SPCS3	TSS1500	shore	TSS1500-shore	chr4:177240935-177241832			
cg08737581	-0.22944138	0.32757954	-4.13020425	0.02006209	0.78005694	-2.83395122	5	7374151	F	II		IGR	opensea	IGR-opensea		rs540036294;rs555130873	15;28	
cg05505103	-0.28190826	0.40068583	-4.12918343	0.02007668	0.78007271	-2.83476659	11	1.1E+08	R	II		IGR	opensea	IGR-opensea		rs539499504;rs557749236;rs566822399	46;36;18	
cg13954541	-0.29404504	0.29667581	-4.12451681	0.02014353	0.78043338	-2.83849615	5	2862136	F	II		IGR	opensea	IGR-opensea		rs550445450;rs571874890;rs16870587	14;29;32	
cg09278646	0.216181222	0.5262504	4.120422185	0.02020241	0.78043338	-2.84177147	3	1.67E+08	R	II	SERPINI1	5'UTR	opensea	5'UTR-opensea		rs193036369;rs185298005	4;1	
cg14357814	-0.24573367	0.699184	-4.11615996	0.02026393	0.78043338	-2.84518375	3	51861073	F	II	IQCF3	1stExon	opensea	1stExon-opensea		rs546221559		39
cg26750446	-0.21869804	0.49117569	-4.11228013	0.02032014	0.78043338	-2.84829246	11	64438853	F	II	NRXN2	Body	opensea	Body-opensea				
cg03419646	0.212062783	0.48793542	4.102234027	0.02046658	0.78043338	-2.85635324	17	47297268	F	I	ABI3	Body	island	Body-island	chr17:47296969-47297314	rs573287028;rs199635084;rs616338	2;26;29	
cg11508001	0.225419161	0.54434416	4.101427729	0.02047839	0.78043338	-2.8570009	8	97399716	F	II		IGR	opensea	IGR-opensea		rs569081179;rs531597015	0;34	
cg18700428	0.22514581	0.57428013	4.097585614	0.02053478	0.78043338	-2.86008858	16	3243304	R	II		IGR	island	IGR-island	chr16:3243303-3243583	rs575170324;rs144106111;rs547294631	43;39;34	
cg01056637	-0.20335311	0.50224067	-4.08921851	0.02065827	0.78043338	-2.86682104	13	26380861	F	II	ATP8A2	Body	opensea	Body-opensea		rs553176162;rs557886007	0;4	
cg16993682	0.207095868	0.502327	4.086970741	0.0206916	0.78044018	-2.86863162	1	1.58E+08	F	II	CD1C	TSS1500	opensea	TSS1500-opensea		rs190508207		1
cg20032280	0.211186745	0.52576822	4.078776123	0.02081368	0.78095369	-2.87523936	3	1.13E+08	F	II	CFAP44	TSS1500	island	TSS1500-island	chr3:113160299-113160641	rs183606005;rs568588213;rs535542797	0;8;45	
cg05342235	-0.25520519	0.4943592	-4.05427736	0.02118408	0.78181452	-2.89505955	10	70426406	R	II	TET1	Body	opensea	Body-opensea		rs541274933		35
cg04100843	0.211067611	0.5791548	4.035592157	0.02147211	0.78277221	-2.9102426	4	4860655	R	II	MSX1	TSS1500	shore	TSS1500-shore	chr4:4861227-4862241	rs537228783		19
cg08164294	0.25887295	0.43841428	4.03339938	0.02150624	0.78277221	-2.91202816	7	27154387	F	II	HOXA3	5'UTR	shore	5'UTR-shore	chr7:27154999-27155426	rs547470262		9
cg00417735	-0.21471232	0.44591439	-4.03214365	0.02152581	0.78277221	-2.91305104	3	28070292	F	II		IGR	opensea	IGR-opensea		rs560607552;rs17020851;rs145663859	0;9;21	
cg23979412	0.204902009	0.29300322	4.027784085	0.02159392	0.78302419	-2.91660425	18	44776850	F	II		IGR	shore	IGR-shore	chr18:44777632-44778084	rs77243045		32
cg21147282	0.211629955	0.64786546	4.023525472	0.02166072	0.78337569	-2.92007821	7	18868877	F	II	HDAC9	Body	opensea	Body-opensea		rs115552810;rs138291818	28;30	
cg11272217	-0.20515846	0.34157985	-4.02062489	0.02170637	0.78337569	-2.92244607	20	15965838	R	II	LOC613266	Body	opensea	Body-opensea		rs564694781;rs576927628	50;1	
cg27606935	0.266940522	0.66905094	4.015430614	0.02178841	0.78337569	-2.92668984	7	1.4E+08	R	II	SLC37A3	Body	opensea	Body-opensea		rs140597201;rs577466422	51;1	
cg00016934	0.20516359	0.39193155	4.014598064	0.0218016	0.78337569	-2.92737046	X	40035961	F	I	BCOR	5'UTR	island	5'UTR-island	chrX:40034239-40036007			
cg00436282	-0.23055573	0.29949971	-4.0138991	0.02181267	0.78337569	-2.92794196	4	70861449	F	II	STATH	TSS200	opensea	TSS200-opensea		rs141720087		9
cg00566038	-0.20610441	0.47276045	-4.00982846	0.02187733	0.78337569	-2.93127186	7	35560296	F	II		IGR	opensea	IGR-opensea		rs557437971		51
cg24242952	-0.23173406	0.55565385	-3.99744182	0.02207554	0.78337569	-2.94142137	13	38020806	R	II		IGR	opensea	IGR-opensea		rs570527719		19
cg13408655	-0.20026997	0.70508272	-3.99528075	0.02211035	0.78337569	-2.94319474	9	1.02E+08	F	II	COL15A1	Body	opensea	Body-opensea		rs559692964;rs528876645	35;39	
cg22930848	0.233356036	0.42846198	3.991115328	0.02217764	0.78337569	-2.94661507	3	8407419	R	II	LMCD1-AS1	Body	opensea	Body-opensea				
cg23054121	0.25957872	0.52087201	3.98840015	0.02222164	0.78337569	-2.94884612	11	2423159	R	II	TSSC4	TSS1500	shore	TSS1500-shore	chr11:2421040-2422474	rs556954315		25
cg15754660	-0.21208228	0.39023855	-3.98497388	0.02227732	0.78337569	-2.95166321	7	34699393	F	II	NPSR1	Body	opensea	Body-opensea		rs537514224;rs554763142;rs574530836;rs147474497	1;7;38;49	
cg23366166	-0.2125917	0.44079865	-3.97919732	0.02237158	0.78337569	-2.95641715	11	1.25E+08	R	II	FEZ1	TSS1500	shore	TSS1500-shore	chr11:125365137-125366319	rs181082316		10
cg11698924	0.222863742	0.5334851	3.978601651	0.02238133	0.78337569	-2.95690769	22	40322751	F	II	GRAP2	1stExon	opensea	1stExon-opensea		rs370366466		0
cg13723989	0.24597804	0.6397008	3.977763055	0.02239507	0.78337569	-2.95759838	8	42127640	F	II	IKBKB	TSS1500	shore	TSS1500-shore	chr8:42128689-42129141	rs17875739;rs193007451;rs7825781	3;14;16	
cg27410271	0.210298012	0.54023971	3.973802428	0.02246007	0.78337569	-2.96086201	12	99549103	R	II	ANKS1B	TSS1500	opensea	TSS1500-opensea		rs576581741;rs544024702	39;34	
cg23144895	0.211378668	0.60174003	3.96422412	0.02261825	0.78337569	-2.96876555	8	90913629	R	II	OSGIN2	TSS1500	shore	TSS1500-shore	chr8:90914197-90915340	rs570502869		2
cg07699991	0.244423127	0.52438766	3.951935868	0.02282322	0.78337569	-2.97892762	22	40228842	F	II	ENTHD1	Body	opensea	Body-opensea		rs552569074;rs188941686;rs77373343;rs550788567	0;1;9;38	
cg25199226	-0.23311434	0.39629169	-3.94368015	0.02296223	0.78337569	-2.98576909	10	26599430	R	II		IGR	opensea	IGR-opensea		rs532107921		44
cg25890050	-0.20641158	0.57154075	-3.92173328	0.02333692	0.78457276	-3.00401189	8	41255897	R	II		IGR	opensea	IGR-opensea		rs187076722;rs192329240	51;1	
cg17960432	-0.26412525	0.47397003	-3.90821709	0.02357147	0.78497277	-3.01528718	2	52022999	F	II		IGR	opensea	IGR-opensea		rs374034298		0
cg04440551	0.322198258	0.36777922	3.902788591	0.0236665	0.78502385	-3.01982435	2	25051151	F	II	ADCY3	Body	opensea	Body-opensea				
cg23171972	0.216317964	0.5899675	3.900489469	0.02370689	0.78521751	-3.02174746	8	1.43E+08	R	I		IGR	shore	IGR-shore	chr8:143202654-143202868	rs148630342;rs10096519;rs10095704;rs555443159;rs574384209;rs538493344	44;43;39;33;23;12	
cg21843573	-0.24922099	0.32904247	-3.89501234	0.02380346	0.78521939	-3.02633243	6	1.18E+08	R	II	ROS1	Body	opensea	Body-opensea				
cg02172711	0.207762402	0.63274947	3.886594999	0.02395282	0.78558449	-3.03338857	15	44964622	R	II	PATL2	Body	opensea	Body-opensea		rs374952072;rs553403732	44;39	
cg01680244	-0.20665271	0.50216895	-3.87438171	0.02417162	0.78611518	-3.04364812	8	59476467	R	II	SDCBP	5'UTR	opensea	5'UTR-opensea		rs530000509;rs189805150	39;12	
cg04281303	-0.21236227	0.44348866	-3.87265484	0.02420275	0.78632817	-3.04510078	15	31763329	F	II		IGR	opensea	IGR-opensea		rs549195859		41
cg09304797	0.26205505	0.76291807	3.872128062	0.02421226	0.78635615	-3.04554402	7	67950674	R	II		IGR	opensea	IGR-opensea				
cg03697809	-0.21476838	0.40208542	-3.86891646	0.02427033	0.78649149	-3.0482473	X	1.07E+08	F	II		IGR	island	IGR-island	chrX:106749879-106750862			
cg04481189	0.22707213	0.6731468	3.868605704	0.02427596	0.78649149	-3.04850896	7	1.38E+08	F	II	SVOPL	TSS1500	opensea	TSS1500-opensea		rs183528140;rs58930234	45;46	
cg14444957	0.203192138	0.32337961	3.862485822	0.02438713	0.78657974	-3.05366537	17	49707886	F	II	CA10	3'UTR	opensea	3'UTR-opensea		rs144362878;rs192457236	14;15	
cg03207666	-0.20822372	0.52761333	-3.86038314	0.02442547	0.78657974	-3.05543849	7	27183950	F	II	HOXA5	TSS1500	island	TSS1500-island	chr7:27182613-27185562	rs183291358;rs566898073;rs535764423;rs555627142;rs575463907	7;19;33;36;44	
cg21200408	0.202271747	0.24685234	3.85948481	0.02444187	0.78657974	-3.05619624	20	21378211	F	I	NKX2-4	TSS200	island	TSS200-island	chr20:21376358-21378245	rs527557171		43
cg27629134	-0.20850387	0.48705647	-3.85890015	0.02445255	0.78657974	-3.05668949	2	2.1E+08	F	II		IGR	opensea	IGR-opensea		rs561567113;rs530360369;rs141887596	0;1;5	
cg14849556	0.252651215	0.56600645	3.845254466	0.02470354	0.78657974	-3.06821814	2	24991672	F	II	NCOA1	3'UTR	opensea	3'UTR-opensea		rs555517622		1
cg09275548	0.324793152	0.42052887	3.829060088	0.02500559	0.78713991	-3.08194124	15	55348908	F	II		IGR	opensea	IGR-opensea		rs114233552		4
cg00377915	0.243189913	0.29280673	3.827187685	0.0250408	0.78713991	-3.0835308	10	70631035	F	II	STOX1	5'UTR	opensea	5'UTR-opensea		rs200160059;rs573777098	0;37	
cg02921824	0.229068948	0.48138599	3.820959507	0.02515839	0.78713991	-3.08882248	3	1.08E+08	R	II	HHLA2	ExonBnd	opensea	ExonBnd-opensea		rs578129688		31
cg19385283	-0.26520148	0.43152798	-3.81527359	0.02526634	0.78713991	-3.09365922	2	75865060	F	II		IGR	opensea	IGR-opensea		rs191330338;rs151015908;rs555710288;rs574298020	0;1;25;51	
cg08800574	-0.26252095	0.64535193	-3.81514937	0.02526871	0.78713991	-3.09376495	14	1.02E+08	F	II		IGR	opensea	IGR-opensea		rs11622062;rs144976013	4;11	
cg06855215	0.223264595	0.43530351	3.806805374	0.02542819	0.78713991	-3.100873	11	3870792	F	II		IGR	opensea	IGR-opensea		rs2193		7
cg01303032	-0.28115268	0.41142874	-3.80339967	0.02549364	0.78713991	-3.10377766	10	25940372	R	II		IGR	opensea	IGR-opensea		rs186427753;rs528930126;rs548648730	24;22;2	
cg02891218	-0.21160038	0.32522987	-3.80271578	0.02550681	0.78713991	-3.10436118	7	99612634	F	II	ZKSCAN1	TSS1500	shore	TSS1500-shore	chr7:99613104-99613797			
cg02292985	0.240923492	0.67104442	3.77644939	0.02601902	0.78718522	-3.12683336	20	61498871	F	II		IGR	opensea	IGR-opensea		rs575427038;rs546119032	1;20	
cg12828483	0.239432694	0.61200023	3.772809607	0.02609101	0.78718522	-3.12995673	20	62792468	R	II		IGR	opensea	IGR-opensea		rs575898253		41
cg12828896	-0.28586058	0.5814325	-3.77160246	0.02611494	0.78718522	-3.13099312	15	45005365	R	II	B2M	Body	shore	Body-shore	chr15:45003460-45004345			
cg17001652	-0.20899244	0.46156335	-3.76715551	0.02620332	0.78718522	-3.13481317	4	78432403	F	II	CXCL13	TSS1500	opensea	TSS1500-opensea		rs180964154		36
cg18436984	-0.20957654	0.41618327	-3.7638985	0.02626829	0.78718522	-3.1376132	7	27198374	F	II		IGR	island	IGR-island	chr7:27198182-27198514	rs189813246;rs578060226;rs568423281	1;11;34	
cg03620962	0.212819298	0.58261046	3.752599149	0.02649523	0.78718522	-3.14734135	3	1.35E+08	R	II	EPHB1	TSS1500	shore	TSS1500-shore	chr3:134514085-134515980			
cg03546739	-0.2006981	0.51749205	-3.74938339	0.02656026	0.78718522	-3.15011399	7	6713037	F	II		IGR	opensea	IGR-opensea		rs532098609		11
cg02095987	0.20194704	0.62432041	3.741114893	0.02672839	0.78731406	-3.15725133	X	71435936	R	II	PIN4	Body	opensea	Body-opensea				
cg09250994	-0.24985397	0.43829124	-3.7258675	0.02704189	0.78811565	-3.1704439	19	8642571	R	II	MYO1F	TSS1500	opensea	TSS1500-opensea		rs148681216;rs7252938	22;21	
cg26545913	-0.24382017	0.4962537	-3.71811493	0.02720304	0.78811565	-3.17716715	6	66819090	F	II		IGR	opensea	IGR-opensea		rs562211785		34
cg13821075	0.204324559	0.54412574	3.716172174	0.02724361	0.78811565	-3.17885361	6	68936152	F	II		IGR	opensea	IGR-opensea		rs532931753		0
cg10239804	0.21606535	0.4856488	3.711013518	0.0273517	0.78830405	-3.18333488	12	48498370	R	II	PFKM	TSS1500	shore	TSS1500-shore	chr12:48499463-48500232	rs11168408;rs563225742	45;14	
cg19660531	-0.23601812	0.69788891	-3.70884479	0.0273973	0.78840768	-3.18522022	12	5937409	R	I	ANO2	Body	shore	Body-shore	chr12:5936876-5937085	rs115973080;rs7136856;rs7310673;rs570765675	44;29;27;7	
cg04989185	-0.2135909	0.32882818	-3.70617713	0.02745353	0.78852214	-3.1875404	8	9790928	F	II		IGR	shore	IGR-shore	chr8:9791236-9791450	rs183498173;rs186952908;rs140908757;rs550667475	20;37;43;51	
cg25448861	-0.25994729	0.33361376	-3.70244709	0.02753238	0.7887003	-3.19078667	12	1.19E+08	R	II	SRRM4	Body	opensea	Body-opensea		rs79171793		2
cg06705930	0.20649452	0.39119754	3.687336449	0.02785469	0.78938653	-3.20396235	11	31823191	R	II	PAX6	Body	shore	Body-shore	chr11:31820060-31821416	rs571551224		12
cg22421661	0.233818128	0.53077326	3.667360484	0.02828799	0.79053457	-3.22144152	8	38643592	F	II	TACC1	TSS1500	shore	TSS1500-shore	chr8:38644473-38645760	rs6981210		48
cg00702593	-0.20161019	0.3446788	-3.65646877	0.02852776	0.79098052	-3.23100129	21	42219853	F	II	DSCAM	TSS1500	shore	TSS1500-shore	chr21:42218489-42219222			
cg14066865	-0.23378162	0.51066127	-3.65498111	0.02856071	0.79098052	-3.23230864	2	2.2E+08	F	II		IGR	shelf	IGR-shelf	chr2:219906107-219906328	rs80319789		20
cg14755712	-0.33188594	0.51570973	-3.65362514	0.02859078	0.79098052	-3.2335006	5	1.81E+08	R	II		IGR	shore	IGR-shore	chr5:180527368-180528782	rs183849381;rs6601174	34;2	
cg02679542	0.209064061	0.41720103	3.645847928	0.028764	0.79102971	-3.24034335	17	6502578	R	II	KIAA0753	Body	opensea	Body-opensea				
cg22606224	0.208535824	0.30056121	3.644198565	0.0288009	0.7911727	-3.2417959	19	12266489	R	I	ZNF625	5'UTR	shore	5'UTR-shore	chr19:12266998-12267686	rs149162705		37
cg17162578	0.249347999	0.51355538	3.643909303	0.02880738	0.79118576	-3.24205069	20	61609595	R	II		IGR	shelf	IGR-shelf	chr20:61612284-61612501	rs555961450		43
cg25631489	0.221902078	0.39925704	3.639071972	0.02891598	0.79151785	-3.2463138	3	1.7E+08	R	II	PHC3	TSS1500	shore	TSS1500-shore	chr3:169898946-169899626			
cg22839447	-0.21172401	0.58329159	-3.62716029	0.02918557	0.79157154	-3.25682903	17	10561350	F	II	MYH3	TSS1500	opensea	TSS1500-opensea		rs78304742		37
cg12363682	-0.20105225	0.46349102	-3.62000362	0.02934904	0.79192673	-3.2631587	5	1.78E+08	R	II	GRM6	Body	shore	Body-shore	chr5:178421225-178422337	rs534525393;rs552799921	25;16	
cg08902683	-0.22725395	0.54152526	-3.61438556	0.02947816	0.79203238	-3.26813388	5	1.79E+08	F	II	ADAMTS2	Body	opensea	Body-opensea		rs139486415;rs544842954;rs183053070	0;1;42	
cg13304297	0.240138498	0.42875958	3.613502093	0.02949853	0.79203238	-3.26891676	3	1.68E+08	R	II	C3orf50	Body	shore	Body-shore	chr3:167967246-167968130			
cg05083977	0.212549033	0.71912634	3.610686574	0.02956356	0.79203238	-3.27141262	3	62536266	F	II	CADPS	Body	opensea	Body-opensea		rs115813148;rs188523922	1;19	
cg04248439	-0.23761295	0.58387255	-3.61008495	0.02957748	0.79203238	-3.27194613	19	11917291	F	II	ZNF491	Body	opensea	Body-opensea		rs151175533		1
cg26485159	0.231728315	0.38268726	3.608264599	0.02961964	0.79207273	-3.27356074	5	4511755	F	II		IGR	opensea	IGR-opensea				
cg26819695	0.207949221	0.40449606	3.606873605	0.02965191	0.79227626	-3.27479493	11	1.23E+08	R	I	ASAM	TSS1500	island	TSS1500-island	chr11:123066517-123066986			
cg02557525	-0.27483192	0.51216397	-3.60386956	0.02972174	0.79248363	-3.27746148	X	54369620	R	II	WNK3	5'UTR	opensea	5'UTR-opensea				
cg01320942	-0.24547808	0.27408381	-3.60273818	0.0297481	0.79261159	-3.27846617	2	1000195	F	II	SNTG2	Body	opensea	Body-opensea		rs139240195		32
cg03261496	0.205216702	0.42031766	3.600266479	0.02980577	0.79271996	-3.28066187	5	37947821	F	II		IGR	opensea	IGR-opensea		rs11740447;rs531969818;rs550854189;rs143836048	0;12;36;46	
cg12893151	0.214802437	0.67064015	3.596013673	0.02990533	0.79293446	-3.28444232	18	25141676	F	II		IGR	opensea	IGR-opensea		rs567008307;rs191908382	0;1	
cg05678733	0.215734236	0.43283139	3.59281675	0.02998045	0.79293446	-3.28728627	5	43010511	F	II		IGR	opensea	IGR-opensea		rs111913557		19
cg23117343	0.259974363	0.55153297	3.578801915	0.0303125	0.7933954	-3.29977504	2	1.7E+08	R	II		IGR	opensea	IGR-opensea		rs141491126;rs150720810	34;2	
cg26388509	0.219742343	0.26091178	3.576599648	0.03036509	0.7933954	-3.30174067	7	1.55E+08	F	II	CNPY1	Body	shelf	Body-shelf	chr7:155302253-155303158	rs144666756		0
cg09136878	0.225998101	0.44512905	3.562216703	0.03071134	0.79341286	-3.31459925	1	2.36E+08	F	II		IGR	opensea	IGR-opensea				
cg13679778	0.214008076	0.38668439	3.559461492	0.03077823	0.79341991	-3.31706664	6	28493019	F	II	GPX5	TSS1500	opensea	TSS1500-opensea				
cg20510272	-0.27329067	0.38500906	-3.54451648	0.03114418	0.79399777	-3.33047392	1	2.04E+08	R	II	GOLT1A	TSS1500	opensea	TSS1500-opensea				
cg08889023	0.227712033	0.70651034	3.543525949	0.03116862	0.79399777	-3.33136393	17	517799	R	II	VPS53	Body	opensea	Body-opensea		rs142795244;rs560299108	35;2	
cg23391041	0.259047401	0.5886127	3.533692374	0.03141258	0.79477653	-3.34020908	2	65136014	R	II	LOC400958	Body	opensea	Body-opensea		rs34318496;rs542666856;rs552786444;rs572750523;rs574693262	47;33;32;11;2	
cg25590826	0.207433274	0.50462279	3.531887791	0.0314576	0.79504406	-3.34183415	15	74557537	F	II	CCDC33	Body	opensea	Body-opensea		rs528824392		7
cg15755295	-0.2837777	0.32325322	-3.52886185	0.03153328	0.79504843	-3.34456038	7	8728722	F	II	NXPH1	Body	opensea	Body-opensea		rs574273091;rs541739018;rs183960507;rs144766452	2;8;27;45	
cg14552491	0.241358289	0.60743069	3.52852647	0.03154168	0.79504843	-3.34486264	4	4355169	R	II		IGR	opensea	IGR-opensea				
cg10326673	0.21878622	0.31172915	3.528279719	0.03154787	0.79504843	-3.34508503	2	30669757	R	II	LCLAT1	TSS1500	shore	TSS1500-shore	chr2:30669988-30670720	rs184507399		23
cg19534723	-0.20095178	0.71576193	-3.52627892	0.03159806	0.79504843	-3.34688876	19	20147046	R	II	ZNF682	5'UTR	shelf	5'UTR-shelf	chr19:20149855-20150175	rs551443591;rs541910410	46;0	
cg21921361	0.201473396	0.45018157	3.507684161	0.03206927	0.79524804	-3.36368611	8	1.46E+08	F	II		IGR	shelf	IGR-shelf	chr8:146126088-146128055	rs543289733		15
cg25502018	0.218522388	0.7448873	3.507500857	0.03207395	0.79524804	-3.363852	2	1.73E+08	F	II	SLC25A12	Body	opensea	Body-opensea		rs573202132		1
cg08718108	-0.21493786	0.6333206	-3.50222753	0.03220919	0.79532481	-3.368627	5	1.78E+08	F	II		IGR	shelf	IGR-shelf	chr5:178367620-178368725	rs189861639;rs567218597;rs527640507;rs552615114;rs145840333	0;1;14;48;50	
cg20992700	0.200704381	0.64848174	3.501147282	0.03223697	0.79540992	-3.36960578	5	94392077	F	II	MCTP1	Body	opensea	Body-opensea		rs570759941;rs534527453	0;12	
cg25596209	0.248025434	0.61740664	3.484699132	0.03266377	0.79555636	-3.38453468	19	47912168	F	II	MEIS3	Body	shore	Body-shore	chr19:47910107-47910563	rs146583722;rs540246891;rs113404913	1;7;35	
cg25745795	0.233131297	0.44269784	3.471689008	0.0330063	0.79572524	-3.39637739	X	25030060	F	II	ARX	Body	shore	Body-shore	chrX:25030461-25032053			
cg01277538	-0.21904105	0.53216458	-3.46838929	0.03309388	0.79575229	-3.39938584	13	19813799	R	II		IGR	opensea	IGR-opensea		rs540081299;rs561526734;rs150490239	32;13;1	
cg16361596	-0.20156427	0.48512496	-3.46551954	0.03317028	0.79582934	-3.40200386	12	22089801	R	II	ABCC9	TSS200	opensea	TSS200-opensea				
cg17237813	0.227330544	0.7479435	3.462516863	0.03325045	0.79603688	-3.40474474	1	84465688	R	II	TTLL7	TSS1500	shore	TSS1500-shore	chr1:84464223-84465232			
cg10336925	0.242362046	0.4884073	3.460488964	0.03330473	0.79643926	-3.40659673	14	77647482	R	II	TMEM63C	TSS1500	shore	TSS1500-shore	chr14:77648108-77648328			
cg07145744	0.225084272	0.53426265	3.45341382	0.03349496	0.79677532	-3.41306396	3	43146836	F	II	C3orf39	5'UTR	shore	5'UTR-shore	chr3:43147184-43147713	rs537316724		29
cg24082680	0.231969723	0.42079896	3.451401093	0.03354933	0.79677532	-3.41490538	1	63249199	F	II	ATG4C	TSS1500	opensea	TSS1500-opensea				
cg04912710	-0.23772341	0.63139779	-3.44956138	0.03359911	0.79677532	-3.41658915	8	72460643	F	II		IGR	shore	IGR-shore	chr8:72459564-72460523	rs181622504;rs535828854	0;1	
cg20417115	-0.20200256	0.71151059	-3.44859804	0.03362522	0.79684115	-3.41747108	4	10443264	F	II	ZNF518B	3'UTR	opensea	3'UTR-opensea		rs565942267;rs140972700	1;51	
cg20485058	-0.20452758	0.568563	-3.44117967	0.03382708	0.79726665	-3.42426811	2	36157995	R	II		IGR	opensea	IGR-opensea		rs139772446		24
cg04764399	0.219713988	0.26375267	3.439924802	0.03386138	0.79728783	-3.42541885	19	40024487	R	II	EID2B	TSS1500	shore	TSS1500-shore	chr19:40022952-40023667			
cg16328558	0.271628187	0.47208047	3.438240703	0.03390747	0.79739912	-3.42696365	1	45766469	F	II		IGR	shelf	IGR-shelf	chr1:45769213-45769917	rs139764869;rs538430173	0;1	
cg20699586	-0.21330597	0.60235372	-3.43377551	0.03403005	0.79779818	-3.43106197	1	2.28E+08	R	I		IGR	island	IGR-island	chr1:227748423-227748860	rs532100028		27
cg05201388	-0.25549304	0.35919691	-3.41879722	0.03444525	0.79887548	-3.44483579	22	42854431	R	II		IGR	opensea	IGR-opensea		rs565568546		20
cg19276727	-0.25719904	0.52686931	-3.41338157	0.03459691	0.79901633	-3.44982588	11	1.24E+08	R	II	OR8G2	TSS1500	opensea	TSS1500-opensea		rs532955781;rs17128530;rs569395056	18;9;2	
cg23286333	-0.20932623	0.53221896	-3.41239717	0.03462457	0.79904785	-3.4507335	18	39112519	F	II		IGR	opensea	IGR-opensea		rs565373772		14
cg01590848	-0.22406941	0.41777345	-3.40120383	0.03494094	0.80007372	-3.46106601	19	39997622	F	II	DLL3	Body	island	Body-island	chr19:39997590-39998291	rs536480700		34
cg19656415	-0.2073198	0.47276361	-3.39798163	0.03503268	0.80011972	-3.46404459	8	41176850	R	II		IGR	opensea	IGR-opensea		rs181934545;rs185389274	29;1	
cg19366346	-0.20747743	0.43565084	-3.39759918	0.03504359	0.80011972	-3.46439825	19	40217838	R	II		IGR	opensea	IGR-opensea		rs385563;rs187054368;rs535235652;rs7249932	46;42;24;20	
cg08093052	-0.26248975	0.39614017	-3.39078413	0.03523866	0.80011972	-3.47070467	1	33407211	R	II	RNF19B	Body	opensea	Body-opensea		rs71278769;rs573825072	51;43	
cg02005231	0.235712467	0.54245125	3.39049624	0.03524693	0.80011972	-3.47097126	16	21115843	F	II	DNAH3	Body	opensea	Body-opensea		rs147238151		1
cg16751193	0.274633692	0.62317353	3.390222246	0.0352548	0.80011972	-3.471225	4	1.15E+08	R	II		IGR	opensea	IGR-opensea		rs186995206;rs533690938;rs569638644	46;45;22	
cg27634991	-0.21064431	0.30900209	-3.38894642	0.03529149	0.80011972	-3.47240666	6	1.38E+08	R	II	IFNGR1	Body	shelf	Body-shelf	chr6:137540126-137540678	rs75998408		26
cg01601188	-0.24137563	0.57550188	-3.37684966	0.03564169	0.80011972	-3.48362527	15	97404046	F	II		IGR	opensea	IGR-opensea		rs12910002		1
cg24350893	-0.20381731	0.43789527	-3.37335422	0.03574367	0.80011972	-3.48687188	7	22797835	F	II		IGR	opensea	IGR-opensea		rs17147254;rs71520380;rs138601086	0;4;45	
cg13924807	0.205203928	0.66955324	3.371291261	0.03580403	0.80011972	-3.48878902	5	1.54E+08	F	II		IGR	shelf	IGR-shelf	chr5:153989957-153990598	rs571053410		36

cg04259358	0.207713347	0.38624934	3.371061416	0.03581077	0.80011972	-3.48900266	10	1.2E+08	R	II		IGR	opensea	IGR-opensea		rs145900349;rs566583202	9;1	
cg00223681	0.210700543	0.48279114	3.369984684	0.03584233	0.80011972	-3.49000364	2	1.77E+08	R	II		IGR	shore	IGR-shore	chr2:177024501-177025692			
cg01970812	0.213827171	0.30084198	3.369631577	0.03585269	0.80011972	-3.49033195	10	1.11E+08	F	II	RNU6-53P	Body	opensea	Body-opensea		rs182514883		1
cg25124045	-0.20647512	0.59546389	-3.36933511	0.03586139	0.80011972	-3.49060761	5	52749655	F	II		IGR	opensea	IGR-opensea		rs529868118;rs78334675;rs187617960	20;27;46	
cg24075412	0.213427275	0.6598358	3.362822049	0.03605315	0.80011972	-3.49666765	17	77479966	R	I	HRNBP3	TSS1500	opensea	TSS1500-opensea				
cg05760182	0.209987606	0.67404064	3.356495027	0.03624065	0.80053425	-3.50256193	6	39078002	R	II	SAYSD1	5'UTR	opensea	5'UTR-opensea		rs566374917		35
cg22164577	-0.22499918	0.5183824	-3.3552789	0.03627682	0.80076787	-3.50369571	2	1.71E+08	F	II	UBR3	Body	shore	Body-shore	chr2:170683860-170684629	rs180704430		38
cg21501097	-0.20556863	0.25000293	-3.34990487	0.03643722	0.80082951	-3.50870905	12	1.33E+08	R	II		IGR	opensea	IGR-opensea		rs28460341;rs192374624;rs536028040	17;16;3	
cg24406162	-0.22300747	0.34676359	-3.34525365	0.03657674	0.80102284	-3.51305231	1	24017943	F	II	RPL11	TSS1500	shore	TSS1500-shore	chr1:24018355-24018567			
cg13753868	0.216647602	0.33897024	3.341118354	0.03670134	0.80102284	-3.51691709	19	2865997	F	II	ZNF556	TSS1500	opensea	TSS1500-opensea		rs143368970;rs550934709	25;34	
cg26154201	0.214843341	0.53925036	3.33204484	0.03697657	0.80135238	-3.52540791	20	238217	F	II	DEFB132	TSS200	opensea	TSS200-opensea		rs530991007;rs550888095;rs62189854	0;3;19	
cg17753390	-0.24456467	0.62472755	-3.33167739	0.03698777	0.80136763	-3.52575207	5	1.7E+08	R	II	KCNIP1	5'UTR	opensea	5'UTR-opensea		rs540996629;rs551495166	50;1	
cg13069322	0.280827438	0.62028934	3.326000249	0.03716133	0.80183329	-3.53107259	7	22047028	R	I		IGR	opensea	IGR-opensea		rs141315331;rs1174968;rs547318600	43;9;1	
cg22282089	0.205315798	0.38817786	3.321812159	0.03729	0.80183329	-3.53500134	13	30686841	F	II		IGR	shelf	IGR-shelf	chr13:30688864-30689335	rs377526591;rs618752;rs565508780	9;24;49	
cg05005604	-0.24345576	0.55102472	-3.32080685	0.03732097	0.80183329	-3.53594488	14	92810338	F	II	SLC24A4	Body	opensea	Body-opensea				
cg11220654	0.285642216	0.39623919	3.317751264	0.03741529	0.8019163	-3.53881381	15	59279345	R	II	RNF111	TSS1500	shore	TSS1500-shore	chr15:59279741-59280720	rs72745097;rs73414877	32;22	
cg03975781	0.222961174	0.53990522	3.317521202	0.03742241	0.8019428	-3.53902989	11	1.2E+08	F	II		IGR	opensea	IGR-opensea		rs538872354;rs557354111;rs575907975	39;45;46	
cg27497857	-0.23807642	0.58215904	-3.31667555	0.03744857	0.80197357	-3.53982422	7	1.29E+08	F	II		IGR	opensea	IGR-opensea				
cg13634918	0.226037581	0.57872537	3.315829583	0.03747476	0.80197357	-3.54061897	16	28984918	R	II	SPNS1	TSS1500	shore	TSS1500-shore	chr16:28985881-28986661	rs534948062		41
cg26892192	0.2730041	0.48286421	3.305316639	0.03780217	0.80215634	-3.55050633	7	25712342	R	II		IGR	opensea	IGR-opensea		rs564161345;rs190526049;rs146512706	23;12;1	
cg23376861	0.204242678	0.39657105	3.300339932	0.03795838	0.80265868	-3.55519389	18	43678713	F	II	ATP5A1	5'UTR	shore	5'UTR-shore	chr18:43677956-43678352			
cg15311873	-0.23669332	0.39364212	-3.29411823	0.03815479	0.80324868	-3.56106042	5	1.66E+08	F	II		IGR	opensea	IGR-opensea				
cg20426806	0.216946734	0.56263288	3.292615156	0.03820242	0.80348226	-3.56247875	13	32606102	R	II	FRY-AS1	TSS1500	shore	TSS1500-shore	chr13:32605320-32605903	rs424118;rs147785987;rs433551	35;27;17	
cg07378312	-0.23085979	0.44133187	-3.28939632	0.03830468	0.80388036	-3.56551747	2	2E+08	F	II		IGR	opensea	IGR-opensea		rs191272188		9
cg11148469	-0.20782323	0.45488107	-3.28760528	0.03836172	0.80402199	-3.5672091	5	1.4E+08	F	II	PCDHA5	TSS1500	shore	TSS1500-shore	chr5:140202573-140203610	rs6885319		16
cg14028400	0.20581618	0.30787042	3.283424366	0.03849529	0.80419764	-3.57116024	6	28793656	R	II		IGR	opensea	IGR-opensea		rs576670650;rs541551798;rs564467400	47;23;2	
cg06185593	0.333918304	0.3372857	3.270632592	0.03890751	0.80444183	-3.58326871	15	55348912	F	II		IGR	opensea	IGR-opensea		rs114233552;rs149078899	0;50	
cg07899997	-0.23106553	0.43345062	-3.26506689	0.03908855	0.80507989	-3.58854639	12	85671892	R	II		IGR	shore	IGR-shore	chr12:85673878-85674700	rs74343919		12
cg19472218	-0.22886705	0.30028337	-3.25123183	0.03954307	0.80526532	-3.60168986	14	90420449	R	II	EFCAB11	5'UTR	shore	5'UTR-shore	chr14:90422142-90422593			
cg03228974	0.259828084	0.56549537	3.248921922	0.03961959	0.80526532	-3.6038877	6	30067855	F	II		IGR	shore	IGR-shore	chr6:30068492-30068794	rs1264695		37
cg04026169	0.20400084	0.46941209	3.245695998	0.03972676	0.80535056	-3.60695873	4	85422265	F	I		IGR	shore	IGR-shore	chr4:85422929-85423190	rs10005941;rs537150735;rs192835192	5;15;18	
cg17586988	-0.20344003	0.54566464	-3.24135932	0.03987138	0.80572074	-3.61109015	18	5892245	F	II	TMEM200C	TSS200	shore	TSS200-shore	chr18:5890292-5891682			
cg24199558	-0.21166498	0.27566541	-3.23962418	0.03992942	0.80586257	-3.61274413	10	1.22E+08	R	II		IGR	opensea	IGR-opensea		rs544637640		5
cg04507598	0.207249088	0.59400112	3.239591046	0.03993053	0.80586257	-3.61277572	12	45990453	R	II		IGR	opensea	IGR-opensea		rs140620534;rs545612979;rs10880824	36;20;13	
cg13315744	0.219031935	0.53351648	3.237979056	0.03998455	0.80586257	-3.61431281	2	1287787	F	II	SNTG2	Body	shore	Body-shore	chr2:1286393-1286642	rs544820175;rs188647699	9;34	
cg12102690	-0.20671956	0.42752344	-3.23396166	0.04011957	0.80586257	-3.61814559	X	29503497	F	II	IL1RAPL1	Body	opensea	Body-opensea				
cg13796843	-0.25404638	0.41506914	-3.22604777	0.04038719	0.80586257	-3.62570439	15	76303634	F	II	NRG4	5'UTR	opensea	5'UTR-opensea		rs541257185		31
cg13784283	0.225644375	0.64222157	3.224484995	0.04044029	0.80586257	-3.62719839	6	33163627	R	II	RXRB	Body	shelf	Body-shelf	chr6:33159991-33160263	rs547479013;rs559052660	29;2	
cg22496559	-0.20721704	0.49057144	-3.22292618	0.04049335	0.80586257	-3.62868904	3	1.96E+08	F	I	TM4SF19	TSS200	opensea	TSS200-opensea		rs563644689;rs531066377	1;9	
cg07889765	-0.25011675	0.44915979	-3.21930943	0.04061677	0.805909	-3.63214937	10	96123159	F	II	NOC3L	TSS1500	shore	TSS1500-shore	chr10:96122540-96122904	rs138366586		20
cg01233718	-0.25336712	0.65971736	-3.21836791	0.04064898	0.80591913	-3.63305055	20	24599115	F	II	SYNDIG1	Body	opensea	Body-opensea				
cg02672759	0.20059884	0.42259034	3.215875441	0.04073439	0.80598808	-3.63543703	19	39739058	R	II		IGR	island	IGR-island	chr19:39737689-39739288	rs117436747		39
cg19724485	-0.24993812	0.4343795	-3.21405316	0.04079697	0.80610548	-3.63718253	11	55999683	F	II	ORST2	1stExon	opensea	1stExon-opensea		rs141189792;rs567353421;rs535373491;rs143289732;rs557241694	1;9;17;38;41	
cg18735473	-0.22965031	0.42407387	-3.20816096	0.04100013	0.80635023	-3.64283061	18	35015946	R	II	BRUNOL4	Body	opensea	Body-opensea		rs541184485;rs151317773	17;2	
cg24254317	-0.21465547	0.36687306	-3.19707612	0.04138571	0.80699061	-3.65347332	7	1.58E+08	F	II	PTPRN2	Body	opensea	Body-opensea				
cg08719486	0.247706774	0.4327996	3.196836607	0.04139409	0.80701683	-3.65370353	9	90112101	R	II	DAPK1	TSS1500	shore	TSS1500-shore	chr9:90112514-90113817	rs189775167;rs557342418	43;27	
cg04846432	-0.23174168	0.39565858	-3.17088667	0.04231443	0.80765045	-3.67870704	3	1.87E+08	R	II	MASP1	3'UTR	opensea	3'UTR-opensea		rs533203765;rs191487026	15;1	
cg00121963	0.296819208	0.58655414	3.170198497	0.04233918	0.80765045	-3.67937178	1	2.1E+08	F	II		IGR	opensea	IGR-opensea		rs150579375;rs537094305;rs555431789;rs181098427	1;45;46;51	
cg20575254	-0.23535806	0.52669915	-3.16737073	0.04244104	0.80765045	-3.68210417	20	54777948	F	II		IGR	opensea	IGR-opensea		rs6024691;rs537838583;rs555256705;rs6024692	0;6;24;25	
cg19709862	-0.20828527	0.65954471	-3.16710034	0.0424508	0.80765045	-3.68236552	16	47239315	R	II	ITFG1	Body	opensea	Body-opensea		rs547227542;rs113459429	32;31	
cg15779586	0.202531676	0.52033166	3.166870493	0.0424591	0.80765045	-3.68258769	4	74486675	F	II	RASSF6	TSS1500	shore	TSS1500-shore	chr4:74486044-74486258	rs557885540		6
cg24746838	-0.20115209	0.74852509	-3.16351552	0.04258041	0.80786542	-3.68583171	7	64452895	F	II	ZNF117	TSS1500	opensea	TSS1500-opensea		rs200900773;rs182355196;rs554302965;rs189142639;rs71534295;rs73365370;rs199931905;rs20	0;1;9;10;11;34;35;36	
cg16747564	0.213031707	0.35623601	3.156590235	0.04283216	0.80791217	-3.69253443	13	1.13E+08	F	I	SOX1	TSS1500	shore	TSS1500-shore	chr13:112720564-112723582	rs563782626;rs531294271	0;38	
cg16588114	-0.21955447	0.54130119	-3.15546084	0.04287339	0.80791217	-3.69362836	2	78578138	F	II		IGR	opensea	IGR-opensea		rs553205373;rs183514998	7;51	
cg23870749	0.217199064	0.41321747	3.146914244	0.04318695	0.80804348	-3.70191409	1	2.27E+08	R	II	PSEN2	Body	opensea	Body-opensea				
cg13863922	-0.204363	0.50653713	-3.14160499	0.04338316	0.80826853	-3.70706798	1	1.57E+08	R	II	C1orf92	TSS1500	shore	TSS1500-shore	chr1:156890243-156890806			
cg23979631	0.237153533	0.43018138	3.14096897	0.04340673	0.80840297	-3.70768573	7	27142427	F	I	HOXA2	TSS200	shore	TSS200-shore	chr7:27143181-27143479	rs113755325		41
cg27521648	-0.21629155	0.57042162	-3.13784142	0.0435229	0.80867532	-3.71072453	3	98293016	R	II		IGR	opensea	IGR-opensea		rs113367850;rs192487158;rs146674218;rs548897998	50;44;38;2	
cg19966955	0.279928523	0.76337906	3.135821151	0.04359814	0.80867532	-3.71268841	16	68267532	F	II	ESRP2	Body	shore	Body-shore	chr16:68269010-68272143	rs541273935;rs150084846;rs578156074;rs138351495	1;20;27;44	
cg12651598	-0.20015858	0.41232313	-3.12798175	0.0438916	0.80933222	-3.72031605	12	1.15E+08	R	II		IGR	opensea	IGR-opensea		rs139666943;rs144638564	43;1	
cg24892433	-0.24481769	0.42597785	-3.12776807	0.04389963	0.80933222	-3.72052412	13	1.12E+08	R	II		IGR	opensea	IGR-opensea		rs532972484		29
cg08924430	0.210142086	0.46642338	3.125629448	0.04398013	0.80933222	-3.72260699	4	1.06E+08	F	II	TET2	TSS1500	shore	TSS1500-shore	chr4:106067473-106067968			
cg02071319	0.201434722	0.64908789	3.120131048	0.04418791	0.80946013	-3.72796589	2	2.32E+08	F	II		IGR	shelf	IGR-shelf	chr2:231692697-231693496	rs75638829		3
cg17647565	0.208070484	0.54703604	3.106970201	0.04469013	0.8101443	-3.74081518	13	78696245	F	II		IGR	opensea	IGR-opensea		rs555487130;rs17068947;rs538045294	0;20;46	
cg23904249	0.221295238	0.55356626	3.102374532	0.04486714	0.81017673	-3.74530948	11	60608951	R	II	CCDC86	TSS1500	shore	TSS1500-shore	chr11:60609392-60609786	rs377268226;rs561285;rs547360784	25;20;9	
cg02310103	0.202542986	0.60877041	3.098757308	0.04500706	0.81040447	-3.74884962	3	50391305	R	II	CYB561D2	3'UTR	shelf	3'UTR-shelf	chr3:50387959-50388681	rs587676191;rs193294004	37;2	
cg10953721	-0.26064135	0.54083114	3.096123815	0.04510927	0.8105621	-3.75142848	11	1.32E+08	R	II	NTM	Body	opensea	Body-opensea		rs554977946;rs573278712;rs544340628	51;49;7	
cg24840099	0.206017886	0.49649516	3.074169399	0.04597242	0.81239061	-3.77297657	4	4864430	F	II	MSX1	Body	shore	Body-shore	chr4:4864456-4864834	rs528951725		15
cg12381370	0.220030305	0.55532987	3.064996165	0.04633902	0.81307545	-3.78200598	14	1.07E+08	F	II		IGR	opensea	IGR-opensea		rs112747173		21
cg10940601	-0.20428654	0.48309486	-3.05917309	0.04657358	0.81342366	-3.78774568	2	90120807	R	II		IGR	opensea	IGR-opensea		rs564244449;rs859741;rs551220209	32;28;2	
cg21079157	0.242178854	0.50193603	3.058096754	0.0466171	0.81342366	-3.78880728	20	60169020	R	II	CDH4	Body	opensea	Body-opensea				
cg15526081	0.203804254	0.19240808	3.056411135	0.04668534	0.81374805	-3.79047025	10	1.19E+08	F	II		IGR	shore	IGR-shore	chr10:119311204-119312104	rs550136549		6
cg26790634	0.21473273	0.57997086	3.048735235	0.04699767	0.81411845	-3.7980495	6	90365125	F	II	LOC101929057	Body	opensea	Body-opensea		rs190997987		9
cg04597312	-0.22634099	0.5918557	-3.04043764	0.04733815	0.81458868	-3.80625466	16	85933163	R	II	IRF8	5'UTR	shore	5'UTR-shore	chr16:85932121-85932942	rs142928841;rs558123454;rs577707345;rs540258616;rs553567847;rs573694304;rs542032446;rs!	47;46;42;37;34;29;23;21;11;9;6	
cg01838728	-0.20114544	0.55597767	-3.03294632	0.04764812	0.81492528	-3.81367323	15	36131223	F	II		IGR	opensea	IGR-opensea		rs549729955		1
cg27132535	0.226419028	0.52935083	3.009935511	0.04861582	0.8166898	-3.83652423	8	20170388	F	II		IGR	opensea	IGR-opensea		rs184772402;rs79305986;rs118143923	6;19;50	
cg06295238	0.28851827	0.5902938	3.00814696	0.04869204	0.8166898	-3.83830438	4	1205447	F	II	CTBP1	3'UTR	shore	3'UTR-shore	chr4:1205817-1206203	rs566302187;rs564855534;rs527281344;rs563184205	11;26;27;28	
cg12201779	0.22892198	0.29864221	3.00187424	0.04896047	0.81687396	-3.84455219	21	42219202	F	II	DSCAM	TSS200	island	TSS200-island	chr21:42218489-42219222	rs561849797;rs78280357;rs550030210	0;25;44	
cg23804454	0.21142216	0.650014	2.999969881	0.04904232	0.81699889	-3.8464504	1	1.17E+08	F	II		IGR	opensea	IGR-opensea		rs148247634;rs189109367	17;35	
cg05768005	0.201550771	0.51927427	2.993875907	0.04930537	0.81740899	-3.8525291	17	8094486	F	II	C17orf59	TSS1500	shore	TSS1500-shore	chr17:8092418-8093706	rs73245443		33
cg17162166	0.284990348	0.5744671	2.993435308	0.04932445	0.81740899	-3.85296885	14	93674922	F	II	C14orf142	TSS1500	shore	TSS1500-shore	chr14:93673128-93673917	rs569477085;rs112511497;rs558347224	12;45;46	
cg18638855	-0.20440036	0.53844232	-2.99040098	0.04945613	0.817421	-3.85599832	13	70544611	R	II	KLHL1	Body	opensea	Body-opensea		rs552214621		38

nature research

Corresponding author(s): Thomas F Meyer

Last updated by author(s): Feb 18, 2019

Reporting Summary

Nature Research wishes to improve the reproducibility of the work that we publish. This form provides structure for consistency and transparency in reporting. For further information on Nature Research policies, see Authors & Referees and the Editorial Policy Checklist.

Statistics

For all statistical analyses, confirm that the following items are present in the figure legend, table legend, main text, or Methods section.

n/a	Confirmed	
☐	☒	The exact sample size (*n*) for each experimental group/condition, given as a discrete number and unit of measurement
☐	☒	A statement on whether measurements were taken from distinct samples or whether the same sample was measured repeatedly
☐	☒	The statistical test(s) used AND whether they are one- or two-sided *Only common tests should be described solely by name; describe more complex techniques in the Methods section.*
☐	☒	A description of all covariates tested
☐	☒	A description of any assumptions or corrections, such as tests of normality and adjustment for multiple comparisons
☐	☒	A full description of the statistical parameters including central tendency (e.g. means) or other basic estimates (e.g. regression coefficient) AND variation (e.g. standard deviation) or associated estimates of uncertainty (e.g. confidence intervals)
☐	☒	For null hypothesis testing, the test statistic (e.g. *F*, *t*, *r*) with confidence intervals, effect sizes, degrees of freedom and *P* value noted *Give P values as exact values whenever suitable.*
☒	☐	For Bayesian analysis, information on the choice of priors and Markov chain Monte Carlo settings
☒	☐	For hierarchical and complex designs, identification of the appropriate level for tests and full reporting of outcomes
☒	☐	Estimates of effect sizes (e.g. Cohen's *d*, Pearson's *r*), indicating how they were calculated

Our web collection on statistics for biologists contains articles on many of the points above.

Software and code

Policy information about availability of computer code

Data collection

Provide a description of all commercial, open source and custom code used to collect the data in this study, specifying the version used OR state that no software was used.

Data analysis

fgsea R package (Sergushichev, A. An algorithm for fast preranked gene set enrichment analysis using cumulative statistic calculation. bioRxiv doi: 10.1101/060012(2016).)
ChAMP package (Morris, T.J., et al. ChAMP: 450k Chip Analysis Methylation Pipeline. Bioinformatics 30, 428-430 (2014).)
limma (Ritchie, M.E., et al. limma powers differential expression analyses for RNA-sequencing and microarray studies. Nucleic Acids Res. 43, e47 (2015))
The networks and functional analyses of microarray data (igure 1 f , g, and S2 a , b and S3) were generated through the use of IPA (QIAGEN Inc., https://www.qiagenbioinformatics.com/products/ingenuity-pathway-analysis; Causal analysis approaches in Ingenuity Pathway Analysis. Bioinformatics. 2014 Feb 15;30(4):523-30.

For manuscripts utilizing custom algorithms or software that are central to the research but not yet described in published literature, software must be made available to editors/reviewers. We strongly encourage code deposition in a community repository (e.g. GitHub). See the Nature Research guidelines for submitting code & software for further information.

Data

Policy information about availability of data

All manuscripts must include a data availability statement. This statement should provide the following information, where applicable:

- Accession codes, unique identifiers, or web links for publicly available datasets
- A list of figures that have associated raw data
- A description of any restrictions on data availability

The microarray and methylation BeadChip data from this manuscript have been deposited in the National Centre for Biotechnology Information Omnibus (GEO)

under accession codes GSE107712 and GSE108202.
Raw data associated with Fig. 3f and Fig 4 can be found in Supplementary Tables 1 and 2, respectively.
Quantitative data supporting the findings of this study are available within the paper and its supplementary information files. All other data supporting these findings are available from the corresponding author upon reasonable request.

Field-specific reporting

Please select the one below that is the best fit for your research. If you are not sure, read the appropriate sections before making your selection.

☒ Life sciences ☐ Behavioural & social sciences ☐ Ecological, evolutionary & environmental sciences

For a reference copy of the document with all sections, see nature.com/documents/nr-reporting-summary-flat.pdf

Life sciences study design

All studies must disclose on these points even when the disclosure is negative.

Sample size	No statistical methods were used to predetermine sample size
Data exclusions	No data were excluded from the experiments
Replication	All attempts at replication were successful. All graphs represent data with at least two biological replicates, all images represent findings reproduced at least twice in the laboratory
Randomization	No specific procedures were carried out for randomization
Blinding	The investigator was blinded for image and quantitative analysis

Reporting for specific materials, systems and methods

We require information from authors about some types of materials, experimental systems and methods used in many studies. Here, indicate whether each material, system or method listed is relevant to your study. If you are not sure if a list item applies to your research, read the appropriate section before selecting a response.

Materials & experimental systems

n/a	Involved in the study
☐	☒ Antibodies
☐	☒ Eukaryotic cell lines
☒	☐ Palaeontology
☒	☐ Animals and other organisms
☐	☒ Human research participants
☒	☐ Clinical data

Methods

n/a	Involved in the study
☒	☐ ChIP-seq
☐	☒ Flow cytometry
☒	☐ MRI-based neuroimaging

Antibodies

Antibodies used	mouse anti-E-Cadherin (1:200 610181, BD Transduction Lab), mouse anti-β-actin (1:200, A5441, Sigma), goat anti-Ctr (OBT0978, AbD Serotec), mouse anti-HSP60 (1:5000, ALX-804-701, Alexis), rabbit anti-Ki67 (9027, Cell Signaling), rabbit anti-pSTAT1 (1:1000, 9167, Cell Signaling), rabbit anti-pSTAT3 (Tyr705) (1:1000 9145, Cell Signaling), cleaved caspase-3 (1:1000, 9664, Cell Signaling), goat anti-LIF (1:500, AF-250-NA, R&D Systems),sheep anti-mouse-HRP (1:3000, NA931, Amersham), donkey anti-rabbit-HRP (1:3000, NA934, Amersham), donkey anti-goat-HRP (1:3000, 800073, Biomol), donkey anti-mouse-Alexa 488 (1:300, 715-546-140, Dianova), donkey anti-goat-Cy3 (1:300, 705-165-003, Dianova), donkey anti-rabbit-Alexa 488 (1:300, 711-546-152, Dianova), donkey anti-mouse-Dylight 647 (1:300, 715-605-150, Dianova), CD326 (EpCAM)-FITC (1:50, 130-080-301, Miltenyi), mouse anti-human CD24-BV711 (1:200, 563371, BD Biosciences), mouse anti IgG1-APC (1:100, 130-098-846, Miltenyi) and mouse anti-human CD133/1 (AC133)-APC (1:100, 130-098-829, Miltenyi).
Validation	Validation was performed by the manufacturers; positive and negative controls were used in the lab for validation of each antibody

Eukaryotic cell lines

Policy information about cell lines

Cell line source(s)	HeLa cells, ATCC® CCL-2

Authentication	HeLa cells were ordered as an authenticated cell line from ATCC
Mycoplasma contamination	All cell lines tested negative for mycoplasma contamination.
Commonly misidentified lines (See ICLAC register)	We used HeLa cells for Chlamydia stock expansion and infectivity assay as they are the standard cell line used for confirming infection with Chlamydia trachomatis.

Human research participants

Policy information about studies involving human research participants

Population characteristics	Tissue was donated by female patients aged 40 to 75
Recruitment	2014-2018
Ethics oversight	Ethics comimssion Charite Medical University Berlin

Note that full information on the approval of the study protocol must also be provided in the manuscript.

Flow Cytometry

Plots

Confirm that:

☒ The axis labels state the marker and fluorochrome used (e.g. CD4-FITC).

☒ The axis scales are clearly visible. Include numbers along axes only for bottom left plot of group (a 'group' is an analysis of identical markers).

☒ All plots are contour plots with outliers or pseudocolor plots.

☒ A numerical value for number of cells or percentage (with statistics) is provided.

Methodology

Sample preparation	CtrD infected as well as non-infected fallopian tube organoids were split at indicated time points into single cells by enzymatic (TrypLE, 15 min, 37°C) and mechanical (needle, 26G) treatment. Single cell suspensions were filtered (0.45 µm), fixed in 3.7% PFA (30 min, RT) and washed with 1%BSA/PBS. Fixed cells were stained in 1%BSA/PBS with either CD24-BV711 and EpCAM-FITC or CD133-APC (30 min on ice). After staining, cells were washed with PBS and analysed using a flow cytometer. For assessing the number of proliferating cells a Click-iT-EdU assay (C10425, Thermo Fisher) was performed. For this organoids were incubated for 2 h with 10 µM EdU, followed by single cell preparation and fixation. Permeabilization and labeling of EdU positive cells with Alexa488 azide was performed according to the manufacturer's protocol.
Instrument	BD FACS CANTOII flow cytometer (BD Biosciences)
Software	BD FACSDiva Software and FlowJo (FlowJo LLC)
Cell population abundance	Only flow cytometric analysis but no sorting was performed.
Gating strategy	From the initial cell population, which was gated in FSC-A/SSC-A by eliminating debris, singlets were discriminated using forward scatter (FSC-H/FSC-W) and side scatter (SSC-H/SSC-W) plots. Boundaries between positive and negative populations were defined using unstained or isotype controls. Representative gating strategies for each analysis are depicted in Supplementary Figures 5a and 6.

☒ Tick this box to confirm that a figure exemplifying the gating strategy is provided in the Supplementary Information.